



University
of Glasgow

Dai, Shaowei (2021) *Adaptive beamforming and switching in smart antenna systems*. PhD thesis.

<https://theses.gla.ac.uk/82507/>

Copyright and moral rights for this work are retained by the author

A copy can be downloaded for personal non-commercial research or study,
without prior permission or charge

This work cannot be reproduced or quoted extensively from without first
obtaining permission in writing from the author

The content must not be changed in any way or sold commercially in any
format or medium without the formal permission of the author

When referring to this work, full bibliographic details including the author,
title, awarding institution and date of the thesis must be given

Enlighten: Theses

<https://theses.gla.ac.uk/>
research-enlighten@glasgow.ac.uk

**ADAPTIVE BEAMFORMING AND SWITCHING IN
SMART ANTENNA SYSTEMS**

Shaowei Dai
Matriculation Number:

Submitted in Fulfilment of the Requirements for the Degree of
Doctor of Philosophy



UNIVERSITY OF GLASGOW
SCHOOL OF ENGINEERING

June 2021

The copyright in this thesis is owned by the author. Any quotation from the thesis or use of any of the information contained in it must acknowledge this thesis as the source of the quotation or information.

Abstract

The ever increasing requirement for providing large bandwidth and seamless data access to commuters has prompted new challenges to wireless solution providers. The communication channel characteristics between mobile clients and base station change rapidly with the increasing traveling speed of vehicles. Smart antenna systems with adaptive beamforming and switching technology is the key component to tackle the challenges.

As a spatial filter, beamformer has long been widely used in wireless communication, radar, acoustics, medical imaging systems to enhance the received signal from a particular looking direction while suppressing noise and interference from other directions. The adaptive beamforming algorithm provides the capability to track the varying nature of the communication channel characteristics. However, the conventional adaptive beamformer assumes that the Direction of Arrival (DOA) of the signal of interest changes slowly, although the interference direction could be changed dynamically. The proliferation of High Speed Rail (HSR) and seamless wireless communication between infrastructure (roadside, trackside equipment) and the vehicles (train, car, boat etc.) brings a unique challenge for adaptive beamforming due to its rapid change of DOA. For a HSR train with 250km/h, the DOA change speed can be up to 4° per millisecond. To address these unique challenges, faster algorithms to calculate the beamforming weight based on the rapid-changing DOA are needed.

In this dissertation, two strategies are adopted to address the challenges. The first one is to improve the weight calculation speed. The second strategy is to improve the speed of DOA estimation for the impinging signal by leveraging on the predefined constrained route for the transportation market. Based on these concepts, various algorithms in beam pattern generation and adaptive weight control are evaluated and investigated in this thesis. The well known Generalized Sidelobe Cancellation (GSC) architecture is adopted in this dissertation. But it faces serious signal cancellation problem when the estimated DOA deviates from the actual DOA which is severe in high mobility scenarios as in the transportation market. Algorithms to improve various parts of the GSC are proposed in this dissertation. Firstly, a Cyclic Variable Step Size (CVSS) algorithm for adjusting the Least Mean Square (LMS) step size with simplicity for implementation is proposed and evaluated. Secondly, a Kalman filter based solution to fuse different sensor information for a faster estimation and tracking of the DOA is investigated and proposed. Thirdly, to address the DOA mismatch issue caused by the rapid DOA change, a fast blocking matrix generation algorithm named Simplified Zero Placement Algorithm (SZPA) is proposed to mitigate the signal cancellation in GSC. Fourthly, to make the beam pattern robust against DOA mismatch, a fast algorithm for the generation of flat beam pattern named Zero Placement Flat Top (ZPFT) for the fixed beamforming path in GSC is proposed. Finally, to evaluate the effectiveness and performance of the beamforming algorithms, wireless channel simulation is needed. One of the challenging aspects for wireless simulation is the coupling between Probability Density Function (PDF) and Power Spectral Density (PSD) for a random variable. In this regard, a simplified solution to simulate Non-Gaussian wireless channel is proposed, proved and evaluated for the effectiveness of the algorithm.

With the above optimizations, the controlled simulation shows that the flat top beam pattern can be generated 380 times faster than iterative optimization method and blocking matrix can be generated 9 times faster than normal SVD method while the same overall optimum state performance can be achieved.

Acknowledgements

I would like to thank my supervisors Dr. Minghui Li, Dr. Qammer H. Abbasi and Professor Muhammad Imran for all their help and invaluable advice during my research. I would also like to thank my wife and two daughters for their support in this tough journey, whom without this would have not been possible. I also appreciate all the support I received from the team. Lastly, I would like to thank the Singapore Economic Development Board and RFNet Technologies Pte. Ltd. that allowed me to conduct this research.

Declaration

I declare that, except where explicit reference is made to the contribution of others, that this dissertation is the result of my own work and has not been submitted for any other degree at the University of Glasgow or any other institution.

Shaowei Dai

Publications from This Thesis

- [1] S. Dai, M. Li, Q. H. Abbasi, and M. A. Imran, “A fast blocking matrix generating algorithm for generalized sidelobe canceller beamformer in high speed rail like scenario,” *IEEE Sensors Journal*, 2020.
- [2] S. Dai, M. Li, Q. H. Abbasi, and M. A. Imran, “A zero placement algorithm for synthesis of flat top beam pattern with low sidelobe level,” *IEEE Access*, vol. 8, pp. 225935–225944, 2020.
- [3] S. Dai, M. Li, Q. H. Abbasi, and M. Imran, “Hardware efficient adaptive beamformer based on cyclic variable step size,” in *2018 IEEE International Symposium on Antennas and Propagation & USNC/URSI National Radio Science Meeting*, pp. 191–192, IEEE, 2018.
- [4] S. Dai, Q. H. Abbasi, M. Li, and M. Imran, “Beamforming optimization based on kalman filter for vehicle in constrained route,” in *2019 IEEE International Symposium on Antennas and Propagation and USNC-URSI Radio Science Meeting*, pp. 1365–1366, IEEE, 2019.
- [5] S. Dai, M. Li, Q. H. Abbasi, and M. Imran, “Improve tracking speed of beamformer with simplified zero placement algorithm,” in *2019 IEEE MTT-S International Wireless Symposium (IWS)*, pp. 1–3, IEEE, 2019.
- [6] S. Dai, M. Li, Q. H. Abbasi, and M. Imran, “Non-gaussian colored noise generation for wireless channel simulation with particle swarm optimizer,” in *2020 14th European Conference on Antennas and Propagation (EuCAP)*, pp. 1–4, IEEE, 2020.
- [7] S. Dai, M. Li, Q. H. Abbasi, and M. Imran, “A fast blocking matrix generating algorithm for generalized sidelobe canceller beamforming,” in *2020 IEEE International Symposium on Antennas and Propagation and North American Radio Science Meeting*, pp. 291–292, IEEE, 2020.

Contents

List of Tables	10
List of Figures	11
Nomenclature	13
1 Introduction	15
1.1 Background	15
1.2 Beamformer Hardware Structure	17
1.3 Beamformer Functions	18
1.4 Motivation	21
1.5 Aims and Objectives	22
1.6 Contributions	22
1.7 Dissertation Organization	23
2 Beamformer Design in Wireless Communication System	25
2.1 Wireless Communication with Smart Antenna Architecture	25
2.2 Beamformer Architecture	26
2.2.1 Analogy to Finite Impulse Response (FIR) Filter	28
2.2.2 Spatial Sampling of Beamformer	29
2.3 Beamforming Algorithm Review	32
2.3.1 Window Method	33
2.3.2 Approximation Problem and Performance Metric	36
2.3.3 Remez Algorithm and Parks-McClellan Method	38
2.3.4 Frequency Sampling Method and Woodward Lawson	39
2.3.5 Minimum Variance Distortionless Response	40
2.3.6 Linear Constraint Minimum Variance	44
2.3.7 Generalized Sidelobe Cancellation	45

2.3.8	Eigen Beamforming	46
2.3.9	Blind Beamforming	47
2.4	Adaptive Optimization Algorithm Review	51
2.4.1	Extension to Complex Domain	51
2.4.2	Mean Square Error	52
2.4.3	Orthogonality	53
2.4.4	Least Square	54
2.4.5	Steepest Descent	55
2.4.6	Least Mean Square	56
2.4.7	Normalized LMS	57
2.4.8	Cyclic Variable Step Size LMS	59
2.4.9	Affine Projection Algorithm	60
2.4.10	Recursive Least Square	62
2.4.11	Kalman Filter	63
2.5	Direction of Arrival Estimation	64
2.5.1	MUltiple Signal Characterization (MUSIC)	64
2.5.2	Kalman Filter Assisted DOA Estimation in Constrained Route	66
2.6	Summary	67
3	Wireless Communication System Simulation	69
3.1	Introduction	69
3.2	Motivation	70
3.3	Problem Formulation	72
3.4	Proposed Solutions	73
3.4.1	Proposed Architecture for Noise Generation	73
3.4.2	Find the Right Filter with the Required $R_x(\tau)$	74
3.4.3	Searching for Optimum Filter Coefficient by PSO	75
3.5	Numerical Simulation and Result Analysis	76
3.6	Summary	78
4	Fast Algorithm for Flat Top Beam Pattern Synthesis	80
4.1	Introduction	80
4.2	Problem Formulation	83
4.3	Proposed Solution	83
4.3.1	Narrow Mainlobe Beam Width with Low SLL Controlled by $C(z)$	84

4.3.2	Zero Placement for Flat Top Constraints Sub-Array $B(z)$	85
4.3.3	Principle Condition for Flattening a Second Order Polynomial with a Broadening Polynomial	87
4.3.4	Main Lobe Pattern Approximation by Taylor Series Expansion	90
4.3.5	Algorithms for the Synthesis of Flat Top Beam Pattern	91
4.4	Numerical Simulation and Analysis	93
4.4.1	Lower SLL or Narrower Null to Null Beamwidth Compared with Window Method	93
4.4.2	Faster Calculation Speed Compared with Numerical Optimiza- tion Method	96
4.4.3	Impact of k Factor and Steering of Main Beam by Angle Shift .	98
4.5	Summary	100
5	Adaptive Beamformer Design and Implementation in Transportation	
	Market	101
5.1	Introduction	101
5.2	Problem Formulation	103
5.2.1	Vehicle to Roadside Challenge	103
5.2.2	GSC Architecture	107
5.3	Proposed Solution	107
5.3.1	Simplified Zero Placement Algorithm	107
5.3.2	Derivative Constraint based Robust Beamforming	109
5.4	Numerical Simulation and Analysis	111
5.4.1	Calculation Performance Simulation	112
5.4.2	Optimum Beam Pattern Performance Simulation	113
5.4.3	Learning Curve and SNR Performance Comparison	114
5.5	Summary	116
6	Conclusion and Future Work	117
6.1	Conclusion	117
6.2	Future Work	119
6.2.1	Further Explore the Knowledge of Constrained Route	119
6.2.2	Extend the SZPA and ZPFT Algorithm to Non-Uniform Dis- tributed Scenario	120

6.2.3 Use the Right Random Variable Profile for Fast Railway Wireless Communication Simulation	120
---	-----

Abbreviations	121
----------------------	------------

Bibliography	125
---------------------	------------

List of Tables

1.1	Minimum Variance Distortionless Response (MVDR) Beamformer Function to Reject Interference	19
3.1	Comparison of Correlation to the Required PSD	77
4.1	Design Parameter for Simulation of Comparison with Window Method Based on FIR	94
4.2	Synthesized ULA for Dolph-Chebyshev, FIR and ZPFT	95
4.3	Design Parameter for Simulation of Comparison with SDR	96
4.4	Synthesized ULA for SDR and ZPFT	97
4.5	Design Parameter for Impact of Shape Factor k Simulation	98
4.6	Design Parameter for Main Beam Shifting Simulation	99
5.1	Adaptive Speed Impact Simulation Setup	114

List of Figures

1.1	Hybrid Beamformer with Shared RF Chain Hardware Structure	18
1.2	Beamformer Rejects Directional Interference	19
1.3	Beamformer Rejects Directional Interference	20
2.1	Smart Antenna System Architecture	25
2.2	Adaptive Beamforming Architecture	27
2.3	Adaptive Temporal Filter Architecture	28
2.4	Beamformer Model of Received Signal	30
2.5	Rectangular Window Effect	32
2.6	Window Shape for Typical Window Algorithms	34
2.7	Various Window Effect on Ideal Beamformer	35
2.8	Chebyshev Polynomial Controlled by Scaling Factor α and Order n	38
2.9	Woodward Lawson Synthesized Pattern with 3 Sampling Point	40
2.10	Beamformer Implementation with GSC Structure	45
2.11	Blind Signal Separation Signal Model	48
2.12	Mixing Independent Signal Causes Dependency	49
2.13	Combined Signal Closer to Gaussian Distribution	50
2.14	Error Signal is Orthogonal to Space Spanned by Input Vector Signal	54
2.15	Adaptive Beamforming Architecture without Reference Response	57
2.16	Update of \mathbf{w} along the Direction of Input Vector \mathbf{x}	59
2.17	Cyclic Variable Step Size Performance Simulation	60
2.18	Affine Projection to Intersect of Affine Subspaces	61
2.19	MUSIC Spectrum	66
2.20	Kalman Filter Assisted Angle Estimation	67
3.1	Changing PSD of a Random Variable by Filtering Affects its PDF	70
3.2	SISO Wireless Channel Model	72
3.3	Architecture of PSO based Non-Gaussian Noise Generation	73

3.4	Generated Noise Follows the Required Rayleigh PDF with Gaussian Noise as Input	77
3.5	Generated Noise Follows the Required PSD for Proposed Method . . .	78
4.1	Norm $ z - r_0 $ for a Zero Placed at $(r_0,0)$	85
4.2	Zero Location Effect on Amplitude Response	87
4.3	Concept to Flatten a Second Order Even Polynomial Function	89
4.4	Synthesized Beam Pattern Comparison between FIR, ZPFT and Dolph-Chebyshev	95
4.5	Synthesized Beam Pattern Comparison between SDR and ZPFT	97
4.6	Beam Pattern Effect of Controlling Factor k	99
4.7	Main Beam Steering Control for ZPFT Algorithm	100
5.1	Base Station Installed along Track Side	104
5.2	DOA Change Effect for Vehicle to Infrastructure	105
5.3	Angle Change Speed Spike when Passing By Base Station	106
5.4	Angle Change Speed Increases when Distance h Decreases	106
5.5	Beamformer Implementation with GSC Structure	107
5.6	Derivative Constraint and Number of Zeros Effect	110
5.7	Each Zero Located at ξ_i Has a Corresponding Peak at $\xi_i + \pi$ for the Norm $ z - \xi_i $	110
5.8	Blocking Matrix Calculation Time Comparison with Respect to Number of Constraints	112
5.9	Converged Beam Pattern Performance Comparison	113
5.10	Learning Curve Performance Comparison with Different Step Size . . .	115
5.11	SNR Performance Comparison	115

Nomenclature

$(.)^*$ Conjugate of matrix or vector.

$(.)^H$ Hermitian of matrix.

$(.)^T$ Transpose of matrix.

$\mathbb{E}\{.\}$ Expectation.

d Antenna Element (AE) space interval.

ω_c Carrier frequency of incoming signal.

$s(t)$ Incoming signal.

$s_i(t)$ The i^{th} incoming signal impinging on AE.

x_m m^{th} AE output.

ξ The spatial frequency.

λ Wave length of signal.

\mathbf{R}_{xx} Correlation matrix for received signal vector.

\mathbf{R} Signal correlation atrix.

$\hat{\mathbf{R}}$ Sample correlation matrix.

\mathbf{r}_{xd} Cross correlation vector.

\mathbf{n} Noise vector.

\mathbf{P} Received signal power array.

\mathbf{x} Received signal column vector.

α Steering vector for incoming signal.

A Steering vectors array.

w Weight vector for combining signals.

Chapter 1

Introduction

The ever increasing requirement for providing large bandwidth and seamless data access to commuters has prompted new challenges to wireless solution providers. The communication channel characteristics between mobile clients and base station change rapidly with the increasing travelling speed of vehicles. Smart antenna systems with adaptive beamforming and switching technology are the key component to tackle the challenges. This dissertation investigates various beamforming algorithms to mitigate challenges faced in wireless communication in the transportation market. One of the focus is on the improvement of Generalized Sidelobe Cancellation (GSC) structure beamformer due to its simplicity for implementation. Various components of GSC include Fixed Beamformer (FB) which produces quiescent beampattern, Blocking Matrix (BM) to avoid signal cancellation and adaptive algorithms to control the noise cancellation are investigated. The results are published in 2 journal paper[1, 2] and 5 conference paper[3, 4, 5, 6, 7].

1.1 Background

The most noticeable attribute of a Smart Antenna system is its multiple Antenna Element (AE) for receiving multiple copies of signal in different location. The AE can be arranged as Uniform Linear Array (ULA), Uniform Circular Array (UCA)[8] or distributed randomly [9, 10]. Controlling of each AE can be through time delay for wide band application or phase shift for narrow band application. Since most of current wireless communication adopts Orthogonal Frequency Division Multiplexing (OFDM) technique [11, p 27], each sub-carrier can be conveniently regarded as a narrow band signal. So most of the discussion in this dissertation assumes the narrow band

model. The controlling can be realized in the analog domain for its low cost, the digital domain for its flexibility, or the hybrid way to balance cost and flexibility. Different weight assignment strategy for each AE makes a huge difference in system performance in interference rejection, channel capacity etc. It can be optimized for diversity gain as with Maximum Ratio Combining (MRC) [12] in receiver or same diversity gain in transmitter [13], channel capacity as in Spatial Multiplexing [14] or Signal to Interference and Noise Ratio (SINR) as in various beamforming algorithm reviewed in next chapter.

As a spatial filter, beamformer has long been widely used in wireless communication [15], radar[16], acoustic[17], medical imaging[18] systems to enhance the received signal from a particular looking direction while suppressing noise from other directions. Data independent beamformer [19, p 222] forms beam based on predefined requirements of beampattern, Sidelobe Level (SLL) etc. Data dependent beamformer like Minimum Variance Distortionless Response (MVDR) is able to adapt to changing environment through adaptive algorithms like Least Mean Square (LMS), Normalized LMS (NLMS), Recursive Least Square (RLS) [20, p 33]. The adaptive beamforming algorithm provides the capability to track the varying nature of the communication channel characteristics. The conventional adaptive beamformer assumes the DOA changes slowly, although the interference direction could be changed dynamically. Many of the existing algorithms and their assumptions need a review under the context of the transportation market.

In the transportation market, many applications require large data bandwidth between the mobile client and fixed base station. Some of the typical usage includes CCTV footage upload, Video Streaming, WiFi Hotspot and Digital Signage Update etc. Different kinds of transportation scenarios like train to trackside, bus to roadside needs to be supported under the name of Vehicle to Everything (V2X) [21, 22] in 5G standard. This kind of application faces some common challenges. Firstly, the channels are crowded in the base station side due to the space constraint. Secondly, the communication channel characteristics are changing rapidly. With the travelling speed up to $500km/h$ as one of the design objectives for 802.11bd, the estimation of the channel becomes obsolete quickly [23]. The environment is highly dynamic with many objects movement. Thirdly, it is desirable for each base station to cover a larger range of mobile clients to reduce cost.

Some of the challenges are solved by the current beamforming technologies. Smart antenna with beamforming is an enabling technology used in current wireless solutions

like 5G and WiFi 802.11ac etc. With the advancement of beamforming, Multiple User Multiple Input Multiple Output (MU-MIMO) becomes possible first in 11AC standard, although it is enabled for downlink only. And currently, MU-MIMO for uplink is also possible in 802.11ax standard.

1.2 Beamformer Hardware Structure

Out of the three hardware structure to implement beamformer as listed in the previous section, Analog Beamformer, Digital Beamformer and Hybrid Beamformer, the hybrid structure is more popular. Analog beamformer is simple and not costly, but the controlling is slow and not flexible. The pure digital structure is most flexible but it is most expensive. One of the costly components in digital beamformer is the RF chain and analog/digital conversion. The strategy to reduce the cost while retaining the benefits of the digital beamformer is to use Single RF Chain to support multiple AE. One way is to use Spatial Modulation to activate the single RF Chain to work with one of the AE at each time instance [24]. Effectively, each antenna's spatial information is used for bits encoding. However, since the receiver needs to use the channel response for each Tx/Rx Channel to identify which Tx antenna is used for the spatial demodulation purpose, the channel probing is a costly process, especially for Massive Multiple In Multiple Out (MIMO). The other popular way is to connect one costly transceiver with multiple AEs equipped with analog phase shifter to reduce the cost as used in hybrid beamformer so that beam pattern can be synthesized in analog beamformer through the phase shifter and digital beamforming through the digital transceiver.

The mapping of transceiver to AE can be classified as fully connected or partially connected [25, 26] in hybrid beamformer. A fully connected hybrid beamformer enjoys more flexibility since each transceiver is connected to all the AEs with much more complexity and cost than the partially connected structure. Each AE can be controlled by Single Phase Shifter (SPS) [25] or Double Phase Shifter (DPS) [27]. The phase shifter imposes a non-convex challenge due to the additional constant modulus constraint [28]. The other major challenge for using phase shifter is frequency invariant when applying the phase shifter in the time domain for wide band signals. Most hybrid beamformer design algorithms thus adopt iterative methods to minimize the Euclidean distance to the optimal digital beamformer [25, 28, 29].

In this thesis, a Hybrid beamformer with potential shared RF Chain is used for

beamformer algorithm investigation. The hardware structure is illustrated in Fig. 1.1.

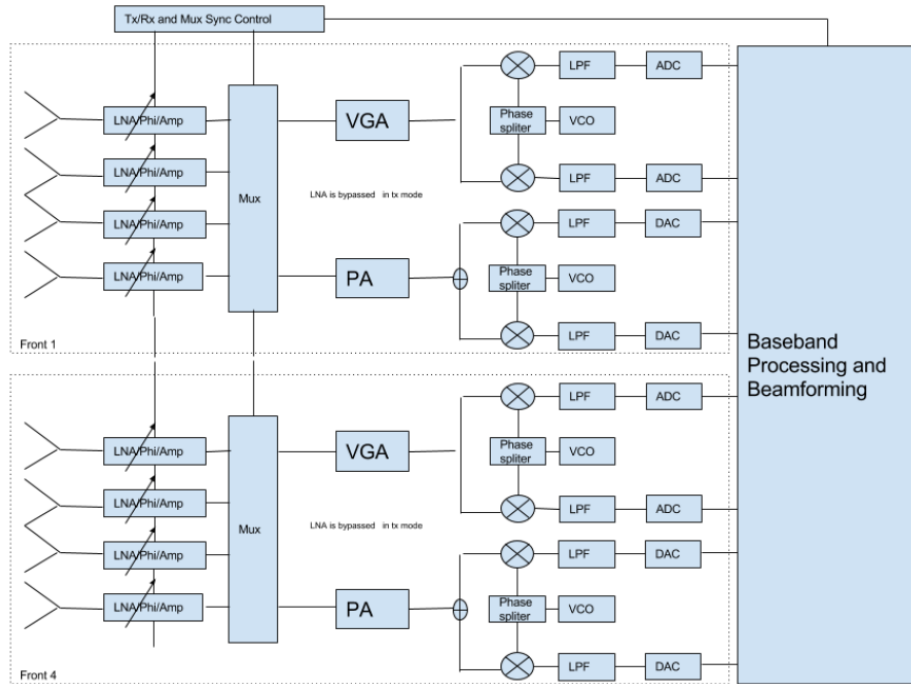


Figure 1.1: Hybrid Beamformer with Shared RF Chain Hardware Structure

As illustrated in Fig. 1.1, each RF chain supports multiple antennae equipped with analog phase shifter and multiplexing for antenna switching. In the targeted constrained route scenario, the speed of adaptation to the DOA change is the main concern. Since the OFDM modulation scheme is used, when analog phase shifter is applied at the post-Inverse Fast Fourier Transform (IFFT) stage, it will cause frequency selective channel. So to eliminate the inherent issue from phase shifter and achieve higher speed following rapid DOA change, the analog AEs are switched instead of phase shifted. The antenna switching is a simple process of activating one of the 4 antenna array with prearranged direction. This dissertation focuses on the beamforming algorithms that could be implemented inside the baseband processing unit.

1.3 Beamformer Functions

In wireless communication, especially the high speed Vehicle to Infrastructure scenario, the beamformer can be used to compensate Doppler Frequency Shift by forming multiple beams in transmitter and compensate each beam before transmitting out [30]. The main usage for beamformer is to reject interference from some known or unknown angle. A simple example below shows the effectiveness of beamformer in rejecting interference. A simple QPSK modulated signal is to be detected with a ten elements

ULA. The parameters to be simulated is listed below:

Table 1.1: MVDR Beamformer Function to Reject Interference

Parameters	Value
Modulation Scheme	QPSK
Number of Sensors	10
Pilot Length	100
Payload Length	1000
Desired Signal Angle of Arrival	0°
Interference Angle of Arrival	-10°
Interference to Signal Ratio	10dB
Signal to Noise Ratio	15dB
Beamforming Algorithm	MVDR

The comparison is conducted between MRC whose main purpose is to address the fading problem to achieve maximum rate in wireless communication. But it has no capability to reject directional interference.

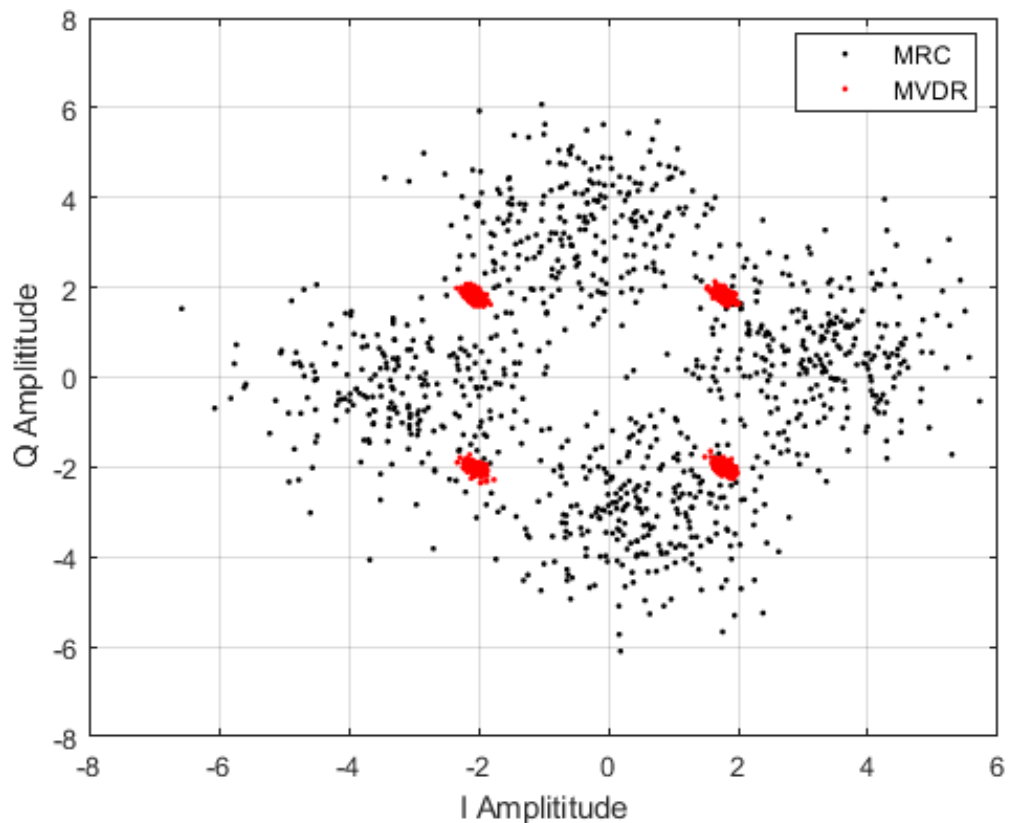


Figure 1.2: Beamformer Rejects Directional Interference

In wireless communication, information is usually modulated using Quadrature Amplitude Modulation (QAM), where the two independent stream of data named as In-phase (I) component and Quadrature component (Q) are modulated into two orthogonal carrier offset by 90° . The demodulated IQ component (I Amplitude and Q Amplitude) could then be used to plot the constellation diagram to show the quality of the received data. The noise or interference tends to spread the constellation point which increases Error Vector Magnitude (EVM) and leads to higher Bit Error Rate (BER). From Fig. 1.2, it is clear that when interference is impinging on the AE, even with just 10 degrees difference, MVDR is able to restore the Quadrature Phase Shift Keying (QPSK) modulated signal. This is because the MVDR beamformer forms a null towards the direction of interference so that the interference is effectively reduced drastically by 55dB as shown in Fig. 1.3. And in this scenario, schemes like MRC that has no consideration of spatial information will fail miserably.

The adaptively formed beam pattern comparison between MRC and MVDR is shown in Fig. 1.3. It clearly shows that a deep null with 55dB attenuation is automatically formed in the interference direction of -10° in MVDR scheme while MRC has no null formed for interference rejection.

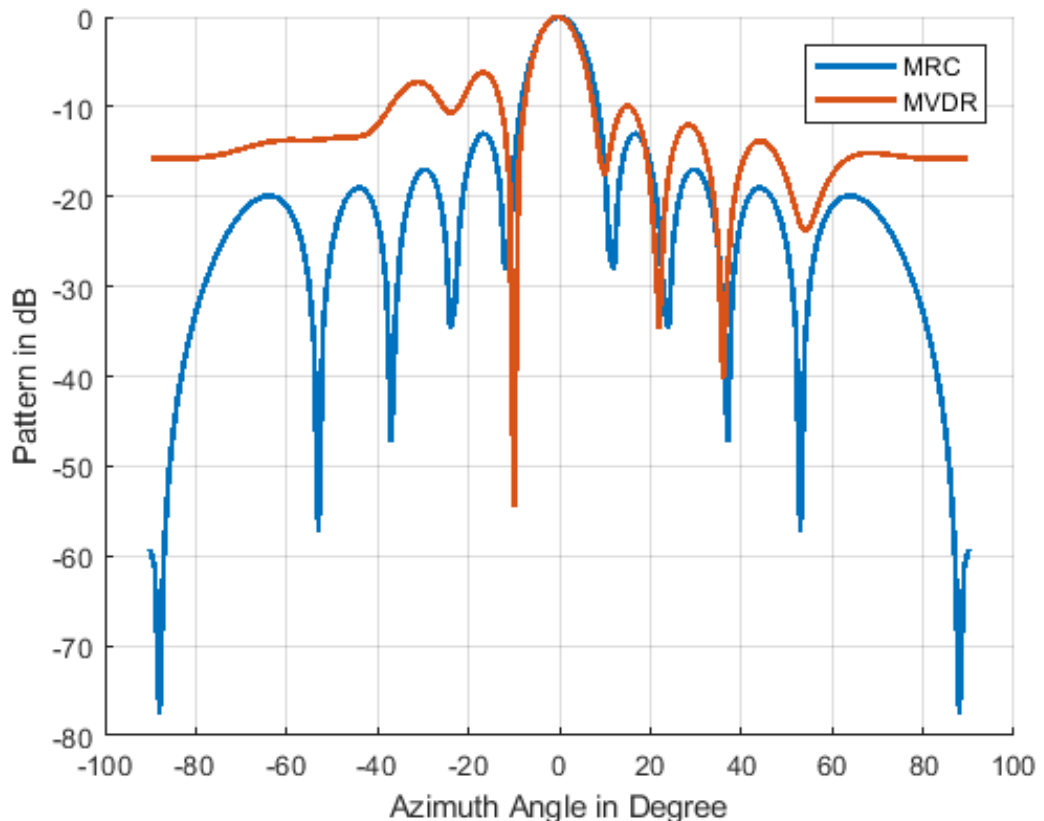


Figure 1.3: Beamformer Rejects Directional Interference

1.4 Motivation

There are many challenges caused by the rapid change of channel statistics like the reduced coherence time, outdated channel estimation and difficulty for beam alignment and management etc. as outlined in [31, 32, 33]. Task groups like New Radio Vehicle to Everything (NR-V2X) and 802.11bd are set up to optimize the existing technologies based on WiFi (802.11p) and Cellular Vehicle to Everything (C-V2X) for reliable wireless communication in high mobility scenarios. One of the main drivers for the enhancement is reducing the latency from up to 100ms to up to 3ms [34]. Various new techniques have been explored in the industry to cater to the fast varying channel. Midamble [33] instead of preamble is introduced in the data stream to estimate the channel more frequently. Predictor antenna concept is introduced to give real time Channel State Information at the Transmitter (CSIT) side that can achieve the delay in the order of 1ms [35] however it requires additional antenna to put in front of the receiving antenna.

But there are still problems that remain unsolved when the current beamforming technologies are directly applied to the transportation market as various field trial has indicated the severe performance drop due to the speed increase [23, 35]. The current WiFi performs poorly when beamforming is enabled in the scenarios where the vehicle is moving rapidly. Under this context, 802.11ac can perform even poorer than 802.11p [23]. It is expected since the intended usage for the beamforming in current WiFi is for scenarios where the movement is not at such high speed. As indicated in [36, p 207], when the multiple path characteristic changes rapidly, the adaptive scheme will fail. The WiFi in the current standard 802.11ac uses explicit beamforming, which requires a sounding process to probe the channel periodically. And the channel statistics needs to be feedback by the beamformee which consumes precious air time and limit the speed of beamforming adaptability.

To make the adaptive beamforming work smoothly as intended in high mobility scenarios, the Channel State Information (CSI) estimation or prediction is only part of the challenge. The other part of the challenge is to improve the beam pattern synthesis speed to match the channel statistics changing speed. This motivates us to investigate various parts of the adaptive beamformer to improve the robustness and beam pattern synthesis speed to match the channel changing speed.

1.5 Aims and Objectives

This project aims to enhance the current WiFi solution with a low-cost smart antenna system that utilizes beamforming technology to address the challenges in the targeted market. The objective of this project includes the following:

- To find ways to simulate the wireless channel with different Power Spectral Density (PSD) and Probability Density Function (PDF) that matches with V2X scenarios,
- To identify cost effective beamformer architecture that can form beam towards mobile clients in a rapidly changing channel condition,
- To investigate and find fast algorithms to form shaped beam pattern to provide robustness against rapid DOA change,
- To investigate and find fast algorithms to derive Blocking Matrix to prevent signal leak when channel is drastically changing.

1.6 Contributions

Faster algorithms to calculate the beamforming weight based on the changing DOA are proposed in this dissertation. It addresses the unique challenges due to the rapid change of DOA for adaptive beamforming brought by the proliferation of HSR and seamless wireless communication between infrastructure (roadside, trackside equipment) and the vehicles (train, car, boat etc.). Two strategies are adopted to address the challenges:

- The first one is to improve the weight calculation speed,
- The second way is to improve the estimation speed of the DOA by leveraging on the predefined constrained route for the transportation market.

Based on these concepts, various algorithms in beampattern generation and adaptive control algorithm are evaluated and investigated in this dissertation:

- A CVSS algorithm [37] for adjusting the weight with simplicity for implementation is proposed and evaluated,
- A Kalman filter based solution to fuse different sensor information to assist on the DOA change and tracking is investigated and proposed in Section 2.5.2,

- A fast algorithm for the generation of flat-top beam pattern that could be used in fixed beamforming path of GSC is detailed in Chapter 4.
- The adaptive beamforming algorithm using GSC architecture that could be used for fast DOA changing scenario is investigated in Chapter 5. A fast blocking matrix generation algorithm is proposed in Chapter 5.
- To further evaluate the effectiveness of beamforming performance, wireless channel simulation is needed. One of the challenging portions for wireless simulation is the coupling between Probability Density Function (PDF) and Power Spectral Density (PSD) for random variable. A simplified solution to simulate a Non-Gaussian wireless channel is proposed, proved and simulated for the effectiveness of the algorithm in Chapter 3.

The contribution of this dissertation can be summarized as the following three points.

- Firstly, by analyzing wireless communication channel in scenarios like the emerging HSR, the necessity for a fast, robust adaptive algorithm is identified.
- Secondly, by arranging the zero placement, a fast blocking matrix generation algorithm and a flat beam pattern generation algorithm for the fixed beamforming path are proposed. The main result of the two algorithms have been published in journal paper [1],[2]. The controlled simulation shows that the flat top beam pattern can be generated 380 times faster than iterative optimization method and blocking matrix can be generated 9 times faster than normal SVD method.
- Thirdly the algorithms to reduce the hardware complexity and to improve the tracking speed using CVSS and Kalman filter method has been investigated, and the result has been published in conference paper.

1.7 Dissertation Organization

The structure of this dissertation is as follows:

The first chapter gives a general introduction, motivation and contributions for the work. The second chapter reviews the existing beamforming algorithms under the context of the transportation market. A Kalman filter based solution for assisting the DOA estimation are also described in this chapter. As the wireless channel is a fundamental

component of wireless communication, Chapter 3 discusses wireless channel modelling, especially the random variable generation for wireless channel simulation where a Particle Swarm Optimization (PSO) based colored noise generation is proposed. Chapter 4 describes a fast algorithm to generate a flat top beam pattern which is critical for making the beamforming process robust. Chapter 5 details a developed algorithm to generate fast blocking matrix. The implementation of the adaptive beamforming algorithms for HSR scenario is investigated. In the last chapter, the conclusion and the future works are described.

Chapter 2

Beamformer Design in Wireless Communication System

2.1 Wireless Communication with Smart Antenna Architecture

The general architecture of a typical smart antenna wireless communication system is illustrated in Fig. 2.1. It contains 3 major parts:

- Wireless Channel \mathbf{H}
- Transmit Beamformer \mathbf{W}_t
- Receive Beamformer \mathbf{W}_r

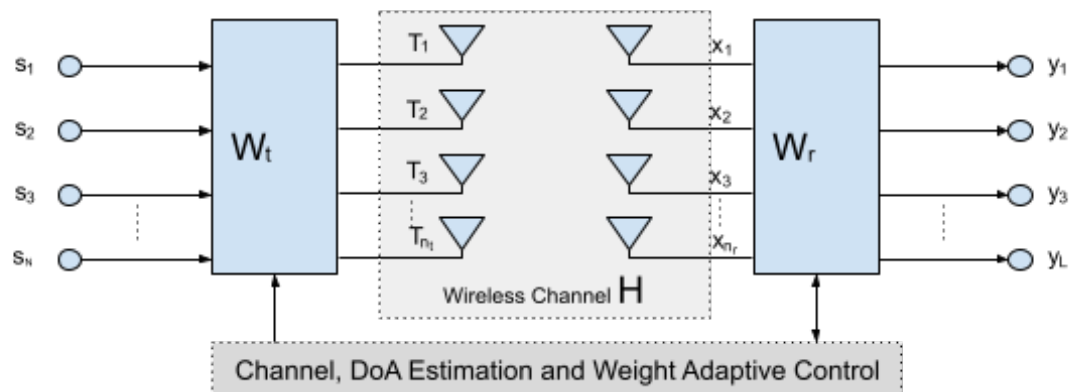


Figure 2.1: Smart Antenna System Architecture

The transmit beamformer $\mathbf{W}_t \in \mathbf{C}^{n_t \times N}$ maps N input signals streams to n_t individual transmit antenna with proper weight. The receive beamformer $\mathbf{W}_r \in \mathbf{C}^{L \times n_r}$ combines the n_r received signal with proper weight to output the recovered signal streams \mathbf{y} . The wireless channel $\mathbf{H} \in \mathbf{C}^{n_r \times n_t}$ is a n_r by n_t complex matrix where n_t and n_r is the number of transmit antenna and receive antenna respectively.

The received signal in receiver could be expressed with the following equation:

$$\mathbf{x} = \mathbf{H}\mathbf{W}_t\mathbf{s} + \mathbf{n} \quad (2.1)$$

where $\mathbf{x} = [x_1, x_2, \dots, x_{n_r}]^T$ is the received signals, \mathbf{H} is the communication channel transfer matrix, $\mathbf{s} = [s_1, s_2, s_3, \dots, s_N]^T$ is the input signal and \mathbf{n} is the additive noise.

The detected signal output from the receive beamformer could be expressed in equation 2.2

$$\mathbf{y} = \mathbf{W}_r\mathbf{x} \quad (2.2)$$

where $\mathbf{y} = [y_1, y_2, \dots, y_L]^T$ is the beamformer output estimation of signal \mathbf{s} , \mathbf{W}_r is the weight matrix for combine the received signals \mathbf{x} .

The wireless channel \mathbf{H} is investigated in chapter 3. This chapter gives a review of various existing beamforming algorithms to derive the transmit beamformer \mathbf{W}_t and \mathbf{W}_r with the focus on the receiving beamformer.

2.2 Beamformer Architecutre

In a typical beamformer scenario, the multiple antenna carries scaled copies of the same information data with the aim to enhance the quality of the received signal. In this case the source signal \mathbf{s} and the combined output \mathbf{y} are both single stream and the \mathbf{W}_t and \mathbf{W}_r then reduces to a vector instead of matrix, which is the focus of this thesis. For simplicity and clarity, we would use \mathbf{w} to represent the weight vector. Since many of the discussions for receive beamformer can be applied to transmit beamformer too, the number of AE (n_t, n_r) is then replaced with N to be consistent.

The core structure of a beamformer is an adaptive linear combiner of multiple inputs as illustrated in Fig. 2.2. As the most important element for adaptive signal processing [36], the weight of the beamformer can be adjusted according to some cost or performance function $J(\mathbf{w})$. For data independent beamformer, the linear combiner is a fixed structure, there is no weight adjustment algorithm involved. This type of fixed

beamformer will not adapt to environment change. For data dependent beamformer, a feedback loop is incorporated to adjust the weight for the linear combiner. It usually works in two modes: Training Mode with known desired signal d for reference and Decision Directed mode where the decoded signal is used as the desired signal d .

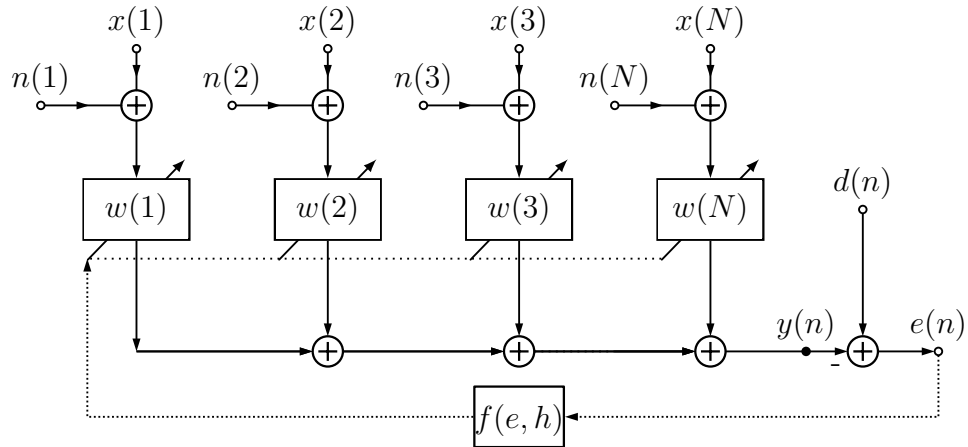


Figure 2.2: Adaptive Beamforming Architecture

It has an architecture that is similar to Finite Impulse Response (FIR) filter. One of the major differences is that FIR works as a temporal filter where the sampling is done in the time domain, while beamformer works as a spatial filter where the sampling is completed in the spatial domain by multiple sensor elements simultaneously.

The output $y(n)$ at time index n could be combined from input vector \mathbf{x} and additive noise vector \mathbf{n} . It could be expressed in vector form as [38, p. 66]:

$$\mathbf{y} = \mathbf{w}^H(\mathbf{x} + \mathbf{n}) \quad (2.3)$$

where the input vector \mathbf{x} could be further decomposed as signal s_0 and interference s_1, \dots, s_K [38, p. 67]:

$$\begin{bmatrix} x_1 \\ x_2 \\ \dots \\ x_N \end{bmatrix} = \begin{bmatrix} \alpha_1 & \alpha_2 & \dots & \alpha_K \end{bmatrix} \begin{bmatrix} s_0 \\ s_1 \\ \dots \\ s_K \end{bmatrix} \quad (2.4)$$

where $\alpha_1, \dots, \alpha_K$ indicates the steering vector for the incoming signal or interference. As illustrated in section (2.2.2), in narrow band scenario with N elements, the steering vector for signal or interference from incoming angle could be expressed as [39, p. 19]:

$$\alpha_i = [1 \quad e^{-j2\pi\xi_i} \quad e^{-j2\pi2\xi_i} \quad \dots \quad e^{-j2\pi(N-1)\xi_i}] \quad (2.5)$$

where ξ_i is the spatial frequency for incoming angle θ_i . There are two labeling method for the antenna elements which leads to different steering vector expression. The other way as defined in [40] is also popular. But in this dissertation, we adopt the same pattern used in [39, 41] as it gives a better match with the Z transform expression in FIR design.

The combined output is then compared with desired input $d(n)$ to derive an error signal. The error signal is then transformed through a cost function $f(e, h)$ to drive the weight vector to converge to the optimum value according to some predefined criteria.

2.2.1 Analogy to Finite Impulse Response (FIR) Filter

As illustrated in Fig. 2.3, the delayed replicas of the same input x is linearly combined to get an estimated output y . The desired signal is then compared to the estimated output y to an error signal e . Through an adaptive algorithm $f(e, h)$, the filter coefficients are updated to drive the error to a minimum following some cost function.

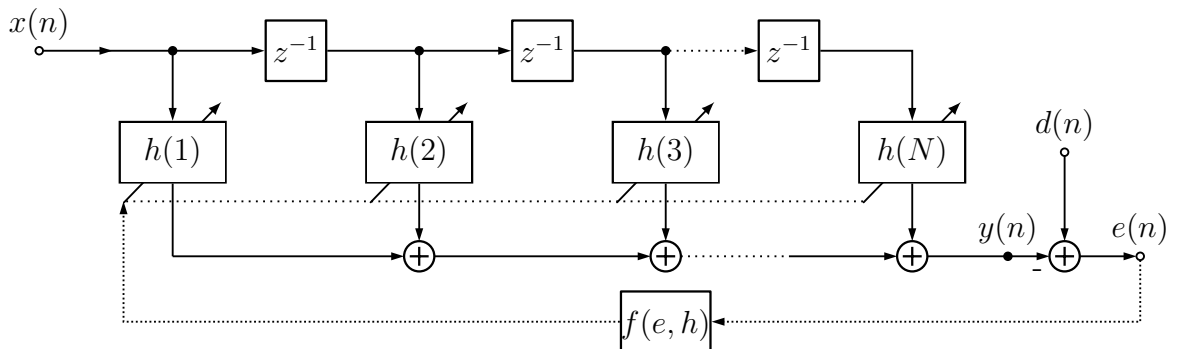


Figure 2.3: Adaptive Temporal Filter Architecture

Comparing Fig. 2.3 and Fig. 2.2, it is found that both are using a linear combiner structure. The difference is just the input to the linear combiner. Due to these structure similarity, many research results in the FIR field like LMS, Normalized LMS (NLMS), Recursive Least Square (RLS) could be directly applied in adaptive beamformer design. The Nyquist threshold [42] is required to both temporal and spatial filter to avoid aliasing effect. In FIR, the sampling frequency needs to be at least twice the highest frequency of the input signal while in beamformer the interval between AE needs to be less than the signal half wave length.

2.2.2 Spatial Sampling of Beamformer

The spatial information added to the signal processing of received signal brings some unique characteristic to beamformer. On top of the time and frequency dimensions of the wireless channel, the additional spatial dimension makes advanced signal processing techniques like DOA estimation and interference nulling in beamformer and MIMO possible. That means also when doing the wireless channel simulation, the model needs to cater for an extra spatial dimension of signal distribution along different directions.

Unlike the temporal filter where the sampling is always uniform, for the sampling in spatial, it usually requires some calibration to get spatial uniform sampling. This creates a well known DOA mismatch problem in beamformer. In distributed beamforming or coordinated beamforming system [43], the location can be totally random. In this dissertation, we focus on the ULA for the clarity and practical usage scenario. But the signal source can still be moving randomly. So the signal spatial signature could be modelled as fixed vector with known or unknown direction in the signal space, or it can be a random vector lies inside a defined signal subspace [44]. Many Robust Adaptive Beamformer (RAB) algorithms are proposed in the literature to overcome the mismatch problem which causes severe signal cancelling. And when applying beamforming technology in high mobility scenarios in transportation market, the mismatch becomes more severe due to the rapid change of DOA and channel characteristics. In chapters 3,4 our proposed method for improving the calculation speed is discussed in more detail.

Fig. 2.4 shows a typical ULA with the antenna elements are placed with distance d apart. Signals impinging from different DOA will create different delay on the receiving antenna elements. The received signal $x_i(t)$ on the i^{th} element from a signal $s_\theta(t)$ incident from an angle θ could be expressed as

$$\begin{aligned} x_i(t) &= s_\theta(t) e^{-j \frac{2\pi d \sin(\theta)}{\lambda} (i-1)} \\ &= s_\theta(t) e^{-j 2\pi (i-1) \xi} \end{aligned} \quad (2.6)$$

where λ indicates the wavelength, and $\xi = 2\pi \frac{d \sin(\theta)}{\lambda}$ is the spatial frequency.

The beamformer output $y(t)$ in this narrow band model could then be expressed as

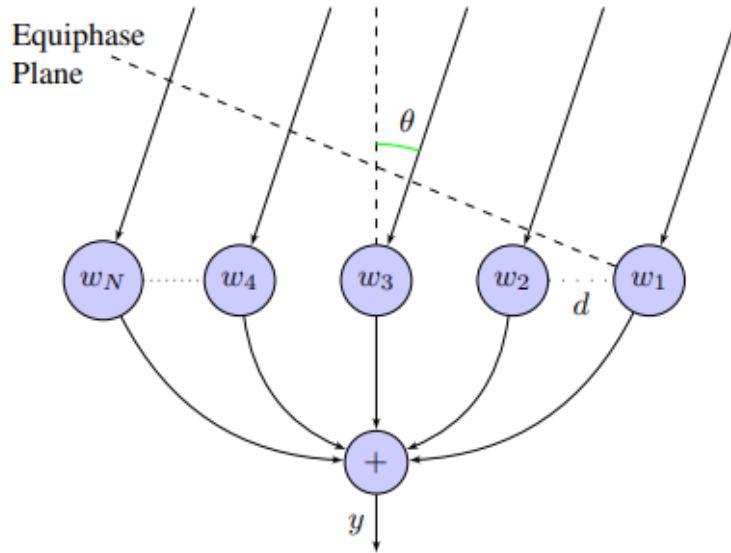


Figure 2.4: Beamformer Model of Received Signal

[39, p. 4]

$$\begin{aligned}
 y(t) &= \sum_{i=1}^N w_i x_i(t) \\
 &= s_\theta(t) \sum_{i=1}^N w_i e^{-j(i-1)\xi}
 \end{aligned} \tag{2.7}$$

So the spatial frequency response could be defined as

$$H(\xi) = \sum_{i=1}^N w_i e^{-j(i-1)\xi} \tag{2.8}$$

It could also be written in the \$Z\$ transform format [45, p. 109] as

$$H(z) = \sum_{i=1}^N w_i z^{-(i-1)} \tag{2.9}$$

It is clear from (2.9) that the weight vector and spatial frequency can be mapped through \$Z\$ transform or Fourier Transform. This can be exemplified through a simple fixed beamformer design in the spatial frequency domain where the beamformer needs to form beam towards the broadside of the array which corresponds to \$\theta = 0\$. For a pencil beam towards a single DOA \$\theta\$, it corresponds to a single spatial frequency impulse \$\xi = 2\pi \frac{d \sin(\theta)}{\lambda}\$. According to Fourier Transform property, the corresponding weight would need to be infinite long. But in practice, the number of AE is always limited. So a window method could be used to reduce the infinite number of AE

to a practical value. And unavoidably, the applied window will produce a widening effect of the final generated beam pattern. As well known in FIR theory, the simplest rectangular window gives the narrowest widening effect while giving long Gibbs effect of rippling in the stop band.

When a rectangular window is applied to an infinitely long weight vector, (2.8) can be used to find the effect of N on the shape of the resulting beam pattern. By normalizing w_i to 1,

$$\begin{aligned} H(\xi) &= 1 + e^{-j\xi} + \dots + e^{-j(N-1)\xi} \\ &= \frac{1 - e^{-jN\xi}}{1 - e^{-j\xi}} \\ &= e^{-j\frac{(N-1)\xi}{2}} \cdot \frac{\sin(\frac{N\xi}{2})}{\sin(\frac{\xi}{2})} \end{aligned} \quad (2.10)$$

The amplitude is simply:

$$|H(\xi)| = \left| \frac{\sin(\frac{N\xi}{2})}{\sin(\frac{\xi}{2})} \right| \quad (2.11)$$

From (2.11), it is clear that the null occurs at:

$$\xi_{null} = \frac{2k\pi}{N} \quad (2.12)$$

where $k = \pm 1, \pm 2, \dots$ and the first null to null beamwidth is $\frac{4\pi}{N}$. For the half wavelength distance apart array, the angle between the first null would be $\arcsin(\frac{4}{N})$. The effect is illustrated in Fig. 2.5.

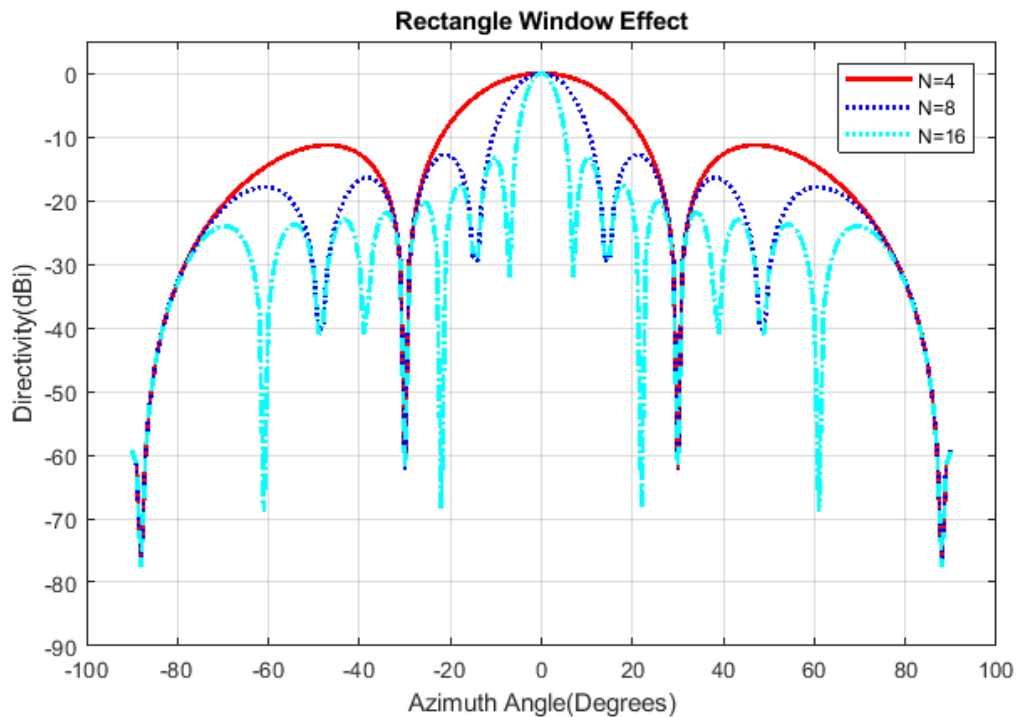


Figure 2.5: Rectangular Window Effect

It is clear that the larger the number of AE, the narrower the beamwidth. But Sidelobe Level (SLL) will not be decreased. To reduce the SLL, various window methods like Hamming, Hanning, Kaiser etc. [46, p 351] could be used to smooth out the transition. The various window method and other beamforming algorithms will be reviewed in the next section.

2.3 Beamforming Algorithm Review

There are different ways to classify beamformers. Based on the processing in analog or digital domain, there are digital beamformer, analog beamformer and hybrid. Based on whether the beampattern can adapt to environmental change, there are data dependent adaptive beamformer and data independent fixed beamformers. Based on the signal bandwidth there are narrow band beamformers and broadband beamformers. Based on whether the explicit signal information like direction or pilot signal training is required, there are blind beamformers and non-blind beamformers. Some of the well known and popular algorithms are reviewed in this section. The proposed algorithm is based on the existing method and improves the speed and robustness for high speed transportation market will be detailed in chapter 4.

2.3.1 Window Method

Window method is the most straightforward way of doing data independent filtering for FIR and beamforming. It is a two steps algorithm that consists of:

- Approximate the filter or beampattern through an ideal filter with infinitely long weight vector,
- Apply a window function to truncate and smooth out the transition to a finite length of weight vector.

As an example, a 30° wide flat top main beam towards the broadside of a ULA array with 9 AE separated half wavelength apart could be designed from the ideal spatial frequency domain as:

$$H(\xi) = \begin{cases} 1 & \theta \in [-30^\circ, 30^\circ] \\ 0 & \theta \in [-90^\circ, 30^\circ) \cup (30^\circ, 90^\circ] \end{cases} \quad (2.13)$$

The infinitely long weight vector could be derived using the Inverse Fourier Transform as:

$$w_i = \frac{\omega_c \sin(\omega_c i)}{\pi \omega_c i} \quad (2.14)$$

where $\omega_c = \pi \sin(\theta)|_{\theta=15^\circ}$.

Various window functions and its characteristics are summarized in [47]. Rectangular window and Bartlett window are easy for implementation, but it has a long transition band and high SLL. Other raised cosine based window function like Hanning and Hamming window have higher suppression of SLL. But it has rather fixed SLL and transition band. In contrast, the Kaiser window is more flexible and can make some trade-off between bandwidth and SLL. But it requires a Bessel function calculation which is more complex and hard to implement in hardware. Some of the widely used window algorithms are illustrated below in Fig. 2.6:

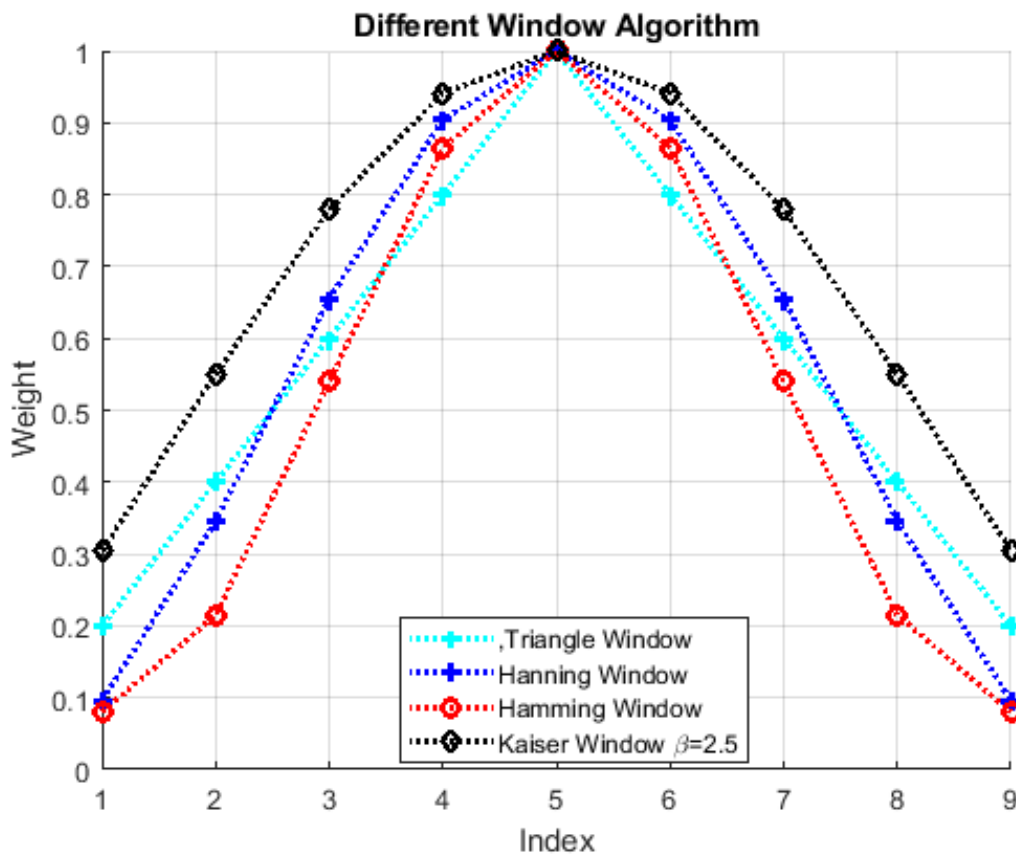


Figure 2.6: Window Shape for Typical Window Algorithms

It is clear from Fig. 2.6 that the window will smooth out the transition for the weight vector. This avoids the abrupt truncation of the filter weights and thus reduce the ring effect in the transformed domain. It plays an important role in beamformer design to control the SLL due to the limited number of taps.

Since the window function is symmetric, it can be fully characterized by half of its value. The function to get the window value could be found in [19, p 62]. The effect of applying the various window to the ideal weight vector is demonstrated in Fig. 2.7 where a nine elements ULA is used for the simulation.

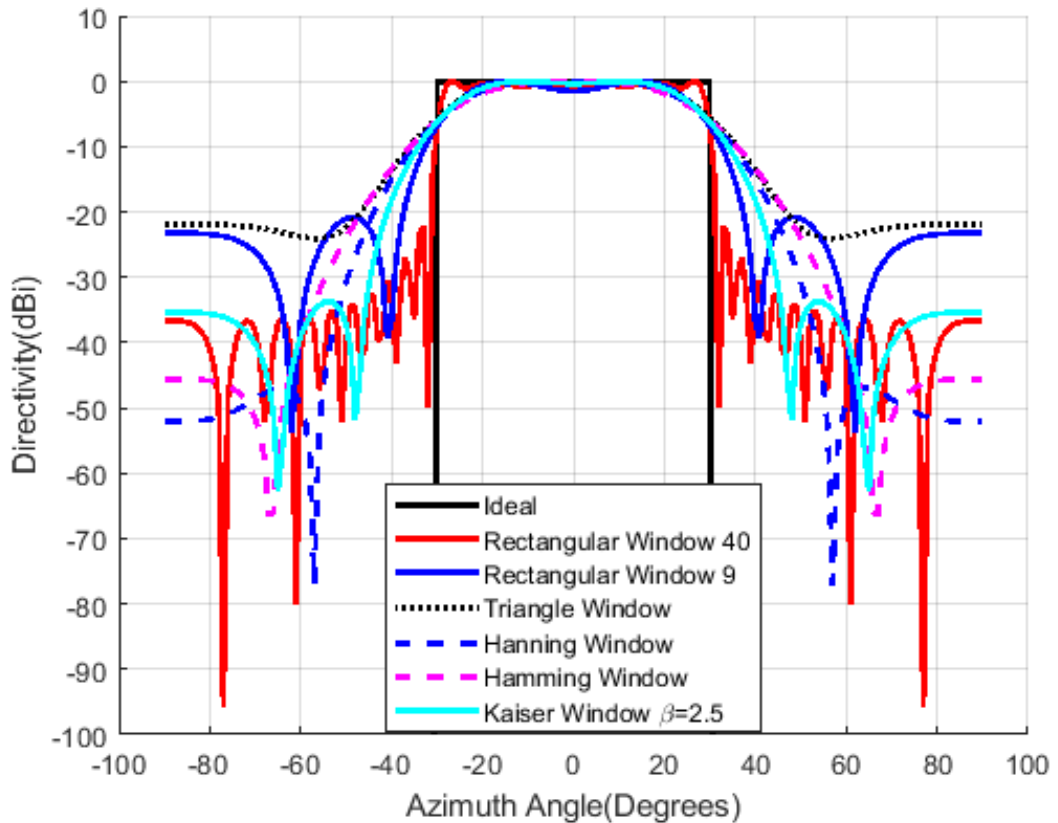


Figure 2.7: Various Window Effect on Ideal Beamformer

It is clear that the rectangular window gives the narrowest main lobe which makes the beam pattern closest to the ideal beamformer. But the SLL is just around -22dB and almost stays unchanged when the rectangular window size changes from 9 to 40, although the null to null width is reduced with the rectangular size increase. The Bartlett (triangle) window has an even longer transition band with a similar level of SLL which is around -22dB too. Hanning and Hamming window gives much better suppression of around -45dB and -51dB respectively, yet resulted in a much wider null bandwidth which has the first null at 57° compared to the 40° for the rectangular window with the same length of 9 elements. The Kaiser window has a SLL of around -35dB while maintaining a relatively narrow transition band which has the first null at 47° . So it can make some trade-off for the transition band and SLL.

One observation for the effect of window is that the sidelobes further away from the mainlobe usually have higher attenuation. This comes at the price of making the first few sidelobes with lower attenuation. So intuitively, when the sidelobes have equal attenuation, the worst sidelobe level would also be the minimum. This is actually achieved as Chebyshev window, which has an optimum performance [48, p 1144] in the sense that with a given bandwidth, it achieves the best attenuation and when the

attenuation is fixed, it has the narrowest beamwidth. The narrower beamwidth will allow the beam pattern to focus on the DOA. The higher attenuation of SLL will give maximum attenuation for other look directions. So a best candidate would give both the narrowest beamwidth and highest attenuation for the SLL. Chebyshev is the one that has this property as indicated in [48, p 1144].

In this research, we adapt the Chebyshev window to make a robust beamformer. Some basic mathematic discussion about the Chebyshev window or in general the approximation problem are discussed in the next section.

2.3.2 Approximation Problem and Performance Metric

Windows methods, in general, are not flexible [49] except for Kaiser and Chebyshev window method. The transition band and attenuation in stop band depends on the filter order or number of AE. The window method can be generalized to an approximation problem where the desired ideal frequency domain response is approximated by a linear combination of a finite set of basis functions [50]. It means to find a parameterized estimation function $\hat{h}(x, \theta)$ with minimum distance to the original function:

$$\theta = \arg \min_{\theta} L(h(x), \hat{h}(x, \theta)) \quad (2.15)$$

where the $L(\cdot)$ is the distance function between two function, $h(x)$ is the ideal response and $\hat{h}(x, \theta)$ is the approximation function characterized by parameter θ .

The similarity of the ideal response and the approximated response could be measured using Minkowski Distance [51]. In discrete version, for two vectors h and \hat{h} , the p norm Minkowski distance is defined as

$$L_p = \sum_i (|h_i - \hat{h}_i|^p)^{\frac{1}{p}} \quad (2.16)$$

where p is the order of the norm and h_i, \hat{h}_i is the i^{th} component of the vector h and \hat{h} respectively. This framework can be applied to Best Linear Unbiased Estimator (BLUE), Adaptive Filter etc. In this research, the optimum weight is the parameter to be searched for minimizing a performance metric.

The commonly used metric to measure distances are Manhattan distance L_1 , Eu-

clidean distance L_2 and Chebyshev distance L_∞ as

$$L_1 = \sum_i |h_i - \hat{h}_i| \quad (2.17)$$

$$L_2 = \left(\sum_i |h_i - \hat{h}_i|^2 \right)^{\frac{1}{2}} \quad (2.18)$$

$$L_\infty = \lim_{p \rightarrow \infty} \left(\sum_i |h_i - \hat{h}_i|^p \right)^{\frac{1}{p}} = \max_i |h_i - \hat{h}_i| \quad (2.19)$$

The widely adopted performance criteria of Least Square (LS) is based on Euclidean distance L_2 . It has an intuitive geometric explanation that gives the orthogonal principle based solution on optimum estimation of a vector in a LS sense by projecting the vector to a sample space. This leads to the popular LS method [52] and many other adaptive filter algorithms includes RLS, Affine Projection Algorithm (APA).

When the input signal is modelled as a Random Process, another L_2 based performance criteria Mean Square Error (MSE) is widely used. This leads to many well known algorithms like LMS and many of its variants.

One of the widely used algorithm Minimum Maximum (MinMax) [53, 54] in Linear Programming (LP) uses Chebyshev distance L_∞ to gauge the maximum error in each step of the optimization process so that the worst case SLL is reduced to the minimum. As proved in [50], the solution will converge to the unique Chebyshev polynomial function, which has equal ripple and the minimum SLL in stop band. The Chebyshev polynomial in the first kind is defined as [55, p 14]:

$$T_n(x) = \cos(n \cdot \arccos(x)) \quad (2.20)$$

In beamformer design, the x is the scaled version of the spatial frequency. The scaled version of Chebyshev polynomial could be defined as:

$$T_n(x) = \cos(n \cdot \arccos(\alpha \cdot x)) \quad (2.21)$$

where the α is the scaling factor which can be used to control the beamwidth of the derived pattern and x is set to $\sin(\theta)$. The effect of order n and scaling factor α is illustrated in Fig. 2.8.

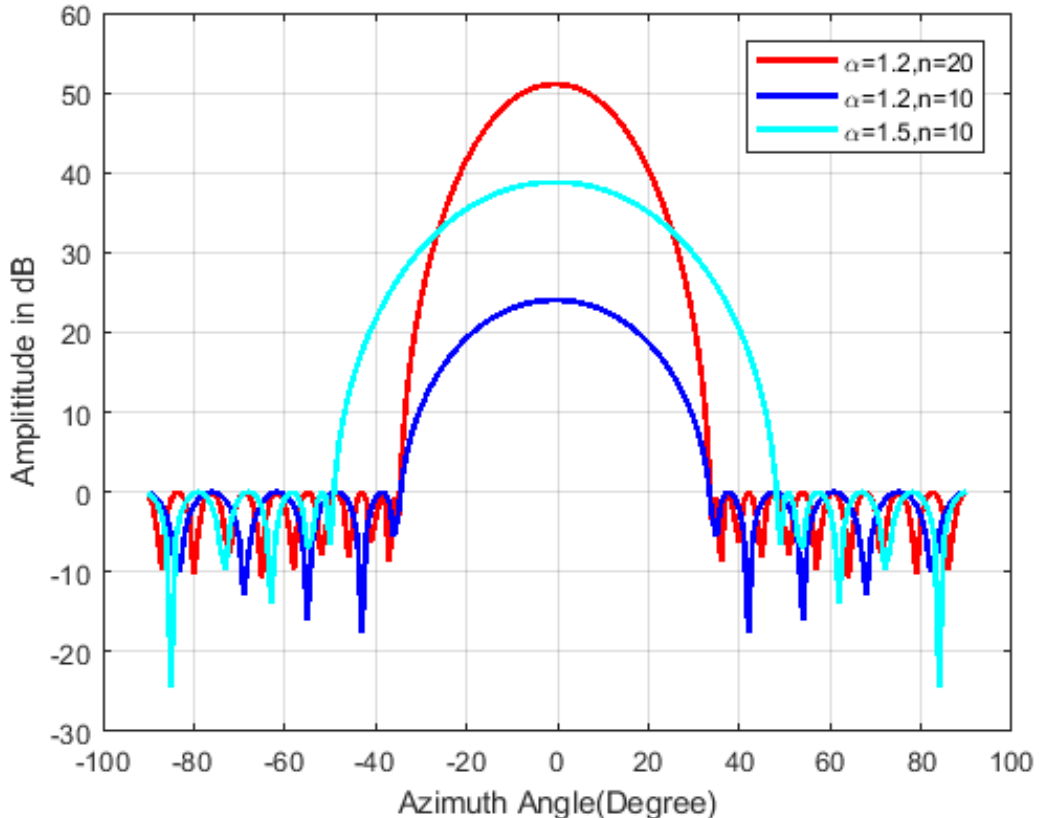


Figure 2.8: Chebyshev Polynomial Controlled by Scaling Factor α and Order n

It is clear that the scaling factor α controls the shape of the pattern as shown in Fig. 2.8. The first null width is fixed around 37° when the order increased from 10 to 20. But when the order is fixed to 10, the scaling factor is the single parameter that affects the attenuation and bandwidth. The higher attenuation of around 40dB at $\alpha = 1.5$ compared with 24dB at $\alpha = 1.2$ comes at the price of a widened main lobe.

2.3.3 Remez Algorithm and Parks-McClellan Method

Following the framework of approximation problem, the ideal filter response can be approximated by minimizing the maximum error compared with the ideal filter over a regulated band using a limited number of elements. In beamformer, that is to minimize the maximum error over the visible regions.

$$\mathbf{w} = \arg \min_{\mathbf{w}} \max |H(\xi) - \hat{H}(\xi, \mathbf{w})| \quad (2.22)$$

In this way, the error between desired and synthesized response is spread evenly across the bands. And this leads to a equal ripple Chebyshev filter. This optimization in the minimax sense is resulted from Alternation Theorem [56] which states that when

the error at the $N + 2$ extreme point has equal magnitude and alternate sign, the approximation error is minimized where N is the number of elements for a low pass filter. Effectively, it means an equal ripple design. Parks and McClellan proposed an iterative method to design this equal ripple filter in [57]. But this method only applies to linear phase filter where it has symmetric structure. Consequently, the frequency response could be expressed as linear combination of cosine function [57]:

$$\hat{H}(\xi) = \sum_{n=0}^M \mathbf{w}(n) \cos(n \cdot \xi) \quad (2.23)$$

As an iterative process, it first assumes the initial $M + 2$ extreme point, which results in the same alternate signed error δ . The $M + 2$ point then are used to build $M + 2$ equation, which can be arranged as below [58, p. 97]:

$$\begin{bmatrix} 1 & \cos(\xi_0) & \dots & \cos(\xi_0) & (-1)^0 \\ 1 & \cos(\xi_1) & \dots & \cos(\xi_1) & (-1)^1 \\ \dots & \dots & \dots & \dots & (-1)^i \\ 1 & \cos(\xi_M) & \dots & \cos(\xi_M) & (-1)^{M+1} \end{bmatrix} \begin{bmatrix} w_0 \\ w_1 \\ \dots \\ w_M \\ \delta \end{bmatrix} = \begin{bmatrix} H(\xi_0) \\ H(\xi_1) \\ \dots \\ H(\xi_M) \\ H(\xi_{M+1}) \end{bmatrix} \quad (2.24)$$

With $M + 2$ system equation for $M + 2$ unknown variables, (2.23) gives a unique solution which identifies $\hat{H}(\xi)$. Then the Chebyshev distance could be calculated between the desired response $H(\xi)$ and the first estimation of $\hat{H}(\xi)$, which gives a new set of extreme frequency points. So iteratively, a new set of \mathbf{w} and δ could be calculated, and the steps repeat until the error is minimized or the number of iteration is reached. Although the Remez algorithm based Parks-McClellan method is efficient and converge rapidly, it is limited to linear phase scenario. But in beamformer scenarios, the number of elements is fixed and can't be expanded easily as in temporal filter scenario. The large number of elements from the requirement of linear phase makes them not attractive in beamformer scenario. In [59], the author extends the Remez algorithm to complex domain. But it still requires an iterative process to converge to the equal ripple Chebyshev solution.

2.3.4 Frequency Sampling Method and Woodward Lawson

Woodward Lawson algorithm [60] is the Frequency Sampling Method in FIR design applied in beamforming synthesis. The synthesized beam can be considered to be the superposition of a composing function in the form of $\text{sinc}(x)$ function. In this way,

the response at the sampling point can be exactly matched, although the rest of point have no control. But it has an advantage of synthesis of arbitrary beam pattern.

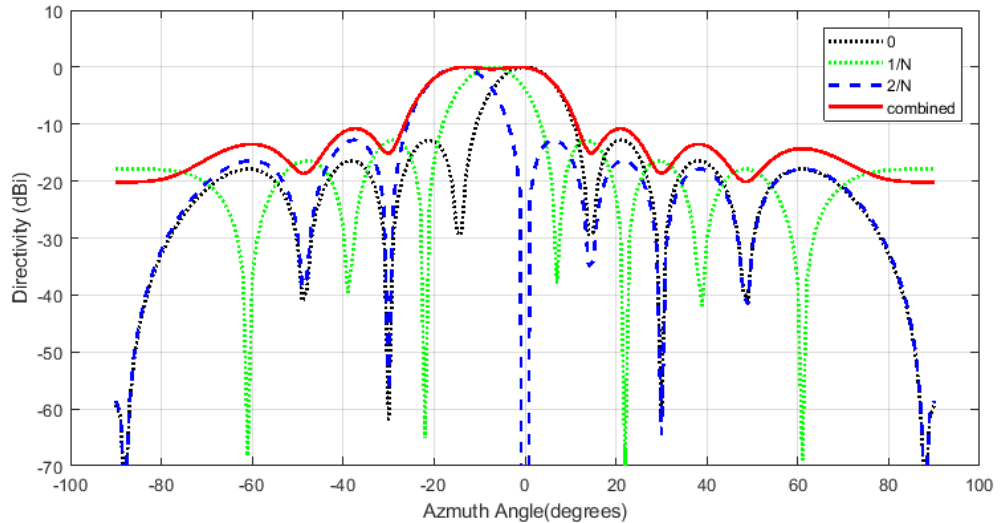


Figure 2.9: Woodward Lawson Synthesized Pattern with 3 Sampling Point

2.3.5 Minimum Variance Distortionless Response

The above beamforming algorithm produces a fixed pattern efficiently. But it can't adapt to environmental change which is quite common in transportation market where the source of interference can vary dramatically. Capon [61] proposed the MVDR beamformer which is also called Capon beamformer. It can adjust the beamformer weight adaptively when the interference characteristics changed so that it still maintains a high SINR by creating null automatically in the strong interference direction while allowing the signal in the interested direction pass without distortion.

MVDR beamformer belongs to a category of beamformer which aims to optimize the output SINR. With the assumption that signal is statistically independent of interference and noise, from (2.3), the output power for a given weight vector could be derived as:

$$P_y = \sigma_0^2 \mathbf{w}^H \boldsymbol{\alpha}_0 \boldsymbol{\alpha}_0^H \mathbf{w} + \mathbf{w}^H \left(\sum_{k=1}^K \sigma_k^2 \boldsymbol{\alpha}_k \boldsymbol{\alpha}_k^H \right) \mathbf{w} + \sigma_v^2 \mathbf{w}^H \mathbf{n} \mathbf{n}^H \mathbf{w} \quad (2.25)$$

where $\sigma_0^2, \sigma_k^2, \sigma_n^2$ is the variance of signal, interference and additive white noise respectively. With the assumption of independent characteristics between signal, interference and noise, the power of output signal component, interference component and noise could be separated as:

$$P_s = \sigma_0^2 \mathbf{w}^H \boldsymbol{\alpha}_0 \boldsymbol{\alpha}_0^H \mathbf{w} \quad (2.26)$$

$$P_i = \mathbf{w}^H \left(\sum_{k=1}^K \sigma_k^2 \boldsymbol{\alpha}_k \boldsymbol{\alpha}_k^H \right) \mathbf{w} \quad (2.27)$$

$$P_n = \mathbf{w}^H \mathbf{n} \mathbf{n}^H \mathbf{w} \quad (2.28)$$

The power of interference and noise could be combined for SINR calculation as:

$$P_{i+n} = \mathbf{w}^H \mathbf{R}_{i+n} \mathbf{w} \quad (2.29)$$

where $\mathbf{R}_{i+n} = \sum_{k=1}^K (\sigma_k^2 \boldsymbol{\alpha}_k \boldsymbol{\alpha}_k^H) + \mathbf{n} \mathbf{n}^H$ is the combined interference and noise covariance matrix. The SINR could be expressed as:

$$SINR = \frac{P_s}{P_{i+n}} = \frac{\sigma_0^2 |\mathbf{w}^H \boldsymbol{\alpha}_0|^2}{\mathbf{w}^H \mathbf{R}_{i+n} \mathbf{w}} \quad (2.30)$$

The problem statement for a optimum beamformer in the maximum SINR sense could be described as:

$$\mathbf{w} = \arg \max_{\mathbf{w}} \frac{P_s}{P_{i+n}} \quad (2.31)$$

To find the maximum value of (2.30), the \mathbf{R}_{i+n} could be decomposed using Cholesky factorization [62]:

$$\mathbf{R}_{i+n} = \mathbf{L} \mathbf{L}^H \quad (2.32)$$

By using the transformed $\tilde{\mathbf{w}} = \mathbf{L}^H \mathbf{w}$, (2.30) could be simplified as:

$$\frac{P_s}{P_{i+n}} = \frac{\sigma_0^2 |\tilde{\mathbf{w}}^H \mathbf{L}^{-1} \boldsymbol{\alpha}_0|^2}{\tilde{\mathbf{w}}^H \tilde{\mathbf{w}}} \quad (2.33)$$

From Cauchy-Schwartz theorem [63, p 100],

$$|\langle u, v \rangle|^2 \leq \langle u, u \rangle \cdot \langle v, v \rangle \quad (2.34)$$

where $\langle u, v \rangle$ indicates the inner product of any two vector. The inner product of two vectors get the maximum value when the two vectors are in parallel. Apply this rule to (2.30), it is clear that the SINR get its maximum value when $\tilde{\mathbf{w}}$ is in parallel to $\mathbf{L}^{-1} \boldsymbol{\alpha}_0$, i.e.:

$$\tilde{\mathbf{w}}_o = \alpha \mathbf{L}^{-1} \boldsymbol{\alpha}_0 \quad (2.35)$$

So the optimum of \mathbf{w} in the SINR sense is

$$\begin{aligned}\mathbf{w}_o &= \alpha(LL^H)^{-1}\boldsymbol{\alpha}_0 \\ &= \alpha\mathbf{R}_{i+n}^{-1}\boldsymbol{\alpha}_0\end{aligned}\quad (2.36)$$

The scale factor α could be derived using the constraints of distortionless in the signal direction. To get the distortionless response for signal s_0 , the optimum value of \mathbf{w} also needs to satisfy:

$$\mathbf{w}_0^H \boldsymbol{\alpha}_0 = 1 \quad (2.37)$$

So that the scale factor for MVDR can be set as:

$$\alpha = \frac{1}{\boldsymbol{\alpha}_0^H \mathbf{R}_{i+n}^{-1} \boldsymbol{\alpha}_0} \quad (2.38)$$

The optimum value for MVDR is then

$$\mathbf{w}_o = \frac{\mathbf{R}_{i+n}^{-1} \boldsymbol{\alpha}_0}{\boldsymbol{\alpha}_0^H \mathbf{R}_{i+n}^{-1} \boldsymbol{\alpha}_0} \quad (2.39)$$

The MVDR beamformer could also be derived from the direct definition as

$$\begin{aligned}\mathbf{w}_o &= \arg \min_{\mathbf{w}} \mathbf{w}^H \mathbf{R}_{i+n} \mathbf{w} \\ &\text{subject to } \mathbf{w}^H \boldsymbol{\alpha}_0 = 1\end{aligned}\quad (2.40)$$

Using Lagrange Multiplier method [63, p 763] we can find the optimum vector \mathbf{w} . The augmented Lagrange function could be defined as:

$$\mathcal{L}(\mathbf{w}, \lambda) = \mathbf{w}^H \mathbf{R}_{i+n} \mathbf{w} + \lambda(\mathbf{w}^H \boldsymbol{\alpha}_0 - 1) \quad (2.41)$$

The gradient of $\mathcal{L}(\mathbf{w}, \lambda)$ respect to \mathbf{w}^H , λ will be:

$$\nabla_{\mathbf{w}^H} \mathcal{L}(\mathbf{w}, \lambda) = \mathbf{R}_{i+n} \mathbf{w} + \lambda \boldsymbol{\alpha}_0 \quad (2.42)$$

$$\nabla_{\lambda} \mathcal{L}(\mathbf{w}, \lambda) = \mathbf{w}^H \boldsymbol{\alpha}_0 - 1 \quad (2.43)$$

By setting the gradients to 0, we can get the optimum of beamformer \mathbf{w} as:

$$\mathbf{w}_o = -\lambda \mathbf{R}_{i+n}^{-1} \boldsymbol{\alpha}_0 \quad (2.44)$$

Using the constraints from (2.43), the Lagrange multiplier can be derived:

$$\lambda = -\frac{1}{\boldsymbol{\alpha}_0^H \mathbf{R}_{i+n}^{-1} \boldsymbol{\alpha}_0} \quad (2.45)$$

So we get the same result as (2.39) which uses the maximum SINR criteria. This shows that MVDR beamformer can really get the maximum SINR. In an interference free scenario, there is only spatial white noise that corrupts the received signal, and the MVDR will be the same as a conventional spatial matched filter to $\boldsymbol{\alpha}_0$.

In practice, it is very difficult to get the covariance of interference and noise matrix due to its unknown and dynamic nature. So instead of minimizing the interference and noise, it is much easier to minimize the received total power which includes both the signal, interference and noise. This is sometimes named as Minimum Power Distortionless Response (MPDR) and in many literature, it is named also as MVDR. The problem statement for MPDR is then

$$\begin{aligned} \mathbf{w}_o &= \arg \min_{\mathbf{w}} \mathbf{w}^H \mathbf{R}_x \mathbf{w} \\ &\text{subject to } \mathbf{w}^H \boldsymbol{\alpha}_0 = 1 \end{aligned} \quad (2.46)$$

Following the same procedure, optimum beamformer could then derived as:

$$\mathbf{w}_o = \frac{\mathbf{R}_x^{-1} \boldsymbol{\alpha}_0}{\boldsymbol{\alpha}_0^H \mathbf{R}_x^{-1} \boldsymbol{\alpha}_0} \quad (2.47)$$

When the incident angle of the signal of interest is estimated accurately and no signal leak into the interference region, MPDR has the same performance as MVDR. Since the power of signal is preserved by the distortionless constraint, the minimization of the power is equivalent to the minimization of interference and noise power. Due to the high resolution of MVDR, slight error in the Signal of Interest (SOI) estimation will cause severe signal cancellation, especially when the signal strength is strong [64]. In practice, the estimation error of SOI is normally not accurate. To mitigate the signal cancellation problem, many RAB are investigated in the literature. The basic concept is to reduce the sensitivity in the region of uncertainty by broadening the region. It includes the Derivative Constraint [65] to broaden the main beam, Diagonal Loading [66] to add a diagonal matrix to the covariance matrix etc. which is equivalent to inject virtual spatial white noise to the system so that its sensitivity is reduced. But how much noise needs to be injected is a challenging task.

2.3.6 Linear Constraint Minimum Variance

Linear Constraint Minimum Variance (LCMV) [67] is a generalized version of MVDR. Instead of having just one constraint on the main lobe, LCMV allows multiple constraints from different angles. By adding constraints to regions of known uncertainty, the synthesized beampattern allows some degrees of the inaccuracy of the DOA. The problem statement for LCMV is summarized as [67]:

$$\begin{aligned} \mathbf{w}_o &= \arg \min_{\mathbf{w}} \mathbf{w}^H \mathbf{R}_x \mathbf{w} \\ &\text{subject to } \mathbf{w}^H \mathbf{C} = \mathbf{f}^H \end{aligned} \quad (2.48)$$

where \mathbf{C} is the M by J constrain matrix for a M elements array with J constraints, \mathbf{f} is the desired response at the each of the constraint angle, \mathbf{w} is the weight vector and $[\cdot]^H$ indicates the conjugate transpose operator. In general, the extreme point of function $f(\cdot)$ with the constraints $g(\cdot) = c$ occurs at the tangent point of the two curves, i.e. their gradients needs to be anti-parallel at the extreme point. So the gradient of the combined output $J(\mathbf{w}) = \mathbf{w}^H \mathbf{R}_x \mathbf{w}$ and the constraint function $\mathbf{w}^H \mathbf{C}$ can be related through:

$$\mathbf{R}_x \mathbf{w}_o = -\mathbf{C} \lambda \quad (2.49)$$

where the λ is the Lagrange multiplier and \mathbf{w}_o is the optimum weight vector. Its value can be derived through the constraints equation. So the optimum solution for LCMV is [67]:

$$\mathbf{w}_o = \mathbf{R}_x^{-1} \mathbf{C} (\mathbf{C}^H \mathbf{R}_x^{-1} \mathbf{C})^{-1} \mathbf{f} \quad (2.50)$$

Since LCMV also uses the covariance of the received signal instead of the interference and noise, it has the same issue as MPDR of the signal cancellation. But since LCMV supports multiple constraints, it can achieve robustness by putting multiple constraints around the estimated DOA to increase the beamwidth of the mainlobe. One novel usage of the multiple constraints is investigated in [44] where the signal spatial signature is classified as deterministic and random vector in the signal subspace. The signal covariance matrix \mathbf{R}_s then can be rank 1 for signals from deterministic DOA or multiple rank for signals from random DOA. By putting constraints on the eigen-vectors of the signal subspace, it can mitigate the signal cancellation. However LCMV doesn't have a good control over synthesized beampattern as it doesn't have a well defined shape for the mainlobe and usually high sidelobe level as reported in [68]. To address this issue,

a flat top beamformer [2] in the fixed path of GSC is proposed in this dissertation. The details of the proposed algorithm is discussed in Chapter 4.

2.3.7 Generalized Sidelobe Cancellation

GSC is an alternative implementation of LCMV. The advantage is that it converts a constrained optimization problem to an unconstrained problem so that many of the adaptive algorithms like LMS, RLS and APA etc. can be used directly. But to apply GSC to the high speed transportation market, many of the components need to adapt to the unique challenge brought by the rapid DOA change.

A typical GSC beamformer is illustrated in Fig. 2.10. It consists of a fixed beamformer \mathbf{w}_f which controls the quiescent response for input vector \mathbf{x} from M receivers, a blocking matrix \mathbf{B} which projects the input vector \mathbf{x} to the null space of the constraint matrix as vector \mathbf{u} that is further adaptively combined to produce the estimated interference \hat{y} for cancellation and an unconstrained beamformer \mathbf{w}_a which is adaptively controlled through an adaptive algorithm block.

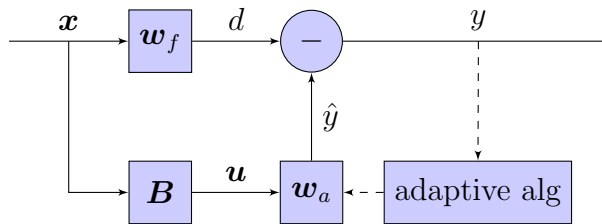


Figure 2.10: Beamformer Implementation with GSC Structure

The required responses for signals from a set of N angles are regulated through a linear equation:

$$\mathbf{C}^H \mathbf{w} = \mathbf{f}^* \quad (2.51)$$

where \mathbf{C} is the M by N constraint matrix with each column specified as a steering vector from a corresponding incoming angle, \mathbf{w} is the overall equivalent weight for the GSC beamformer, \mathbf{f} is the column vector with each element being the required response from the beamformer and $[\cdot]^*$ is the conjugate operator and $[\cdot]^H$ is the hermitian operator.

The fixed beamformer \mathbf{w}_f works in the column space of the constraint matrix \mathbf{C} to make sure that after processing the received input vector \mathbf{x} , the signals from a specified direction follow the desired response. It could be calculated as [69]:

$$\mathbf{w}_f = \mathbf{C}(\mathbf{C}^H \mathbf{C})^{-1} \mathbf{f}^* \quad (2.52)$$

The blocking matrix \mathbf{B} is in the left null space of the constraint matrix \mathbf{C} so that any signal coming from the regulated angle would be blocked by blocking matrix. Thus an unconstrained adaptive algorithm like LMS could be used to adjust \mathbf{w}_a . In this way, any interference not from the regulated angle would be adaptively reduced or eliminated. The conventional way of computing the blocking matrix using SVD is denoted as Normal GSC in this chapter for comparison. The beamformer in its unconstrained format could then be expressed as [69]:

$$\underset{\mathbf{w}_a}{\operatorname{argmin}} E\{|y|^2\} = (\mathbf{w}_f - \mathbf{B}\mathbf{w}_a)^H \mathbf{R}_{xx} (\mathbf{w}_f - \mathbf{B}\mathbf{w}_a) \quad (2.53)$$

where \mathbf{R}_{xx} is the covariance matrix of the input signal x .

Taking the derivative of (2.53) with respect to \mathbf{w}_a and force it to 0, we could find the optimum value of \mathbf{w}_a .

$$(\mathbf{w}_f - \mathbf{B}\mathbf{w}_a)^H \mathbf{R}_{xx} \mathbf{B} = 0 \quad (2.54)$$

So that the optimum value of \mathbf{w}_a , denoted as $\mathbf{w}_{a_{opt}}$, would be [69]:

$$\mathbf{w}_{a_{opt}} = (\mathbf{B}^H \mathbf{R}_{xx} \mathbf{B})^{-1} \mathbf{B}^H \mathbf{R}_{xx} \mathbf{w}_f \quad (2.55)$$

To block desired signal from leaking to the cancellation path, the i^{th} column vector of the blocking matrix \mathbf{B} denoted as \mathbf{b}_i needs to satisfy:

$$\mathbf{C}^H \mathbf{b}_i = 0 \quad (2.56)$$

where $i = 1, 2, \dots, M - N$ stands for the $M - N$ degree of freedom for an M element array with N constraints.

2.3.8 Eigen Beamforming

Wireless channel has a big impact on the performance of communication system, many systems like 802.11AC WiFi will explicitly probe the channel to get the CSI. The Access Point (AP) as beamformer sends Null Data Packet (NDP) packet to wireless client. The wireless client as beamformee will feedback the received channel characteristics to AP.

When both transmitter and receiver has perfect knowledge of CSI, the optimum

value for \mathbf{W}_t and \mathbf{W}_r could be derived from the Singular Value Decomposition (SVD) of \mathbf{H} :

$$\mathbf{H} = \mathbf{U}\mathbf{\Lambda}\mathbf{V}' \quad (2.57)$$

where the columns of \mathbf{U}, \mathbf{V} are orthogonal eigenvectors of $\mathbf{H}\mathbf{H}', \mathbf{H}\mathbf{H}$ respectively and $\mathbf{\Lambda}$ is eigenvalue of $\mathbf{H}\mathbf{H}'$ and $[\cdot]'$ is the conjugate transpose of a matrix.

\mathbf{U}, \mathbf{V} are orthogonal matrix, so $\mathbf{U}\mathbf{U}' = \mathbf{I}$ and $\mathbf{V}\mathbf{V}' = \mathbf{I}$. By choosing

$$\mathbf{W}_t = \mathbf{V} \quad (2.58)$$

$$\mathbf{W}_r = \mathbf{U}' \quad (2.59)$$

(2.2) could be simplified as:

$$\mathbf{y} = \mathbf{U}'\mathbf{U}\mathbf{\Lambda}\mathbf{V}'\mathbf{V}\mathbf{s} = \mathbf{\Lambda}\mathbf{s} \quad (2.60)$$

In this way, the source signal is separated and transmitted to receiver without cross talk.

2.3.9 Blind Beamforming

Blind beamforming aims to estimate the desired signal without the DOA information and pilot signals assistance. Instead, it uses some a priori knowledge about the signal. Some of the properties that could be exploited in wireless communication includes constant modulus of the phase modulated signal like Binary Phase Shift Keying (BPSK), QPSK, power difference between interference and desired signal [41].

2.3.9.1 Constant Modulus Algorithm

By setting the cost function $\mathbf{J}(\mathbf{w})$ to keep the modulus of the received input to a constant, Constant Modulus Algorithm (CMA) beamformer [70] is able to filter out noise and interference that corrupts the received input of phase modulated signals. The algorithm could be expressed as:

$$\mathbf{w}_o = \arg \min_{\mathbf{w}} \mathbf{E}[|\mathbf{w}^H \mathbf{x}| - 1]^2 \quad (2.61)$$

2.3.9.2 Power Inversion Beamformer

When a reference signal is not available and even the estimated DOA is not available, but the interference is stronger than signal, it is possible to separate the signal and interference through power. A power inversion beamformer [41] or power separator [36, p 371] use the property of a MVDR which creates a deep null for strong interference. In Fig. 2.2, when any one of the omni-antenna element is used as a desired input $d[n]$, the output $e[n]$ will contain the input signal minus any correlated input to the selected $d[n]$. When interference is stronger than signal, the adaptive beamformer will form a null in the direction of interference and allow signal pass without attenuation. But when the signal is stronger, this method will experience severe signal cancellation as expected since it only inverts the power by rejecting the strongest input.

2.3.9.3 Blind Source Separation

A large family of blind beam forming algorithms falls under Blind Source Separation (BSS). It makes use of the non-gaussianness to separate different signal if the signal sources that need to be separated is non-gaussian.

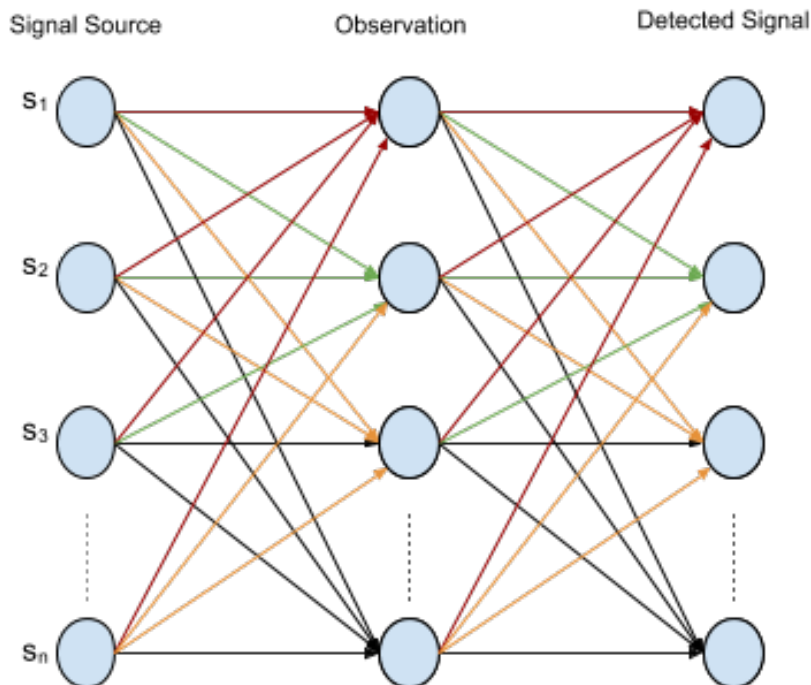


Figure 2.11: Blind Signal Separation Signal Model

The typical signal model of BSS consists of source signals, observed signals and detected signal as described in [71] and illustrated in Fig. 2.11 where the number of

signal source and number of sensor for observation both are n . The observation vector of the mixed signal \mathbf{x} is described below [72]:

$$\mathbf{x}(t) = \mathbf{A}_{mm} * \mathbf{s}(t) \quad (2.62)$$

where \mathbf{A} is the mixing matrix to combine all the unknown signal sources vector $\mathbf{s}(t)$.

As shown in Fig. 2.12, the mixing of two independent uniformly distributed random variables combined by a mixing operation might cause dependency on each other.

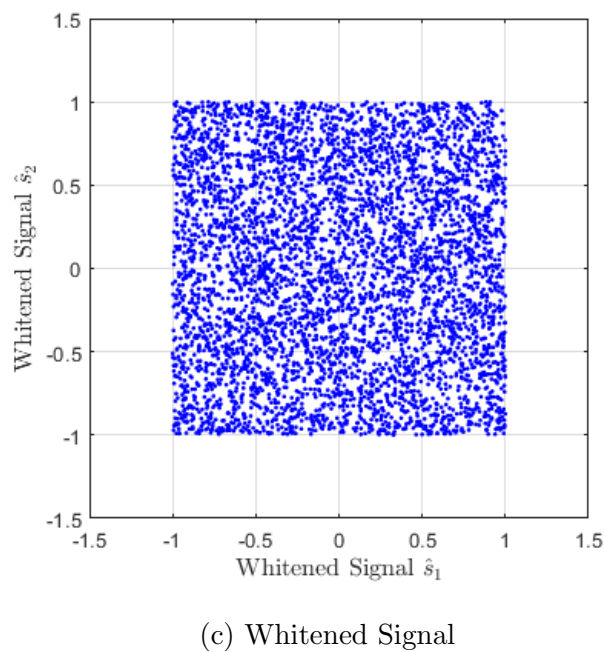
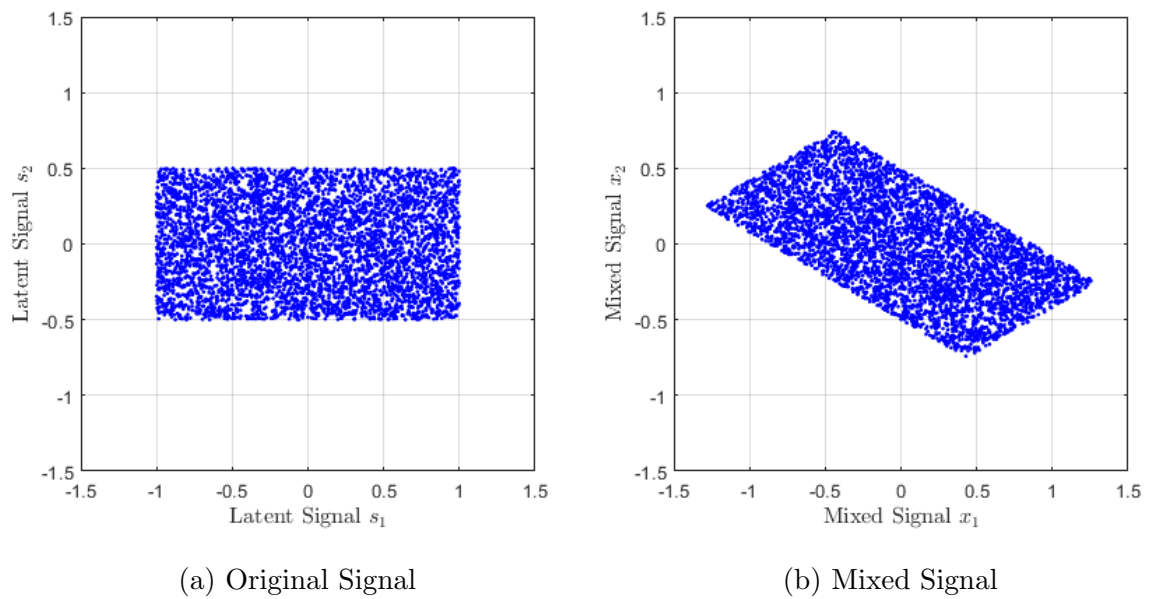


Figure 2.12: Mixing Independent Signal Causes Dependency

The original signal vector \mathbf{s} contains two independent component s_1 and s_2 as

illustrated in Fig. 2.12a. The mixing matrix is a linear map that rotates axis s_1 by 30° and s_2 by 60° . As clearly show in Fig. 2.12b, the mixed signal x_1 and x_2 is now dependent with each other.

From the distribution edge of the mixed signal, we can derive the mixing operation. But it only works for uniformly distributed original signals. According to Central Limit Theorem (CLT), the combination of non-Gaussian signals tends to become more and more Gaussian in PDF. For the above mixed signal, it can be verified from the histogram as illustrated in Fig. 2.13

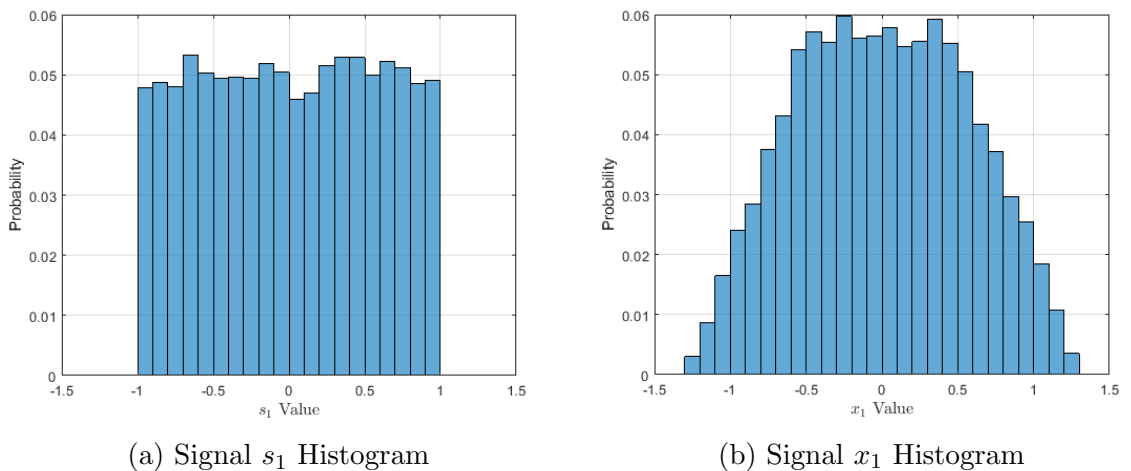


Figure 2.13: Combined Signal Closer to Gaussian Distribution

Since the mixing operation of the channel has the above effects, the ideal un-mixing operation would reverse those effects. To achieve that, a measure of those effects needs to be defined. As defined in [73, p.38], kurtosis could be used to measure the gaussianity of a random variable :

$$kurt(x) = \frac{\mathbf{E}\{x^4\}}{\mathbf{E}\{x^2\}^2} - 3 \quad (2.63)$$

The $kurt(x)$ has the following property which makes it suitable for measuring the gaussianity of random variable:

- $kurt(x) = 0$ when x is Gaussian distributed random variable,
- $kurt(x) > 0$ when x is super Gaussian distributed random variable with peak center PDF,
- $kurt(x) < 0$ when x is sub Gaussian distributed random variable with strong tail PDF.

2.4 Adaptive Optimization Algorithm Review

2.4.1 Extension to Complex Domain

In wireless communication, source information in baseband is usually represented using complex numbers and modulated through QAM to carrier. The cost function of the desired signal and filtered signal thus are all in the complex number domain, which makes the extension of the adaptive algorithm to complex domain necessary.

2.4.1.1 Complex Derivative Operator

There are different ways to extend the adaptive algorithm to the complex domain. Widrow[74] extended the LMS algorithm to the complex domain by treating the real and imaginary part of the complex weight separately. So instead of getting the derivative to complex weight directly, it seeks to get the partial derivative independently as follows:

$$\nabla_{\Re} = \frac{\partial}{\partial \Re(\mathbf{w})} \quad (2.64)$$

$$\nabla_{\Im} = \frac{\partial}{\partial \Im(\mathbf{w})} \quad (2.65)$$

In [75, p 77], the similar concept is used where a special derivative is defined to get the gradient of a cost function with respect to the complex variable:

$$\nabla_w = \frac{\partial}{\partial \Re(\mathbf{w})} + j \frac{\partial}{\partial \Im(\mathbf{w})} \quad (2.66)$$

Although this definition works in getting the optimum value of a global minimum through a quadratic cost function, in general, the definition of gradient for complex function doesn't hold. One obvious example is:

$$f(z) = z \quad (2.67)$$

where z is a complex variable. By using the definition of (2.66), the gradient would be calculated as 0. This is apparently not consistent to analytic complex functions[76, p 35]. In this dissertation, we adopt the Wirtinger derivative[77] definition which is

also used in many adaptive filter theory literatures [78, p 62].

$$\nabla_w = \frac{1}{2} \left(\frac{\partial}{\partial \Re(\mathbf{w})} - j \frac{\partial}{\partial \Im(\mathbf{w})} \right) \quad (2.68)$$

One of the benefit of Wirtinger definition is that w and w^* could be treated as independent complex variable when comes to the differential operator as shown below.

$$\nabla_w(w) = 1 \quad (2.69)$$

$$\nabla_w(w^*) = 0 \quad (2.70)$$

2.4.2 Mean Square Error

The cost function is defined as a function of mismatch between the desired signal and the combined output as (2.71).

$$e = d - \mathbf{w}^H \mathbf{x} \quad (2.71)$$

where the e is the mismatch value, d is the desired signal, \mathbf{w} is the weight of the linear combiner or beamformer and \mathbf{x} is the input signal vector. The desired signal d and input vector \mathbf{x} are random variables. \mathbf{w} is an unknown weight vector to be found to minimize the mismatch value which is also a random variable.

Usually a quadratic function is chosen due to its convex nature with a global minimum location so that the adaptive algorithm could converge to the global optimized solution. Other cost functions of error might lead to multiple local minimum.

The most popular and simplest cost function could then be defined as MSE:

$$\begin{aligned} J(\mathbf{w}) &= \mathbb{E}(|e|^2) \\ &= \mathbb{E}(ee^*) \\ &= \mathbb{E}|d|^2 + \mathbf{w}^H \mathbb{E}(\mathbf{x}\mathbf{x}^H) \mathbf{w} - \mathbb{E}(d\mathbf{x}^H) \mathbf{w} - \mathbb{E}(d^* \mathbf{w}^H \mathbf{x}) \end{aligned} \quad (2.72)$$

The global optimum of value of \mathbf{w} that minimize the cost function (2.72) depends on the first derivative with respect to \mathbf{w} :

$$J'_w(\mathbf{w}) = R_{xx}^T \mathbf{w}^* - \mathbb{E}(d\mathbf{x}^*) \quad (2.73)$$

where $R_{xx} = \mathbb{E}(\mathbf{x}\mathbf{x}^H)$

By setting (2.73) to 0, the optimum value of \mathbf{w} needs to satisfy:

$$R_{xx}^T \mathbf{w}^* = d\mathbf{x}^* \quad (2.74)$$

Conjugate both sides of the equation, the equation for getting \mathbf{w} is

$$R_{xx}^H \mathbf{w} = \mathbb{E}(\mathbf{x}d^*) \quad (2.75)$$

Since R_{xx} is a hermitian matrix, (2.75) could easily be transformed to:

$$R_{xx} \mathbf{w} = R_{xd} \quad (2.76)$$

where $R_{xd} = \mathbb{E}(\mathbf{x}d^*)$ is the cross correlation of received input vector and the desired input. This is the well known Winer-Hopf equation which gives the best weight vector in the MSE sense when the statistical moments of the input vector and design signal is known. The optimum beamformer weight vector then can be described as:

$$\mathbf{w}_0 = \mathbf{R}_{xx}^{-1} \mathbf{R}_{xd} \quad (2.77)$$

In a practical scenario, those statistical moment is not available in general. Many optimization algorithms use various approximation values in place of the true value. For example, LMS use instantaneous value of to replace the \mathbf{R}_{xd} , Direct Matrix Inversion (DMI) use sample covariance matrix inversion in place of the \mathbf{R}_{xx}^{-1} .

2.4.3 Orthogonality

In converged state, the expected error variable and the expected random input signal are orthogonal to each other. By rearranging (2.76) as:

$$\begin{aligned} \mathbb{E}(\mathbf{x}\mathbf{x}^H)\mathbf{w} &= \mathbb{E}(\mathbf{x}d^*) \\ \mathbb{E}[\mathbf{x}(d^* - \mathbf{x}^H\mathbf{w})] &= 0 \\ \mathbb{E}[\mathbf{x}(d - \mathbf{w}^H\mathbf{x})^*] &= 0 \\ \mathbb{E}(\mathbf{x}e^*) &= 0 \end{aligned} \quad (2.78)$$

it is clear that the random variable of error value is orthogonal to the random input variable.

Geometrically, it shows that the error variable is perpendicular to the space spanned by the input vector and the combined output as illustrated in Fig. 2.14.

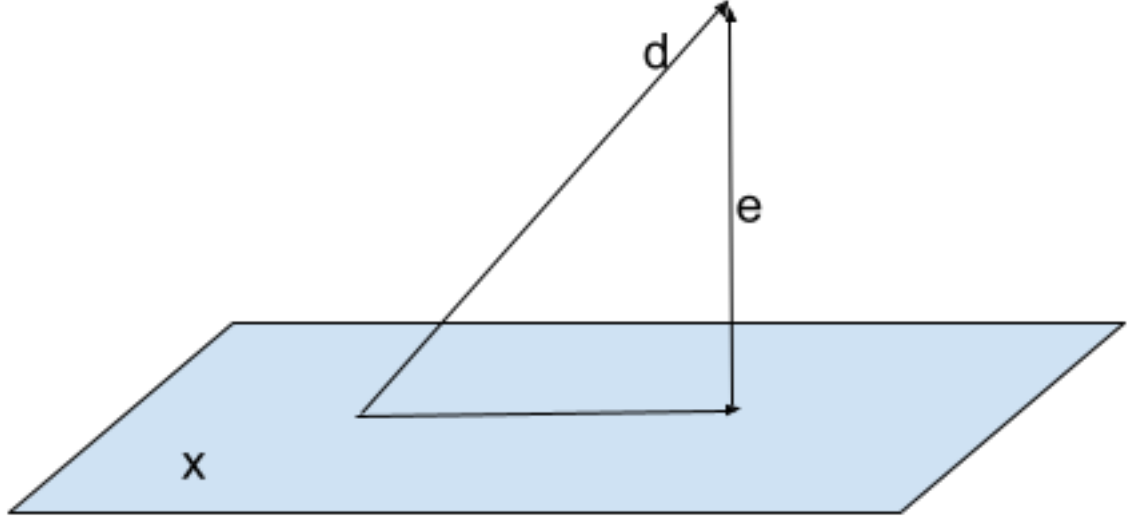


Figure 2.14: Error Signal is Orthogonal to Space Spanned by Input Vector Signal

2.4.4 Least Square

Other than treating the input signal and errors as random variable, another popular criteria for evaluating the quality of the estimation by the linear combiner to the desired signal is the LS criteria.

In this criteria, the system is modelled as a set of overdetermined linear equations from different samples. For an M element system with N samples, the system could be modelled as below:

$$\mathbf{X}\mathbf{w} = \mathbf{d} \quad (2.79)$$

where \mathbf{X} is a N by M matrix as listed below. The expanded expression is illustrated in (2.80)

$$\begin{pmatrix} x_{11} & x_{12} & \cdots & x_{1M} \\ x_{21} & x_{22} & \cdots & x_{2M} \\ \cdots & \cdots & \cdots & \cdots \\ x_{N1} & x_{N2} & \cdots & x_{NM} \end{pmatrix} \begin{pmatrix} w_1 \\ w_2 \\ \cdots \\ w_M \end{pmatrix} = \begin{pmatrix} d_1 \\ d_2 \\ \cdots \\ d_M \end{pmatrix} \quad (2.80)$$

where the X_{ij} indicates i^{th} snapshot of the j^{th} element detected input.

From the same geometric view as in Fig. 2.14, the optimum estimator $\hat{\mathbf{d}}$ is a

projection of \mathbf{d} onto the space spanned by \mathbf{X} . It could be expressed as

$$\mathbf{X}\mathbf{w}_o = \hat{\mathbf{d}} \quad (2.81)$$

where \mathbf{w}_o is the optimum value of \mathbf{w} that minimize the Least Square of $|\mathbf{d} - \hat{\mathbf{d}}|^2$. By applying the orthogonal principle, the difference vector should be orthogonal to the column space of \mathbf{X} as follows:

$$\mathbf{X}^H(\mathbf{d} - \hat{\mathbf{d}}) = 0 \quad (2.82)$$

So the optimum value of \mathbf{w} in the LS sense could be derived as:

$$\mathbf{w}_o = (\mathbf{X}^H \mathbf{X})^{-1} \mathbf{X}^H \mathbf{d} \quad (2.83)$$

And the estimated value is:

$$\hat{\mathbf{d}} = \mathbf{X}(\mathbf{X}^H \mathbf{X})^{-1} \mathbf{X}^H \mathbf{d} \quad (2.84)$$

2.4.5 Steepest Descent

Although (2.77) gives the optimum value in a closed form, in general, an iterative method to reach this optimum value is more desirable due to the real time requirement in wireless communication and the need to avoid computation intensive matrix inversion in mobile devices. The general iterative method could be expressed as:

$$\mathbf{w}_i = \mathbf{w}_{i-1} + \mu \mathbf{p} \quad (2.85)$$

where μ is the step size and \mathbf{p} is the direction to move for the next weight vector. The moving direction should ensure the resultant cost function $\mathbf{J}(\mathbf{w})_i$ smaller than $\mathbf{J}(\mathbf{w})_{i-1}$ so that the cost will converge to the minimum point eventually [78, p 144].

In Steepest Descent (SD) the direction \mathbf{p} is chosen to be the opposite of the gradient conjugate of the cost function $\mathbf{J}(\mathbf{w})$. It reaches to the optimum beamformer iteratively through the following procedure:

$$\begin{aligned} \mathbf{w}_i &= \mathbf{w}_{i-1} - \mu \nabla \mathbf{J}(\mathbf{w})^* \\ &= \mathbf{w}_{i-1} + \mu (\mathbf{R}_{xd} - \mathbf{R}_{xx} \mathbf{w}_{i-1}) \end{aligned} \quad (2.86)$$

that leads to the global minimum value of $\mathbf{J}(\mathbf{w})$. To get the condition of convergence, (2.86) could be rearranged as:

$$\begin{aligned}\mathbf{w}_i &= (\mathbf{I} - \mu\mathbf{R}_{xx})\mathbf{w}_{i-1} + \mu\mathbf{R}_{xd} \\ &= (\mathbf{Q}\mathbf{Q}^T - \mu\mathbf{Q}\mathbf{\Lambda}\mathbf{Q}^T)\mathbf{w}_{i-1} + \mu\mathbf{R}_{xd} \\ &= (\mathbf{Q}(\mathbf{I} - \mu\mathbf{\Lambda})\mathbf{Q}^T)\mathbf{w}_{i-1} + \mu\mathbf{R}_{xd}\end{aligned}\quad (2.87)$$

where $\mathbf{Q}, \mathbf{\Lambda}$ are the normalized eigenvectors and eigenvalues of \mathbf{R}_{xx} respectively. So clearly, for \mathbf{w}_i to converge to the optimum point, μ needs to satisfy [79]:

$$|1 - \mu\lambda_i| < 1 \quad (2.88)$$

where λ_i is the i^{th} eigen value of the auto covariance matrix \mathbf{R}_{xx} .

2.4.6 Least Mean Square

In practice, most system would not have the auto-covariance or cross covariance information available as stated by Widrow [80]. LMS algorithm uses instantaneous value to approximate the true value of $\mathbf{R}_{xd}, \mathbf{R}_{xx}$ as [81]:

$$\mathbf{R}_{xd} \approx d^* \mathbf{x} \quad (2.89)$$

$$\mathbf{R}_{xx} \approx \mathbf{x}\mathbf{x}^H \quad (2.90)$$

With this approximation, (2.86) is transformed to [82]:

$$\begin{aligned}\mathbf{w}_i &= \mathbf{w}_{i-1} + \mu\mathbf{x}e^* \\ &= \mathbf{w}_{i-1} + \mu\mathbf{x}(d - \mathbf{w}_{i-1}^H\mathbf{x})^*\end{aligned}\quad (2.91)$$

which is the well known LMS iterative algorithm for adaptive filter. But the selection of μ is a challenge. Although smaller μ gives a better converged state error, the convergence rate is slow. One of the bigger issues for LMS is that the μ effectively varies following the amplitude of the input. The step size plays an important part in the converged state MSE and converging speed. In this dissertation a variable step size named CVSS is proposed and evaluated below.

Another challenging task is to get the desired response d . In practical wireless system, d is usually not available. Otherwise, there would be no need to setup the

wireless communication channel. Several schemes could be used to get the desired response. The first widely used scheme is to use pilot signal. The second is to use a Decision Directed mode to replace the pilot signal with the detected signal. The third one is proposed by Griffith in [83] where instead of replacing the cross covariance \mathbf{R}_{xd} and auto-covariance \mathbf{R}_{xx} with instantaneous value, it assumes the knowledge of the cross-covariance is known and only \mathbf{R}_{xx} is replaced with the instantaneous value. In this way, no desired response d is required as shown below:

$$\mathbf{w}_i = \mathbf{w}_{i-1} + \mu \mathbf{R}_{xd} - \mu \mathbf{x}y \quad (2.92)$$

The adaptive beamformer architecture without reference can then be transformed from Fig. 2.2 to Fig. 2.15:

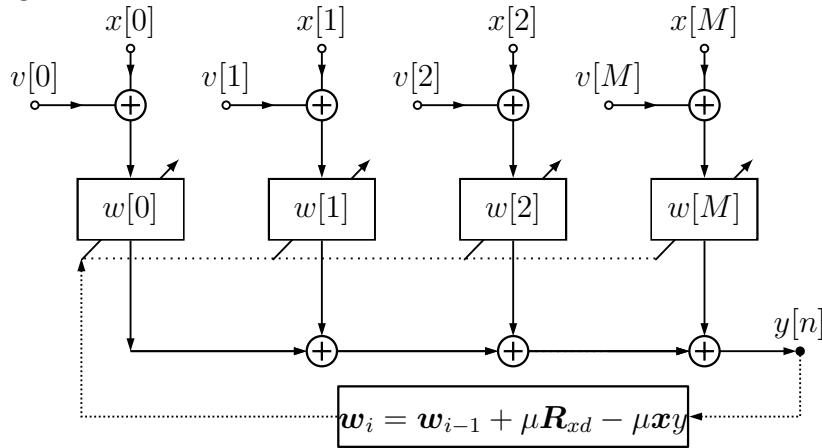


Figure 2.15: Adaptive Beamforming Architecture without Reference Response

In practice, the \mathbf{R}_{xd} is also not easily obtained, but with the advancement in DOA estimation technique, the DOA could be estimated with a satisfactory level of accuracy, the reference signal could be derived and applied in beamformer structures like GSC.

2.4.7 Normalized LMS

To get a uniform value for the step size μ over different amplitude, NLMS could be used to normalize the range of input signal. From (2.91), it can be easily verified that when the received input vector \mathbf{x} is scaled by a scalar a , the reference input d is also scaled by a . The second term of (2.91) will be scaled by a^2 as $a^2 \mu \mathbf{x} (d - \mathbf{w}_{i-1}^H \mathbf{x})^*$. So clearly the effective step size μ is scaled by a^2 to $a^2 \mu$. To get a uniform step size regardless of input signal power, the update formula in NLMS could be derived as [75, p 495]:

$$\mathbf{w}_i = \mathbf{w}_{i-1} + \mu \frac{\mathbf{x}}{|\mathbf{x}|^2 + \gamma} e^* \quad (2.93)$$

where γ is a regularization factor for numerical stability.

The step size μ has a different meaning in NLMS as compared with LMS. It acts as a relaxation factor [84]. When $\gamma = 0$ and $\mu = 1$, conjugate and multiply both sides of (2.93) by \mathbf{x} , it is shown that \mathbf{w}_i is at the best estimation to get the desired signal d :

$$\begin{aligned}\mathbf{w}_i^H \mathbf{x} &= \mathbf{w}_{i-1}^H \mathbf{x} + d - \mathbf{w}_{i-1}^H \mathbf{x} \\ &= d\end{aligned}\tag{2.94}$$

The characteristics of one step to reach to the optimum point is not coincident. It is actually a well known property of Newton's recursion algorithm [63, p 632]. Actually, NLMS can also be derived from Newton's recursion algorithm to find the root of the function $f(w)$

$$w_i = x_{w-1} - \frac{f(w_{i-1})}{f'(w_{i-1})}\tag{2.95}$$

where $f'(w)$ is the first derivative of $f(\mathbf{w})$. In NLMS context, $f(\mathbf{w}) = \mathbf{R}_{xx}\mathbf{w} - \mathbf{R}_{xd}$ and $f'(\mathbf{w}) = \mathbf{R}_{xx}$. So in Newton's recursion algorithm, the weight vector could be obtained iteratively as follows:

$$\mathbf{w}_i = \mathbf{w}_{i-1} + \mu \mathbf{R}_{xx}^{-1} (\mathbf{R}_{xd} - \mathbf{R}_{xx} \mathbf{w})\tag{2.96}$$

For numerical stability of the inverse of \mathbf{R}_{xx} , a regularization factor γ could be added in and (2.96) could be transformed as:

$$\begin{aligned}\mathbf{w}_i &= \mathbf{w}_{i-1} + \mu (\gamma \mathbf{I} + \mathbf{R}_{xx})^{-1} (\mathbf{R}_{xd} - \mathbf{R}_{xx} \mathbf{w}) \\ &\approx \mathbf{w}_{i-1} + \mu (\gamma \mathbf{I} + \mathbf{x} \mathbf{x}^H)^{-1} (\mathbf{x} d^* - \mathbf{x} \mathbf{x}^H \mathbf{w}) \\ &= \mathbf{w}_{i-1} + \mu \gamma (\mathbf{I} + \gamma^{-1} \mathbf{x} \mathbf{x}^H)^{-1} (\mathbf{x} d^* - \mathbf{x} \mathbf{x}^H \mathbf{w}) \\ &= \mathbf{w}_{i-1} + \mu \gamma \left(\mathbf{I} - \frac{\gamma^{-1} \mathbf{x} \mathbf{x}^H}{1 + \gamma^{-1} \mathbf{x}^H \mathbf{x}} \right) (\mathbf{x} d^* - \mathbf{x} \mathbf{x}^H \mathbf{w}) \\ &= \mathbf{w}_{i-1} + \mu \gamma^2 \frac{\mathbf{x}}{\gamma + |\mathbf{x}|^2} e^*\end{aligned}\tag{2.97}$$

where the second step of approximation is conducted by using the instantaneous value in place of the true value. So it is clear that NLMS is actually a Newton method with approximation and when $\mu = 1$, it can reach the optimum value in one step only.

But in practice, although when step size $\mu = 1$, it arrives at the best estimation at step i with one update, this might cause over fitted noise. So as LMS a small step size gives a better converged state error.

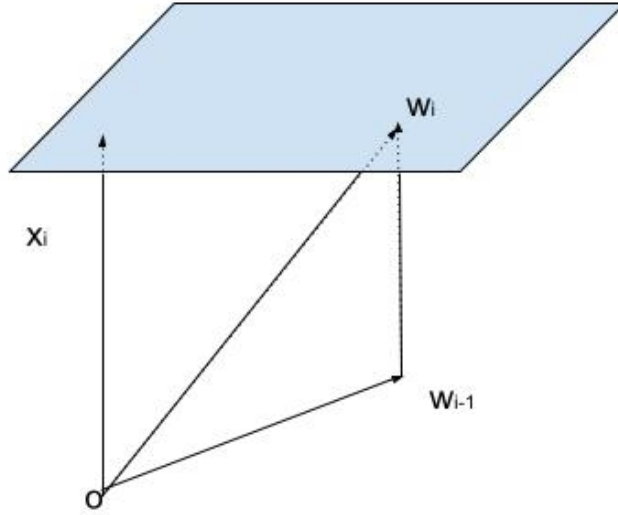


Figure 2.16: Update of \mathbf{w} along the Direction of Input Vector \mathbf{x}

As geometrically illustrated in Fig. 2.16, a smaller μ will need multiple steps to advance \mathbf{w} in the direction of adjustment.

2.4.8 Cyclic Variable Step Size LMS

For high speed adaptive design, it is important to reduce the calculation complexity. It is popular to use the signed data in place of the actual data for simplicity [85]. When the error signal is replaced with its sign as $sign(e)$, it is named the Signed Error Algorithm (SEA). Or the data input could be replaced with its signed version as $sign(x)$ in Signed Data Algorithm (SDA). Another way to simplify the selection of μ without losing the data information is CVSS as proposed in [3]. By cycling through the maximum allowed step size and the reduced step size, it has the potential to achieve higher convergence speed and a lower converged state MSE.

The proposed algorithm CVSS could be implemented by a simple shift operation. The selection of μ could be simplified as the following formula:

$$\mu_k = \mu_{base} * 2^{(\lfloor \frac{k}{T_p} \rfloor \text{ mod } T_c)} \quad (2.98)$$

where μ_{base} , T_p , T_c and $\lfloor \cdot \rfloor$ indicates the starting step size, number of iterations before changing step size, number of different step sizes and the nearest integer operator respectively. In this way, the change of μ is simply a shift operation in fixed point algorithm. Since there is no dependence on error signal detection or input vector norm calculation as in NLMS, it is light weight and robust.

The performance of CVSS is illustrated in Fig. 2.17 where a SNR 15dB signal is used for testing with the following parameter setting: $\mu_{base} = 0.00024, T_p = 30, T_c = 3$. For comparison, the standard LMS and SDA and SEA is also simulated with the same data input. The simulation results shows that CVSS LMS has the potential to achieve both faster convergence speed and low converged state MSE.

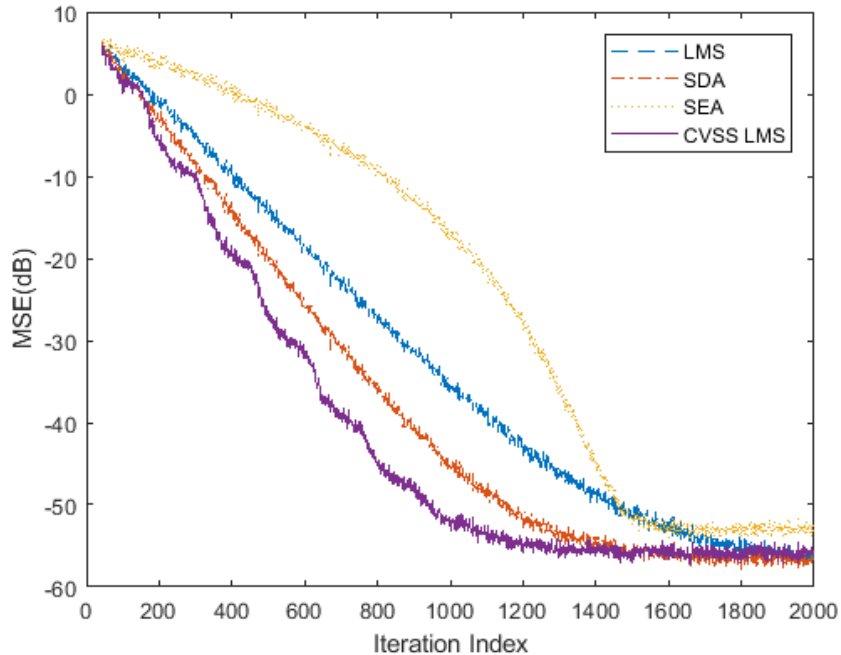


Figure 2.17: Cyclic Variable Step Size Performance Simulation

The periodic nature of the step size adjustment is manifested from the periodic change of the convergence speed before getting to the final optimum solution at around iteration step 1200. Before get to the convergence point, it is clear that when the steps size cycled to the higher value, it will converge faster than SDA or SEA and then it will get to a slower convergence speed when it cycled to the lower value.

2.4.9 Affine Projection Algorithm

Although NLMS gives an improvement in the step size selection, it still makes use of the instantaneous input vector for the estimation of adjustment direction. To improve the adjustment direction, the past input vectors could be used to enhance the estimation accuracy as investigated in [84]. APA is a generalized version of NLMS. The i^{th} updated weight vector \mathbf{w} is actually lies in the affine space defined by the i^{th} step input vector \mathbf{x}^i as follows:

$$\{\mathbf{w} | \mathbf{w} \in \mathbb{C}^M, \langle \mathbf{x}^i, \mathbf{w} \rangle = d\} \quad (2.99)$$

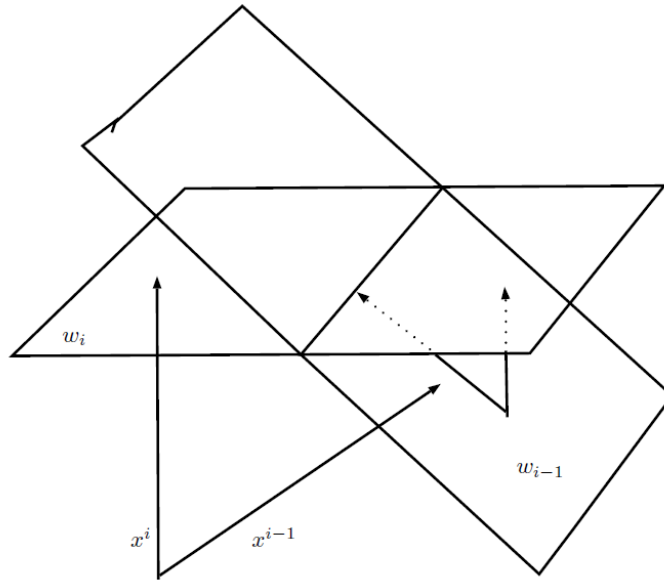


Figure 2.18: Affine Projection to Intersect of Affine Subspaces

where $\langle \mathbf{x}^i, \mathbf{w} \rangle$ indicates the inner product of two vector \mathbf{x}^i and \mathbf{w} . So NLMS could be generalized as a projection from \mathbf{w}_{i-1} to the affine space defined by (2.99). In general, for an affine subspace defined by $\mathbf{A}\mathbf{x} = \mathbf{b}$, the affine projector for a vector \mathbf{v} in the row space of \mathbf{A} is defined as [86, p 45]:

$$P_{affine} = \mathbf{v} + \mathbf{A}^\dagger(\mathbf{b} - \mathbf{A}\mathbf{v}) \quad (2.100)$$

where \mathbf{v} is the vector to be projected, \mathbf{A}^\dagger indicates the pseudo inverse of matrix \mathbf{A} . While NLMS only use a simple affine space defined by the latest input vector and desired signal, APA arrange multiple of input vectors and project the next update of weight vector \mathbf{w} to the intersect of all such affine subspace. Since the intersect of any affine subspace is still a affine subspace, (2.100) can still be used to project the weight vector \mathbf{w}_{i-1} to the intersected affine space. And the location is closer to the global optimum point. As illustrated in Fig. 2.18, instead of projection to the affine space defined by the single input vector, the APA algorithm projection to the intersect of two or more affine space. This gives one additional advantage for APA to handle the correlated input more efficiently.

When K measurement is arranged in a vector form, the APA algorithm can be described as:

$$\mathbf{w}_i = \mathbf{w}_{i-1} + \mu \mathbf{X}(\mathbf{X}^H \mathbf{X})^{-1} \mathbf{e} \quad (2.101)$$

where $\mathbf{X} = [\mathbf{x}_1, \mathbf{x}_2, \dots, \mathbf{x}_K]$ is the K instance of input vector arranged in matrix form, $\mathbf{e} = [e_1, e_2, \dots, e_K]^H$ is K instance of the measured error between desired signal and

beamformer output.

It is clear that NLMS is just a special case of APA when the order K is 1.

2.4.10 Recursive Least Square

Other than using the instantaneous value to approximate the \mathbf{R}_{xx} by the instantaneous value, a more accurate calculation can be achieved by using the past vectors for the calculation. But to retain the tracking capability, some forget factor needs to be incorporated so that the oldest data will have less weight. The concept of RLS is to use a recursive way to calculate the required \mathbf{R}_{xx} and its inverse as follows:

$$\mathbf{R}_{xx}^i = \beta \mathbf{R}_{xx}^{i-1} + \mathbf{x}\mathbf{x}^H \quad (2.102)$$

where \mathbf{R}_{xx}^i indicates the k^{th} estimate of the auto-covariance and β is the forgetting factor. So the inverse of the auto-covariance could be derived by using Woodbury formula [87, p 82] as:

$$\mathbf{P}_i = \beta^{-1} \left[\mathbf{P}_{i-1} - \frac{\beta^{-1} \mathbf{P}_{i-1} \mathbf{x}\mathbf{x}^H \mathbf{P}_{i-1}}{1 + \beta^{-1} \mathbf{x}^H \mathbf{P}_{i-1} \mathbf{x}} \right] \quad (2.103)$$

Using the recursively calculated matrix inversion in (2.97), the weight update formula for RLS could be expressed as:

$$\mathbf{w}_i = \mathbf{w}_{i-1} + \mathbf{P}_i \mathbf{x} e^* \quad (2.104)$$

Multiply both sides of (2.103) with \mathbf{x} , it is easily transformed to:

$$\mathbf{P}_i \mathbf{x} = \frac{\beta^{-1} \mathbf{P}_{i-1} \mathbf{x}}{1 + \beta^{-1} \mathbf{x}^H \mathbf{P}_{i-1} \mathbf{x}} \quad (2.105)$$

So the final version to update the weight vector of RLS is:

$$\mathbf{w}_i = \mathbf{w}_{i-1} + \frac{\beta^{-1} \mathbf{P}_{i-1} \mathbf{x}}{1 + \beta^{-1} \mathbf{x}^H \mathbf{P}_{i-1} \mathbf{x}} e^* \quad (2.106)$$

RLS brings an iterative way of calculating the \mathbf{R}_{xx} that covers longer history of data instead of just the latest input vector. The more accurate estimation reduces the eigenvalue spread thus improves convergence rate. But its computation requirement is quite intensive.

2.4.11 Kalman Filter

Kalman filter [88] is a well known recursive adaptive algorithm to improve estimation accuracy by combining state transition based prediction and measurement update. The core concept behind this accuracy improvement builds on the calculation of the joint PDF of two uncorrelated Normal Distribution. For Normal Distributed random variable vector $\mathbf{x}_1 \sim \mathcal{N}(\boldsymbol{\mu}_1, \Sigma_1)$ and $x_2 \sim \mathcal{N}(\boldsymbol{\mu}_2, \Sigma_2)$, their joint PDF still follows Normal Distribution as $\mathcal{N}(\boldsymbol{\mu}, \Sigma)$. Its mean $\boldsymbol{\mu}$ and covariance matrix Σ can be calculated as [89, p 52]:

$$\begin{aligned} \mathbf{K} &= \Sigma_1(\Sigma_1 + \Sigma_2)^{-1} \\ \boldsymbol{\mu} &= \boldsymbol{\mu}_1 + \mathbf{K}(\boldsymbol{\mu}_2 - \boldsymbol{\mu}_1) \\ \Sigma &= \Sigma_1 - \mathbf{K}\Sigma_1 \end{aligned} \quad (2.107)$$

where the \mathbf{K} is the gain.

In Kalman Filter, the underline random process and its measurement are modeled in the State Space as follows:

$$\mathbf{s}_i = \mathbf{A}\mathbf{s}_{i-1} + \mathbf{n}_{i-1} \quad (2.108)$$

$$\mathbf{z}_i = \mathbf{C}\mathbf{s}_i + \mathbf{v}_i \quad (2.109)$$

where \mathbf{s}_i captures the internal state of the random variable that needs to be estimated, \mathbf{A} , \mathbf{C} are state transition matrix, and measurement matrix respectively, \mathbf{n}_{i-1} and \mathbf{v}_i are the process model noise and measurement noise respectively.

The estimation of Kalman filter is a two step update [78, p 110]. The first step uses transition matrix in (2.109) to get the new i^{th} estimation \mathbf{s}_i^- based on state model. Here the $(\cdot)^-$ indicates the snapshot before the final i^{th} data. The predicted measurement then follows $\mathcal{N}(\mathbf{C}\boldsymbol{\mu}_i^-, \mathbf{C}\mathbf{P}_i^- \mathbf{C}^H)$ where $\boldsymbol{\mu}_i^-$ and \mathbf{P}_i^- is the mean vector and covariance matrix of predicted measurement of s_i respectively. The second step then uses the actual observed measurement to refine the estimation of \mathbf{s}_i^- to the final \mathbf{s}_i and covariance matrix Σ_i . It is described as below:

$$\begin{aligned} \mathbf{C}\boldsymbol{\mu}_i &= \mathbf{C}\boldsymbol{\mu}_i^- + \mathbf{K}(\mathbf{z}_i - \mathbf{C}\boldsymbol{\mu}_i^-) \\ \mathbf{C}\mathbf{P}_i \mathbf{C}^H &= \mathbf{C}\mathbf{P}_i^- \mathbf{C}^H - \mathbf{K}\mathbf{C}\mathbf{P}_i^- \mathbf{C}^H \\ \mathbf{K} &= \mathbf{C}\mathbf{P}_i^- \mathbf{C}^H (\mathbf{C}\mathbf{P}_i^- \mathbf{C}^H + \mathbf{R}_i)^{-1} \end{aligned} \quad (2.110)$$

with simple manipulation, the recursive update could be derived as:

$$\begin{aligned}\boldsymbol{\mu}_i &= \boldsymbol{\mu}_i^- + \mathbf{K}_k(\mathbf{z}_i - \mathbf{C}\boldsymbol{\mu}_i) \\ \mathbf{P}_i &= \mathbf{P}_i^- - \mathbf{K}_k\mathbf{C}\mathbf{P}_i^- \\ \mathbf{K}_k &= \mathbf{P}_i^- \mathbf{C}^H (\mathbf{C}\mathbf{P}_i^- \mathbf{C}^H + \mathbf{R}_i)^{-1}\end{aligned}\tag{2.111}$$

where \mathbf{K}_k is the refined gain, $\boldsymbol{\mu}_i$ and \mathbf{P}_i is the updated mean and covariance matrix of the state variable \mathbf{s}_i .

2.5 Direction of Arrival Estimation

Many of the beamforming algorithm like MVDR, LCMV, GSC requires the knowledge of the DOA to form the correct pattern when pilot signal not available. This section reviews the well known algorithms to get the high resolution DOA. And our proposed algorithm for getting stable DOA estimation in constrained routes.

2.5.1 Multiple Signal Characterization (MUSIC)

Multiple Signal Characterization (MUSIC) [90] is the first high resolution algorithm that explores the signal and null subspace of the received input's covariance matrix. By analyzing the eigenvalues of the received input's covariance matrix, the eigenvectors in the null space corresponding to noise could be identified. It can then be used to find a pseudo spectrum peak that corresponds to DOA.

As described in (2.25), the input vectors for signal and interference could be treated the same in DOA estimation except that they might have a different level of power. And their respective steer vectors are collected as an array \mathbf{A} . Then the input covariance matrix could be described as

$$\begin{aligned}\mathbf{R} &= E\{\mathbf{x}\mathbf{x}^*\} \\ &= \mathbf{A}\mathbf{P}\mathbf{A}^* + \sigma^2\mathbf{I}\end{aligned}\tag{2.112}$$

where \mathbf{P} , \mathbf{A} , σ^2 , \mathbf{I} , indicates the power matrix for each signal source, steer vector array, noise power and identity matrix respectively. The power matrix for all the signal source

is expressed as:

$$\mathbf{P} = \begin{pmatrix} \sigma_1^2 & & 0 \\ & \ddots & \\ 0 & & \sigma_K^2 \end{pmatrix} \quad (2.113)$$

where $\sigma_1, \dots, \sigma_I$ is the power of the I signal source.

Since \mathbf{R} is a hermitian matrix, its eigenvalues are non-negative real value. And their corresponding eigenvectors are orthogonal. For K uncorrelated signals, $\text{rank}(\mathbf{P}) = K$, to differentiate these K signals, the necessary constrain on number of AE is $M > K$. In that scenario, $\text{rank}(\mathbf{A}\mathbf{P}\mathbf{A}^*) = K$. So that we can have K largest eigenvalue and $M - K$ smaller eigenvalue correspond to σ^2 . The eigenvectors of \mathbf{R} could be split into two groups: \mathbf{S} corresponds to the largest K eigenvalues and \mathbf{G} correspond to the rest $M - K$ smallest eigenvalues.

By multiplying both sides of equation 2.112 with \mathbf{G} , we've the following

$$\begin{aligned} \mathbf{R}\mathbf{G} &= \sigma^2\mathbf{G} \\ &= \mathbf{A}\mathbf{P}\mathbf{A}^*\mathbf{G} + \sigma^2\mathbf{G} \end{aligned} \quad (2.114)$$

where the first equation is derived from the definition of eigenvalue. From (2.114) It is clear that

$$\mathbf{A}^*\mathbf{G} = 0 \quad (2.115)$$

which shows that \mathbf{G} is in the null space of \mathbf{A} . It means that any steering vector $\boldsymbol{\alpha}(\theta)$ in \mathbf{A} is perpendicular to \mathbf{G} . So that we have $\boldsymbol{\alpha}^*\mathbf{G}\mathbf{G}^*\boldsymbol{\alpha} = 0$. It suggests a way to find incoming signal's DOA θ through the pseudo MUSIC spectrum formula: $\frac{1}{\boldsymbol{\alpha}^*\mathbf{G}\mathbf{G}^*\boldsymbol{\alpha}}$ that peak at the each of actual incoming angle.

Since it uses the null space vector for spectrum calculation, MUSIC algorithm requires that the number of antenna element must be larger than the number of the signal source.

Although MUSIC algorithm has high resolution, it doesn't work well in the environment where some signals are correlated.

Figure 2.19 illustrates the pseudo spectrum of three mixed signal with DOA of 10° , 25° and 39° resolved by a 10 elements ULA.

Once the direction of arrival is identified, the beamformer weight could then be derived through MVDR, GSC etc. Since any angle mismatch might cause severe signal

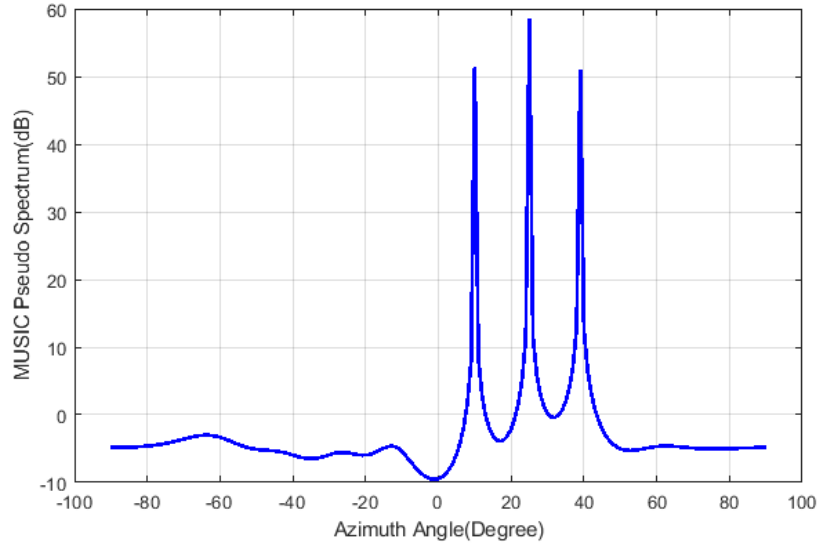


Figure 2.19: MUSIC Spectrum

cancellation, it is important to get the DOA estimation accurate and fast. The following section describes one of the algorithms that this dissertation explores to improve the estimation speed with the assistance of sensors.

2.5.2 Kalman Filter Assisted DOA Estimation in Constrained Route

As described in Section 2.4.11, Kalman filter is good at fusion multiple sensor input with the underline model. For vehicles in constrained routes, it is possible that Kalman filter could be used to improve the DOA estimation accuracy [4].

As the vehicle speed v could be easily detected by a speed sensor, a Kalman filter could be used to fuse the DOA estimation θ and sensor detected speed v with the DOA estimation run at a lower rate. The state space transition of Kalman filter could then use the linear interpolated version of the DOA estimation. The discrete Kalman filter for DOA tracking using (2.4.11) could be described as:

$$\begin{aligned} \mathbf{A} &= \begin{bmatrix} 1 & T_s \\ 0 & 1 \end{bmatrix} \\ \mathbf{x}_k &= \begin{bmatrix} p_k \\ v_k \end{bmatrix} \\ \mathbf{C} &= \begin{bmatrix} 1 & 0 \\ 0 & 1 \end{bmatrix} \end{aligned} \quad (2.116)$$

where p_k, v_k are position and speed at time index k , T_s is the sampling interval as the train speed is assumed to be constant over the sampling period. As for the observation matrix \mathbf{C} , although the observed parameters are speed v and angle θ , distance parameter p can be easily obtained through (5.1).

The simplified model is simulated with a train moving with speed $20m/s$ and the Sampling interval is set to $10ms$.

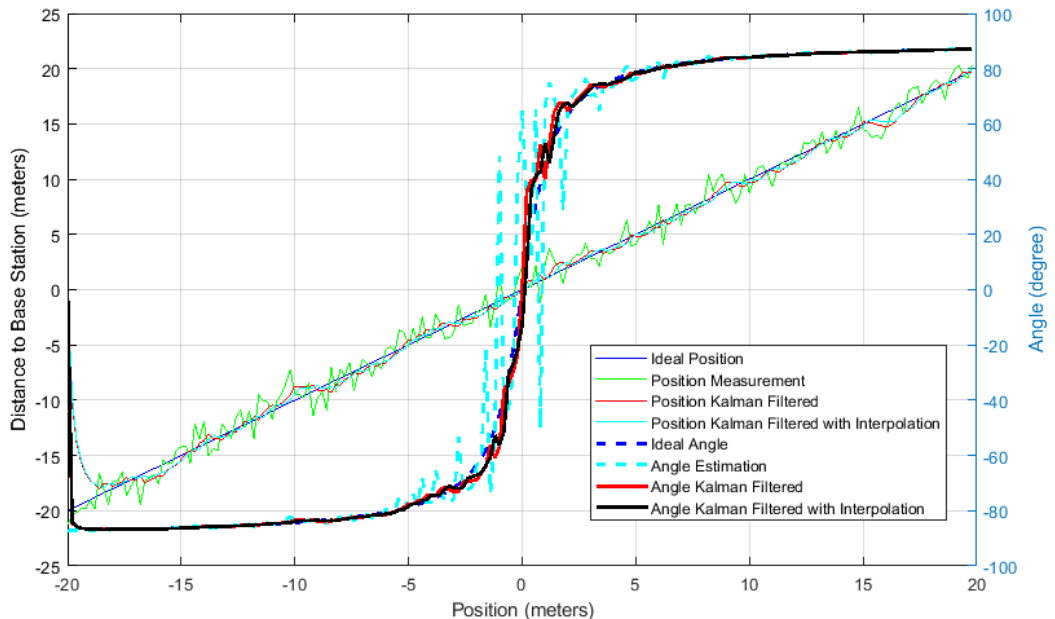


Figure 2.20: Kalman Filter Assisted Angle Estimation

As illustrated in Fig. 2.20, it shows that the Kalman filtered output of the DOA helps smooth the DOA estimation. The estimated DOA could be refined using covariance reconstruction algorithm proposed in [91, 92]

2.6 Summary

In this chapter, the architecture of the smart antenna system, the adaptive structure to implement the beamformer and various algorithms to derive the weight vector are reviewed. Due to the similarity to FIR, many existing algorithms in designing FIR like Window methods, Remez algorithm, Frequency Sampling methods etc. can be used for beampattern synthesis. Data dependent algorithms like MVDR, LCMV, GSC are briefly discussed and reviewed as in the following chapter we'll be focusing on improving GSC to implement the adaptive beamformer for the transportation market. Blind algorithms like CMA, Power Inversion beamformer do not rely on the DOA.

They have some advantages to save the channel probing cost. But the longer time that it needs to converge makes them not very suitable for high mobility scenarios. Various adaptive algorithm is reviewed including stochastic algorithms like LMS, SD and deterministic algorithms like LS,RLS. For high speed adaptive design, a CVSS LMS is proposed and simulated, which shows potential to achieve fast convergence speed and low optimum MSE as published in [3]. In the end the techniques to estimate DOA is briefly introduced and the algorithm to improve the estimation speed by using Kalman filter to fuse with other position or speed sensor is proposed.

Chapter 3

Wireless Communication System Simulation

3.1 Introduction

Wireless channel simulation is critical for the verification of transceivers with different algorithms in various channel situations. Multipath is a unique character of the wireless channel that causes fading. To simulate the multipath effect, mainly there are two approaches, namely Ray Tracing [93] and Stochastic Modeling method [94].

Ray tracing method is a site-specific algorithm where multiple communication paths are traced directly for a particular site model. Although it is computing-intensive, the channel's characteristics like coherence bandwidth, coherence time etc., are reflected in the ray modelling. On the other hand, the Stochastic Model method is generic and simpler for simulating different fading scenarios by modelling the channel gain as a Random Variable (RV) with different Power Spectral Density (PSD) and Probability Density Function (PDF), which could be considered as an aggregated effect from multipath. There are many random distributions like Rayleigh, Rician, Nakigami, and Weibull etc., which have been proposed, tested and verified in the field with varying levels of accuracy. This chapter focuses on the Stochastic Modeling method.

The PSD of the channel gain random variable represents the Doppler spectrum of the wireless channel model. The wider the Doppler spread [95], the faster the change of the channel gain, hence the shorter the coherence time [95] of the channel. So to properly model a wireless channel characteristic, it is necessary to implement specific PSD for the channel gain random variable. Different Doppler spectrum like U-Shaped [96, p.148], Bell shaped [97, p.45] etc. have been proposed in the literature for various

fading model.

3.2 Motivation

The challenge for stochastic modeling method is that changing of PSD and PDF of a random variable is highly related to each other except for the Gaussian distribution case. In Fig. 3.1, two random noise with uniform and Gaussian distribution is illustrated for the impact of filtering. It is clear from the comparison that although the output of filtering a Gaussian random noise still follows Gaussian distribution, filtering a uniform distribution random variable to get a specific PSD would transform the random variable to a different distribution. According to Central Limit Theorem, the filter actually makes the distribution more Gaussian-like.

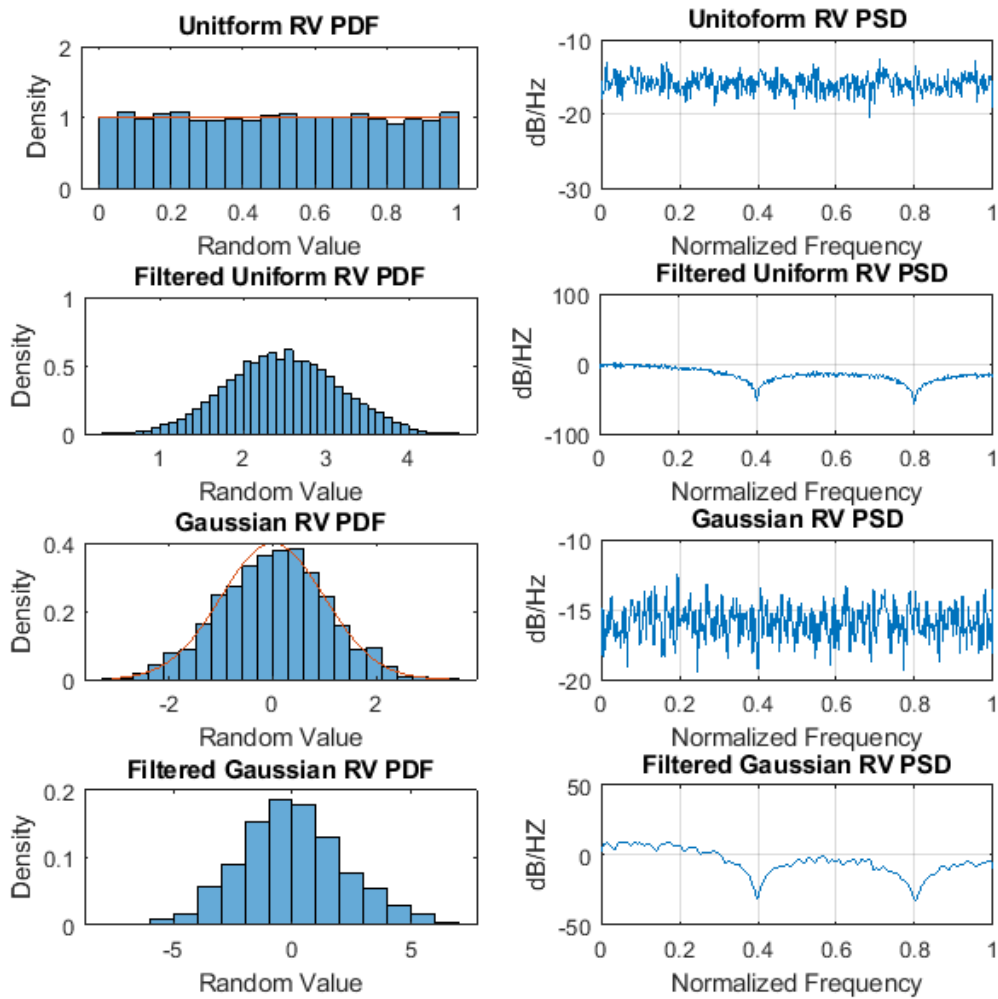


Figure 3.1: Changing PSD of a Random Variable by Filtering Affects its PDF

But in most of the wireless channel simulations, the channel gain doesn't follow

Gaussian distribution. Many system design and simulation need to consider Non-Gaussian noise [98, 99, 100]. Thus many literatures have investigated how to generate colored Non-Gaussian noise. Non-Gaussian distributed random variable could be generated from well know distribution like Gaussian or uniform variables using Inverse Transform Sampling (ITS) [101, p.104] method. Since generally the inverse of the required Cumulative Distribution Function (CDF) is non-linear, complicated methods like Hermite Expansion are needed to compensate for the effect of the non-linear transformation. In [102], the concept of rearranging the random sequence to follow a reference sequence is explored to reshape the PSD without modifying the PDF. It is referred to as Sequence Rearrangement Block Method in this chapter since it can only generate random variables in a block manner. Since the rearranged sequence only asymptotically approaches the required PSD, the block size needs to be set to relatively large. This makes it ineffective for wireless communication simulation. In [103], the summation of real sinusoid is explored where all the amplitude, phase and frequency of the sinusoids could be used to derive the final random variable. So that the PDF could be controlled by amplitude and phase. And the PSD could be controlled by the selection of frequency components. But it can only be used to generate symmetric PSD.

To eliminate the limitations of existing methods, this chapter uses Gaussian random variable filter method so that once the filter coefficients are determined, the channel gain random variable can be generated in real time. But in contrast to using complex Hermite Expansion to find the non-linear effect of Inverse Transform Sampling, our proposed method considers the ITS non-linear effect for PSD as distortion for the filter response. By taking into consideration of the non-linear effect of the ITS directly, Particle Swarm Optimization (PSO) is then used to find the pre-distorted filter solution. PSO is widely used to optimize various non-linear problems since it is first proposed in [104] due to its simpleness and effectiveness for implementation. As a population based stochastic algorithm, the concept of PSO is simple and inspired by birds flocking and fish schooling. It uses a preset number of random particles which represents a point in the solution space to search for a globally optimized solution to minimize a cost function.

This chapter uses PSO to search for a pre-distorted filter that can correct the distortion caused by the non-linear effect of ITS so that the combined output generates the required PSD while the ITS will guarantee the generated variable meets the required

PDF. Compared to existing methods, it has no assumption for PSD and PDF and it can generate the channel gain random variable in real time after the filter coefficients are found by PSO. The rest of the chapter is organized as follows. Firstly a wireless channel model is illustrated where the channel gain could be modeled as a random variable following the Non-Gaussian distribution with a specific Doppler spectrum. Then the proposed solution for the generation of the Non-Gaussian variable is discussed in detail. Finally the numerical simulation for random variable with specific distribution and required PSD is presented to validate the proposed solution.

3.3 Problem Formulation

A Single Input Single Output (SISO) wireless channel model is shown in Fig. 3.2.

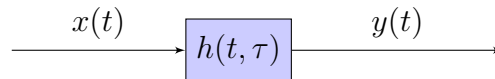


Figure 3.2: SISO Wireless Channel Model

The channel convolution effect could be described as [105, p.44]

$$y(t) = \int_{-\infty}^{\infty} x(t - \tau)h(t, \tau)d\tau \quad (3.1)$$

where $y(t)$, $x(t)$, $h(t, \tau)$ are the received signal, transmitted signal and channel impulse response at time t respectively. For a SISO channel with N multiple paths, $h(t, \tau)$ is modeled as (3.2) [105].

$$h(t, \tau) = \sum_{i=1}^N a_i(t)\delta(\tau - \tau_i(t)) \quad (3.2)$$

where $a_i(t)$, $\tau_i(t)$ is the gain and delay at time t for i^{th} path respectively. The received signal could then be described in (3.3)

$$y(t) = \sum_{i=1}^N a_i(t)x(t - \tau_i(t)) \quad (3.3)$$

To simplify the discussion, we assume the channel is one tap wideband channel which is a valid assumption nowadays due to the wide use of Orthogonal Frequency Division Multiplexing (OFDM) in wireless communication [106]. Then (3.3) could be further simplified as

$$y(t) = g(t)x(t - \tau) \quad (3.4)$$

where $g(t) = \sum_{i=1}^N a_i(t)$ is the aggregated channel gain and τ is the one tap delay. The channel gain $g(t)$ is assumed to be a Wide Sense Stationary Process (WSS) which is normally valid for wireless channel simulation for symbol recovery.

The problem could be summarized as to generate a random variable G which represents the channel gain $g(t)$ that satisfies the two requirements at the same time: a specific Cumulative Distribution Function (CDF) F_G and a specific autocorrelation function $R_G(\tau)$. This is equivalent to meet the requirement of PSD and PDF at the same time.

3.4 Proposed Solutions

3.4.1 Proposed Architecture for Noise Generation

Fig. 3.3 shows the model for the generation of the required non-Gaussian variable from a Gaussian distributed variable W .

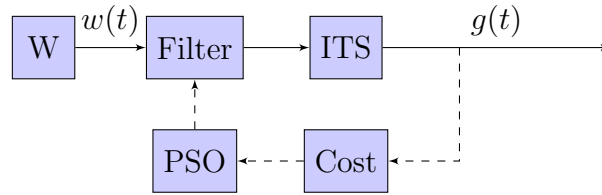


Figure 3.3: Architecture of PSO based Non-Gaussian Noise Generation

The Gaussian random variable sequence $w(t)$ is filtered before feeding into the ITS block. Since the filtered version of Gaussian variable is also Gaussian distributed, the ITS could be designed with the assumption that its input is Gaussian random variable. So that the ITS could be designed as:

$$G = F_G^{-1}(F_W(w)) \quad (3.5)$$

where G is the generated random variable, F_G^{-1} is the inverse of the desired CDF of G , F_W is the CDF of Gaussian variable and w is the sample from a Gaussian random Variable W .

The generated random number $g(t)$ follows distribution function F_G no matter what filter coefficients are used since the input to ITS is always Gaussian. So we can focus on getting the right filter that can generate the right PSD for the output of ITS.

3.4.2 Find the Right Filter with the Required $R_x(\tau)$

The algorithm could be summarized as follows [102]:

1. Generate a realization sequence X_0 from Gaussian distribution $\mathcal{N}(0, 1)$,
2. Filter X_0 through a filter to make sure that the output sequence X follows standard distribution and have a specially defined autocorrelation $R_X(\tau)$,
3. Apply G_X to the X to get the final samples that follow the required CDF F_Y and $R_Y(\tau)$.

To find the right $R_X(\tau)$ for the input Gaussian variable, a relationship between the input and output autocorrelation function needs to be established. Since Hermite polynomials are orthogonal under weight $\frac{1}{\sqrt{2\pi}}e^{-\frac{x^2}{2}}$ as indicated in (3.6).

$$\int_{-\infty}^{\infty} H_n(x)H_m(x)p(x)dx = n!\delta_{nm} \quad (3.6)$$

where H_n, H_m are the n^{th} and m^{th} order Hermite polynomial respectively, $p(x)$ is the PDF of normal distribution, it could be used as the basis for decomposing G_X as follows

$$G_X(x) = \sum_{n=0}^{\infty} f_n H_n(x) \quad (3.7)$$

By multiplying and integrating both sides of (3.7) by Hermite polynomial and $p(x)$, the coefficient f_n could be derived as

$$f_n = \frac{1}{n!} \int_{-\infty}^{\infty} G_X(x)H_n(x) \frac{e^{-x^2/2}}{\sqrt{2\pi}} dx \quad (3.8)$$

Putting the derived coefficient f_n back to equation (3.7), $G_X(x)$ could be used to derive $R_Y(\tau)$

$$R_Y(\tau) = \mathbf{E}[Y_{t_1}Y_{t_2}] \quad (3.9)$$

where $\tau = t_2 - t_1$. Expand the random variable Y_{t_1}, Y_{t_2} will have:

$$\begin{aligned} \mathbf{E}[Y_{t_1}Y_{t_2}] &= \sum_{n=0}^{\infty} f_n H_n(x_1) \sum_{m=0}^{\infty} f_m H_m(x_2) \\ &= \sum_{n=0}^{\infty} \sum_{m=0}^{\infty} f_n f_m \mathbf{E}[H_n(x_1)H_m(x_2)] \\ &= \sum_{n=0}^{\infty} \sum_{m=0}^{\infty} f_n f_m \int_{-\infty}^{\infty} H_n(x_1)H_m(x_2)p(x_1, x_2)dx_1 dx_2 \end{aligned} \quad (3.10)$$

where $p(x_1, x_2)$ is the joint probability density for the two Gaussian variable. According to Mehler Formula [107], $p(x_1, x_2)$ can be further expanded to Hermite polynomial.

$$p(x_1, x_2) = p(x_1)p(x_2) \sum_{k=0}^{\infty} \frac{\rho^k}{k!} H_k(x_1)H_k(x_2) \quad (3.11)$$

where ρ is the cross correlation coefficient. Since X_1, X_2 are standard normal distribution at t_1 and t_2 , $\rho = R_X(\tau)$. Based on (3.6) and (3.11), (3.9) could be further simplified to

$$R_Y(\tau) = \sum_{n=0}^{\infty} n! f_n^2 R_X(\tau)^n \quad (3.12)$$

For a required $R_Y(\tau)$, a $R_X(\tau)$ satisfying (3.12) could be found or at least in a Mean Square Error (MSE) sense.

The proposed solution works in two stages. In the first stage, PSO is used to find the optimum filter coefficients. In the second stage, the Filter process the input of Gaussian random numbers with the optimum coefficients.

3.4.3 Searching for Optimum Filter Coefficient by PSO

The number of filter coefficients defines the search space for PSO. For filters with n coefficients, the i^{th} particle p_i could be represented by the coefficients vector as:

$$p_i = [a_{i1} \ a_{i2} \ \cdots \ a_{in}]^T \quad (3.13)$$

where a_{i1}, a_{i2}, a_{in} is the filter coefficients for the i^{th} particle and $[\cdot]^T$ denotes the transpose operator. Each particle then tracks its local and global best location based on a performance cost measurement function.

The cost function in PSO is to measure the error caused by the deviation of each particle position to the optimum position. In this chapter, the error e is designed to be the Mean Squared Error of generated PSD compared with the required PSD as follows:

$$e = \frac{1}{K} \sum_{k=1}^K (P_g(k) - P_r(k))^2 \quad (3.14)$$

where K is the number of frequency point to be measured, $P_g(k)$ is the k^{th} frequency point of the generated random variable PSD and $P_r(k)$ is the k^{th} frequency point of the required PSD.

The location of each particle is then updated iteratively. The $(m + 1)^{th}$ iteration of position p_i^{m+1} is then updated by its m^{th} position p_i^m and $(m + 1)^{th}$ velocity v_i^{m+1} [108]:

$$p_i^{m+1} = p_i^m + v_i^{m+1} \quad (3.15)$$

The velocity v_i^{m+1} is also derived iteratively from the m^{th} iteration of velocity v_i^m , the detected local best location p_{i_lbest} , the global best location p_{gbest}^m and their weight and random number as follows[108]:

$$v_i^{m+1} = w_i v_i^m + w_l r_l (p_{i_lbest}^m - p_i^m) + w_g r_g (p_{gbest}^m - p_i^m) \quad (3.16)$$

where w_i is the inertial weight, w_l is the self adjustment weight, w_g is the social adjustment weight. The uniform distributed random numbers r_l and r_g are used to explore the solution space by adjusting the steps and direction randomly.

Once the error e reaches the required level of accuracy before the number of iterations exceeds the threshold, it would be concluded that the PSO has found proper filter coefficients with the required pre-distortion. Otherwise, a manual check or adjustment might be needed on PSO parameters.

3.5 Numerical Simulation and Result Analysis

A first order AutoRegressive Model is used to verify the effectiveness of the proposed algorithm. The required channel gain is modeled as:

$$g(t) = \rho g(t - 1) + w(t) \quad (3.17)$$

where $\rho = 0.4$ is used for the simulation, w is the Gaussian random variable for reference. The required channel gain needs to follow Rayleigh distribution for simulation. The PSO is designed with the self adjustment weight set to 0.3 and the social adjustment weight set to 0.6 for the simulation. 25000 random numbers are generated for the comparison.

Fig. 3.4 illustrates the PDF of the original Gaussian noise input and the generated Rayleigh noise to simulate the channel gain. It shows that the generated noise follows Rayleigh distribution after ITS.

Fig. 3.5 illustrates the PSD of the generated Non-Gaussian noise using the proposed

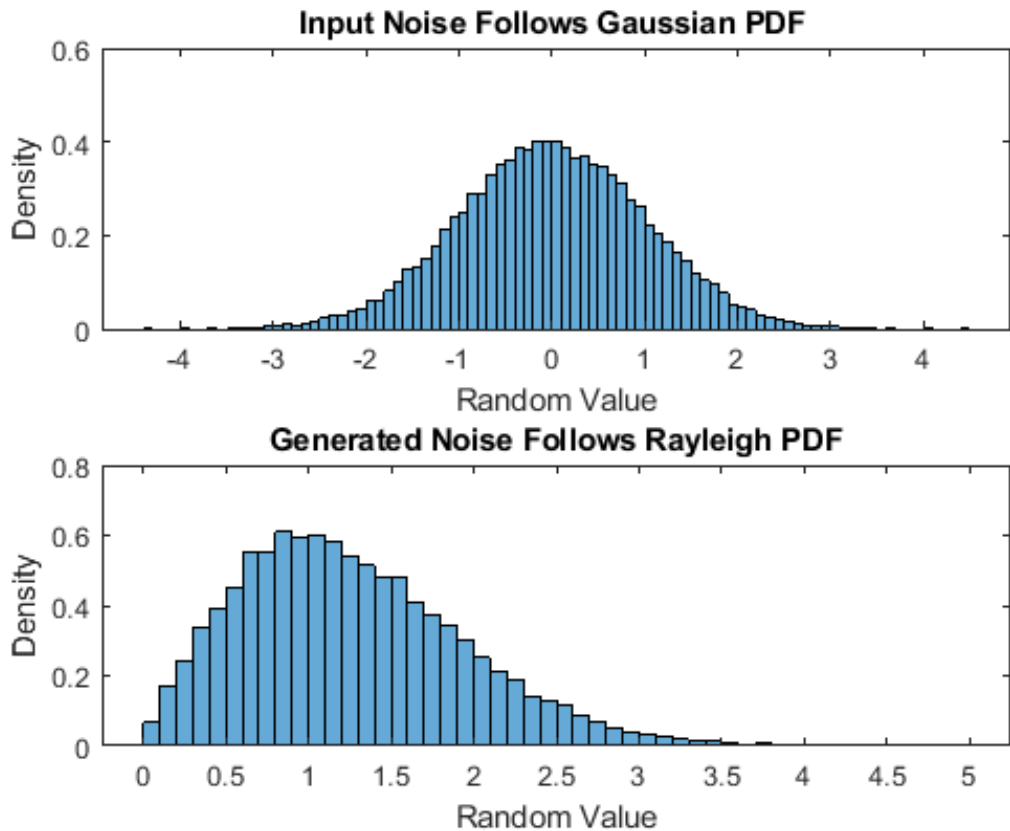


Figure 3.4: Generated Noise Follows the Required Rayleigh PDF with Gaussian Noise as Input

PSO based filter and the Sequence Rearrangement Block Method.

To compare the similarity of the generated noise PSD to the required PSD, the correlation between the generated PSD and the required PSD is calculated in Table 3.1. It shows that the generated random variables by both methods match to the required PSD. PSO based Filter method has a slightly lower correlation value. This is also evidenced from Fig. 3.5 where at higher frequency it deviates slightly from the required PSD. Part of the reason could be due to the numerical error generated from the optimization process. But the proposed PSO based filter method could be used to generate continuous noise while the Sequence Rearrangement Block method can only generate noise block by block thus delay is unavoidable.

Table 3.1: Comparison of Correlation to the Required PSD

Algorithm Name	Correlation to Required PSD
PSO Based Filter Method	0.9126
Sequence Rearrangement Block Method	0.9158

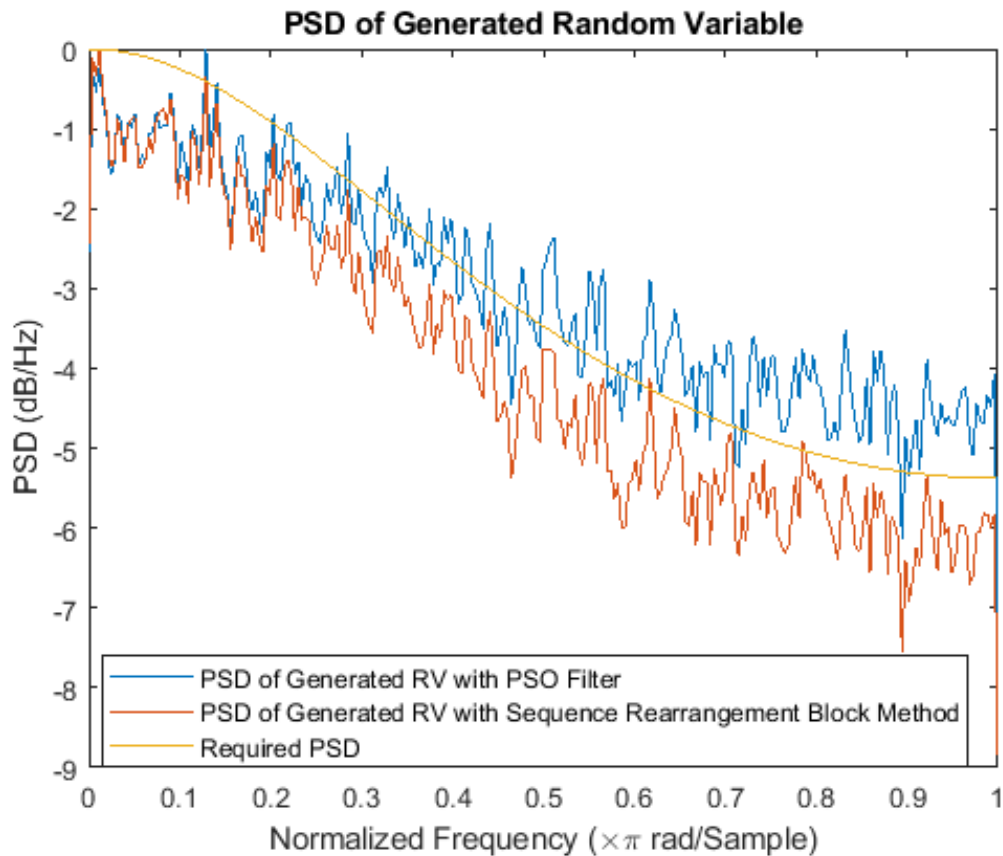


Figure 3.5: Generated Noise Follows the Required PSD for Proposed Method

3.6 Summary

A PSO based method for generating colored Non-Gaussian noise that meets both the requirements of PSD and PDF is proposed. The numerical simulation result confirms its effectiveness. The benefit of this new method is that the complexity of deriving the required pre-distortion for the filter is replaced with a simple PSO search method. And once the required filter coefficients are found, the generation of non-Gaussian noise could be done in real time by filtering and ITS. Compared to block based methods or other analytical methods, it is more suitable for real time wireless channel simulation. The limitation for the proposed method is that the inverse of the required PDF needs to be available. Future investigation would be suggested on the verification of the validity for various PDFs and PSDs that might be useful for wireless channel gain simulation.

To evaluate the performance of various adaptive beamforming algorithms in wireless communication context, simulation is much more cost effective and fast than the field trial method. Different delay spread, angle spread and relative speed etc. of incoming signal will produce different profile of PDF and PSD. Colored Non-Gaussian noise that implements various PDF and PSD is thus important for adaptive beamforming system

simulation in wireless communication. When each antenna elements are not highly correlated, the steering vector alone is not enough to capture the wireless channel characteristics. A combination of mean DOA and a Random Variable represented complex channel gain would be used for each path [109]. The proposed noise generation method could then be used for the beamforming simulation.

Chapter 4

Fast Algorithm for Flat Top Beam Pattern Synthesis

4.1 Introduction

Beamforming is widely used in wireless communication as a spatial filter to enhance signals from a specific Direction of Arrival (DOA) and suppress noise and interference from other directions. In high mobility scenarios, wireless communication with beamforming faces unique challenge [1] where the DOA changes rapidly which makes the beamforming performance degrade or fail if not addressed properly. It is always desirable to tune the beamwidth of the mainlobe to cater for the mismatch of DOA due to estimation error or inaccuracy of element calibration. Various robust algorithms [65, 110, 111] have been proposed to cater for the mismatch of DOA by putting in constraints to broaden the main beam. The Flat Top shaped beam pattern [112, 113, 114, 115, 116] is thus increasingly attractive due to its flat response to large DOA mismatch, especially in high mobility scenarios when the DOA changes more rapidly.

Beam pattern synthesis is an extensively investigated area in antenna array beamforming design. Many algorithms have been proposed in the literature to achieve the optimization of low Sidelobe Level (SLL) [117, 118], high gain and narrow mainlobe. Schelkenoff [119] established the link between nulls of the beam pattern and the complex roots of the polynomials that represent the Z transform of the beamformer weights. By spacing out the zeros in the unit circle differently, many patterns could be synthesized. Dolph [120] proposed to use the properties of Chebyshev polynomials [121] of the first kind to achieve equal Sidelobe Level and the narrowest main beam. Subsequently, Riblet [122] discovers that Dolph's method only applies to scenarios where the antenna

elements spaced at least half wavelength. The original Dolph-Chebyshev array is then extended to scenarios with less than half wavelength inter-element space where a different mapping could be applied to use the Chebyshev polynomials. A similar pattern for continuous apertures is proposed by Taylor [123] with a modification that the far out of the sidelobes can decay faster following a uniform array pattern while keeping the sidelobes close to the mainlobe with equip-ripple as in Dolph-Chebyshev array. To implement the same pattern directly for a discrete array, Villeneuve [124] proposed a method to replace the last few zeros of the array response with the zeros of a uniform array. Different window methods like Gaussian [125] and the derivative of Chebyshev [126] have been reported to get a decaying sidelobe shape with narrower main lobe for improved efficiency. In [127], a modified Chebyshev array is proposed to make the SLL, beamwidth to be adjustable independently. But since the modified function is non-linear and can't be expressed as polynomials, an iterative method has to be used to derive the converged weight.

Although these methods synthesize beam patterns with low SLL, narrow or adjustable main beam, the shaped beam pattern is not part of their optimization goal. To get flat-top beam pattern, Finite Impulse Response (FIR) based algorithms and various numerical optimization algorithms over an objective or cost function could be used. Window method [112] based on FIR algorithm is popular due to its robustness and ease of implementation. But due to its extra constraints of the same level of ripples in pass band and stop band, it is not optimum for the filter order [52]. Iterative methods based on numerical optimization algorithms like minimum mean squared optimization [128], or stochastic based Genetic Evolution algorithm [129], Particle Swarm Optimization algorithm [113, 130] and various convex optimization based algorithms [131] normally are used for getting shaped main beam. However iterative methods might not be suitable for high mobility scenarios where real-time calculation usually is needed.

In this chapter, the Zero Placement method based on Schellkenoff polynomial is used to synthesize Flat Top beam pattern directly. Although a similar concept of zero replacement is used in [124], their adjustment is still restricted on the unit circle. So its effect in the main beam is limited to the null-to-null beamwidth and gain. And the main beam shape can not be controlled. In this chapter, by relaxing this restriction, the zeros can be placed off the unit circle instead of replacing part of the Dolph-Chebyshev zeros with uniform array zeros located on the unit circle. This step makes

the main beam shape controlling possible. The proposed Zero Placement Flat Top (ZPFT) algorithm breaks the array factor into two parts. For an N elements antenna array which has $N - 1$ zeros of freedom for beam pattern control, two of the zeros are reserved for synthesizing the flat-top shaped main beam. The rest $N - 3$ zeros can be used for any other existing low SLL window methods. Due to the unique feature that forms narrowest mainlobe with a given Sidelobe Level (SLL) or lowest SLL with a given null to null beamwidth of mainlobe, Dolph-Chebyshev array is chosen for the $N - 3$ zeros allocation. But other window functions could also be used. The key innovation for the algorithm proposed in this chapter is two folds. Firstly, the off unit circle zeros are explored directly to mix with unit circle zeros from Dolph-Chebyshev to control the main beam shape. Secondly, the quadratic function approximation is used to investigate the flat-top effect of the proposed zero location and an algorithm is developed to identify the location of zeros for flat-top control. So that it achieves lower SLL compared with FIR method with the same flat-top pattern directly with simple zero placement in the spatial angle domain. This also makes the steering of the main beam straightforward. Furthermore, when comparing to iteration based global optimization methods, it achieves the same optimum beam pattern and takes 380 times less computing time in an Intel Core i7 Windows platform as the simulation shows for an ULA with 8 elements. All these make ZPFT an ideal candidate for high mobility applications where the DOA changes rapidly. To the best of our knowledge, it is the first time Dolph-Chebyshev zeros are combined with the off unit circle zeros to realize flat-top main beam shape while preserving the narrow main beam property. This different way of zero arrangement makes ZPFT simple yet effective and gives ZPFT the advantage of synthesizing flat-top shaped beam patterns while maintaining low SLL in a steering adjustment efficient way compared with existing methods in the literature.

The chapter is organized as follows, after the problem model is established in section 4.2, the zero placement algorithm for synthesizing flat-top beam pattern is described in section 4.3. Numerical simulation is conducted in section 4.4 which compares the proposed algorithm with the existing algorithms. In the end section 4.5 concludes the chapter.

4.2 Problem Formulation

For clarity of the discussion, the system model for Uniform Linear Array (ULA) with N antenna elements as illustrated in Fig. 2.4 is used. As indicated by Schelkunoff [119], every ULA could be represented as a polynomial and vice versa. According to fundamentals of polynomial, the Array Factor (AF) defined by (2.9) could be factored by its $(N - 1)$ roots as

$$\begin{aligned} H(Z) &= \sum_{i=1}^N w_i z^{-(i-1)} \\ &= \prod_{i=1}^{N-1} (z - z_i) \end{aligned} \quad (4.1)$$

where each z_i gives a null response for the angle that defined by $e^{j\xi_i} = z_i$ and $z = e^{j\xi}$ is evaluated along the unit circle. As indicated in (4.1), the Array Factor for a N elements array could be uniquely characterized by its $N - 1$ zeros.

So the objective of this chapter is to synthesize a flat-top beam pattern with low SLL by identifying the proper location of zeros.

4.3 Proposed Solution

For ULA, the number of zeros uniquely defines the Z transform of the weight vector thus also defines the array factor. Inspired by the concept of [1], the polynomial of Z (2.9) could break into two parts.

$$H(z) = C(z)B(z) \quad (4.2)$$

where $C(z)$ corresponds to the sub-polynomial that generates beam pattern without flattening constraints, and $B(z)$ represents the portion that compensates and flattens the main lobe. $N - 3$ zeros are allocated for $C(z)$ as

$$C(z) = \prod_{i=3}^{N-1} (z - z_i) \quad (4.3)$$

which represents the sub-array that controls the main beam width and SLL. Two zeros are allocated for $B(z)$ as

$$B(z) = (z - z_1)(z - z_2) \quad (4.4)$$

which represents the broadening sub-array that creates the flat-top and decaying far-out sidelobes.

4.3.1 Narrow Mainlobe Beam Width with Low SLL Controlled by $C(z)$

In this chapter, the sub-array represented by $C(z)$ is implemented through the Dolph-Chebyshev algorithm due to its simplification. For clarity, the inter element space is assumed to be half wavelength. Since two zeros represented by $B(z)$ are reserved for the flat-top control, the actual elements for implementing the Dolph-Chebyshev array will be $N - 2$ elements.

In Dolph-Chebyshev array, there is only one scaling parameter R_0 that controls both the main beam width and SLL which maps the spatial frequency ξ range to the abscissa of the Chebyshev polynomial range [122]. The Chebyshev polynomial used for $C(z)$ could be defined as

$$T_{N-3}(x) = \begin{cases} \cos((N-3) \cdot \arccos(x)), & \text{for } |x| \leq 1 \\ \cosh((N-3) \cdot \operatorname{acosh}(x)), & \text{for } |x| > 1 \end{cases} \quad (4.5)$$

where $x = R_0 \cos(\frac{\xi}{2})$ is the scaled input for the Chebyshev polynomial. The scaling factor R_0 could be derived from the null to null beam width as:

$$R_0 = \cos\left(\frac{\pi}{2(N-3)}\right) \cdot 1 / \cos\left(\pi \frac{d}{\lambda} \cdot \sin(bw/2)\right) \quad (4.6)$$

where bw is the required null to null beam width.

By setting $T_{N-3}(x) = 0$ for $|x| \leq 1$, all the $N - 3$ zeros could be found as [48, p. 1147]

$$\xi_i = 2 \cdot \arccos\left(\frac{x_i}{R_0}\right) \quad (4.7)$$

where $x_i = \cos\left(\frac{(i-1/2)\pi}{N-3}\right)$, $i = 1, 2, \dots, N - 3$.

4.3.2 Zero Placement for Flat Top Constraints Sub-Array $B(z)$

To find the zero locations of $B(z)$ to flatten the beam pattern of the main lobe, it would be necessary to understand the pattern around the main lobe and the impact of the location of zero $(r_0, 0)$ on the pattern.

As illustrated in Fig. 4.1, each angle $\xi = \frac{2\pi d}{\lambda} \sin(\theta)$ corresponds to a DOA θ . The main lobe is assumed at point c which corresponds to 0 degree measured from the broadside. It is clear from Fig. 4.1 that $|z - r_0|$ reaches the minimum when z is at c which corresponds to the main lobe.

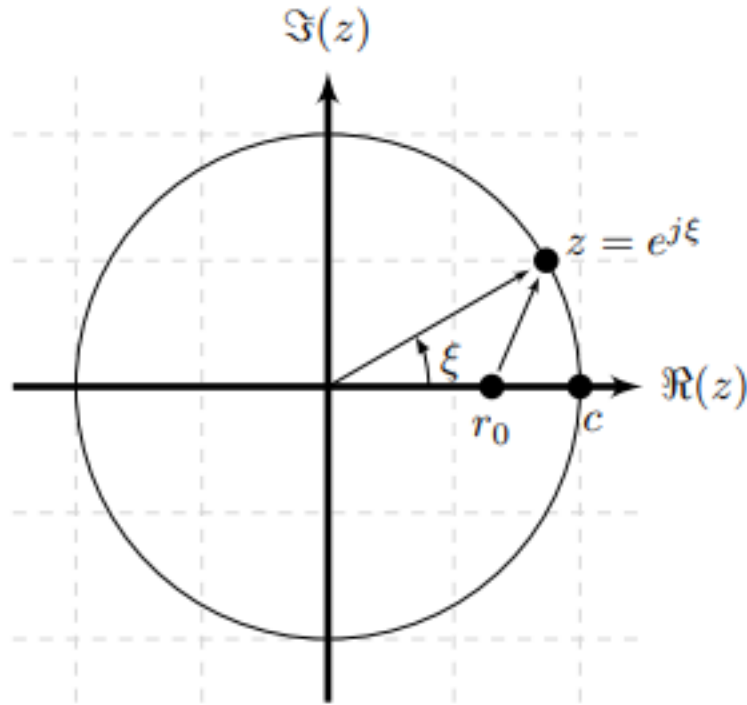


Figure 4.1: Norm $|z - r_0|$ for a Zero Placed at $(r_0, 0)$

The distance d_{r_0} between z and r_0 could be described as (4.8).

$$\begin{aligned} d_{r_0}(\xi) &= |z - r_0| \\ &= \sqrt{1 - 2 \cos(\xi)r_0 + r_0^2} \end{aligned} \quad (4.8)$$

To further investigate the curve effect of r_0 , $d_{r_0}(\xi)$ could be expanded using the second order Taylor series around point c which corresponds to the main lobe at $\xi = 0$ as

$$d_{r_0}(\xi) \approx \hat{d}_{r_0} = d_{r_0}(0) + d'_{r_0}(0)\xi + \frac{1}{2}d''_{r_0}(0)\xi^2 \quad (4.9)$$

where d'_{r_0}, d''_{r_0} indicates the first and second derivative of d_{r_0} respectively. After taking

derivative of (4.8), it is easy to find out that:

$$d'_{r_0}(0) = \frac{r_0 \sin(\xi)}{\sqrt{1 - 2 \cos(\xi)r_0 + r_0^2}} \Big|_{\xi=0} = 0 \quad (4.10)$$

$$d''_{r_0}(0) = d''_{r_0}(\xi) \Big|_{\xi=0} = \frac{r_0}{1 - r_0} \quad (4.11)$$

So the second order Taylor series could be expressed:

$$\hat{d}_{r_0}(\xi) = \frac{r_0}{2(1 - r_0)} \xi^2 + 1 - r_0 \quad (4.12)$$

For using this as a broadening function, the shaping parameter is derived as

$$\begin{aligned} k_b &= \frac{d_{r_0}}{\frac{1}{2}d''_{r_0}} \\ &= \frac{2(1 - r_0)^2}{r_0} \end{aligned} \quad (4.13)$$

Fig. 4.2 shows the effect of zero location on the amplitude response. It is clear that when r_0 moves to the origin, it gives an all-pass response that will not change the amplitude response. On the other hand, when r_0 moves towards the unit circle, it creates a dip at the main lobe.

By examining the effect of zeros in Fig. 4.2, the dip effect at angle 0 could be used for creating the flat-top pattern in the mainlobe. So the z_1 could be just located in the real axis and off the unit circle at $(r_0, 0)$. Fig. 4.2 shows that the broadening zero at z_0 has a side effect of raising the far-out sidelobe level as also indicated in [132]. An extra zero $(-1,0)$ could then put in to compensate for the effect. So the two zeros for $B(z)$ could be designed as:

$$B(z) = (z - r_0)(z + 1) \quad (4.14)$$

With (4.2),(4.5),(4.14), the transfer function could be derived as:

$$H(z) = T_{N-3}(R_0 \cos(\pi \frac{d}{\lambda} \sin(\theta)))(z - r_0)(z + 1) \quad (4.15)$$

where θ is the azimuth angle. The power distribution of the beam pattern could then

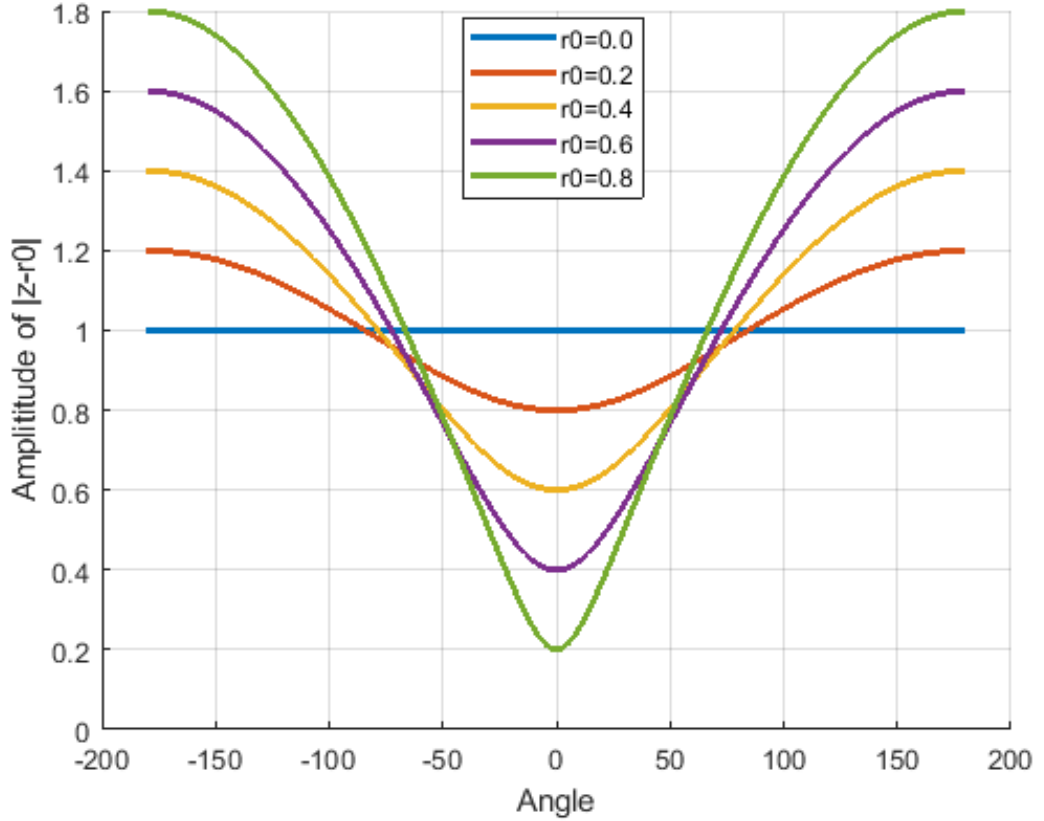


Figure 4.2: Zero Location Effect on Amplitude Response

be evaluated along the unit circle as:

$$P(\theta) = |T_{N-3}(R_0 \cos(\frac{\pi d}{\lambda} \sin(\theta))(z - r_0)(z + 1))|_{z=e^{j\frac{2\pi d}{\lambda} \sin(\theta)}}^2 \quad (4.16)$$

4.3.3 Principle Condition for Flattening a Second Order Polynomial with a Broadening Polynomial

The flat-top effect of the zero z_0 is investigated through an approximation with a second order polynomials in this section. For a second order even polynomial that have a curvature peak at $x = 0$,

$$f(x) = -a_1x^2 + b_1 \quad (4.17)$$

where $a_1 > 0$ and b_1 can be any real value, a broadening polynomial

$$b(x) = a_2x^2 + b_2 \quad (4.18)$$

where $a_2 > 0$ could be applied to obtain a flat-top function

$$p(x) = f(x)b(x) \quad (4.19)$$

where $p(x)$ represents a resultant function that has a flat-top. To get the condition for broadening function $b(x)$ to be effective, the derivative of (4.19) could be investigated

$$\begin{aligned} p'(x) &= \frac{d}{dx}(-a_1x^2 + b_1)(a_2x^2 + b_2) \\ &= x(-4a_1a_2x^2 + 2(-a_1b_2 + a_2b_1)) \end{aligned} \quad (4.20)$$

where $\frac{d}{dx}$ indicates the derivative operator.

By forcing (4.20) to 0, the peak of $p(x)$ could be located as

$$x_0 = 0 \quad (4.21)$$

$$x_{1,2}^2 = \frac{1}{2}\left(\frac{b_1}{a_1} - \frac{b_2}{a_2}\right) \quad (4.22)$$

where x_0 represents the original peak location, $x_{1,2}$ is the two possible peak locations introduced by the broadening polynomial.

By defining shape parameters as

$$k_f = \frac{b_1}{a_1} \quad (4.23)$$

$$k_b = \frac{b_2}{a_2} \quad (4.24)$$

and controlling factor as

$$k = \frac{k_b}{k_f} \quad (4.25)$$

where k_f, k_b is the shape parameter for original function and broadening function respectively, and k is the controlling factor for regulating the broadening effect, (4.22) could be simplified as:

$$x_{1,2}^2 = \frac{1-k}{2}k_f \quad (4.26)$$

In the practical beamforming context, $k_f > 0$ is always satisfied. With this assumption,

the principle condition for the broadening polynomial could be summarized as:

$$p(x) = \begin{cases} \text{no flat top,} & \text{for } k > 1 \\ \text{flat top,} & \text{for } k = 1 \\ \text{flat top with variation,} & \text{for } k < 1 \end{cases} \quad (4.27)$$

This concept is illustrated with an example polynomial $f_1(x) = 2x^2 + 20$ in Fig. 4.3. It shows that with $k = 1$, the production patched function $p(x)$ has a flat-top without variation. When $k = 0.2, 0.5, 0.7$, the top is broadened but also exhibit a dip in the original top. The smaller the k value, the deeper the dip and the wider the broadening effect. As a contrast, it barely shows the broadening effect when $k = 3$. It could be explained from (4.22), when $k > 1$, there is no real roots for (4.20) except at $x = 0$ which means there is only one extreme point: the original top point.

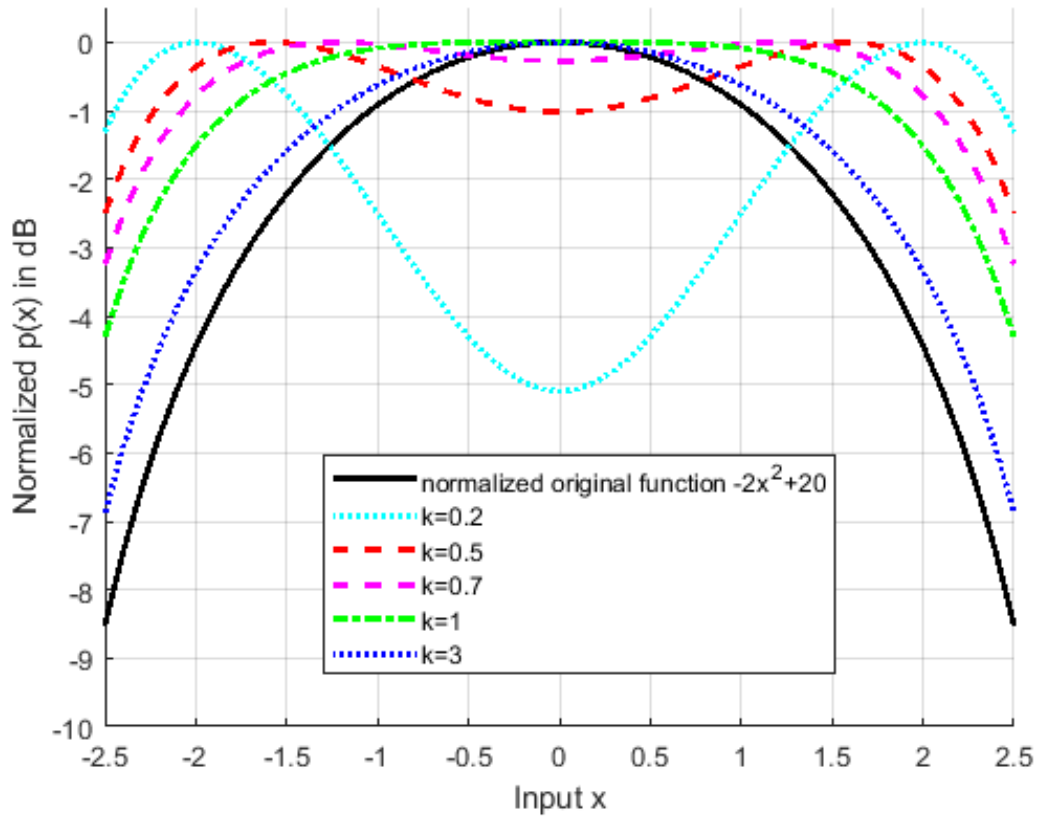


Figure 4.3: Concept to Flatten a Second Order Even Polynomial Function

Since the peak occurs at the extreme point x_1, x_2 and the dip occurs at x_0 , the

variation within the broadened range could be easily calculated as:

$$\begin{aligned}\delta &= \frac{p(x_1)}{p(x_0)} \\ &= \frac{(1+k)^2}{4k}\end{aligned}\quad (4.28)$$

where the δ represents the variation within the broadened band and k is the controlling factor as defined in (4.22).

So for a given δ , the controlling factor k could be derived as

$$k = 2(\delta - \sqrt{\delta^2 - \delta}) - 1 \quad (4.29)$$

by finding the roots of (4.28).

4.3.4 Main Lobe Pattern Approximation by Taylor Series Expansion

In the main lobe region, the beam pattern could be Taylor expanded to get a second order polynomial approximation as

$$\begin{aligned}f(\xi) &= \cosh(Nx) \\ &\approx \hat{f}(\xi) = f(0) + f'(0)\xi + \frac{1}{2}f''(0)\xi^2\end{aligned}\quad (4.30)$$

where $x = a\cos(R_0\cos(\xi))$ represents the normalized angle, and $f'(\cdot)$, $f''(\cdot)$ indicates the first and second derivative operator of $f(x)$ respectively. With simple manipulation, the the derivatives could be derived as:

$$f'(0) = N \cdot \sinh(Nx) \frac{(-R_0 \sin(\xi))}{\sqrt{R_0^2 \cos(\xi)^2 - 1}} \Big|_{\xi=0} = 0 \quad (4.31)$$

$$f''(0) = f''(\xi)|_{\xi=0} = N \cdot \sinh(Nx) \frac{-R_0}{\sqrt{R_0^2 - 1}} \quad (4.32)$$

Treat this expansion as the original function to be broadened, the shape parameter

could be derived as

$$\begin{aligned}
k_f &= \frac{f(0)}{-\frac{1}{2}f''(0)} \\
&= \frac{2\sqrt{R_0^2 - 1}}{R_0 N \cdot \tanh(Nx)} \\
&\approx \frac{2\sqrt{R_0^2 - 1}}{R_0 N}
\end{aligned} \tag{4.33}$$

where the approximation is made due to $\tanh(Nx)|_{\xi=0} \approx 1$. The location of r_0 for the broadening could then be derived according to (4.25) as

$$\frac{(1 - r_0)^2}{r_0} = \frac{k\sqrt{R_0^2 - 1}}{N \cdot R_0} \tag{4.34}$$

Solving (4.34), r_0 could be derived as:

$$r_0 = 1 + \frac{1}{4}(kk_f \pm \sqrt{(kk_f)^2 + 8kk_f}) \tag{4.35}$$

where k is the controlling factor as defined in (4.25) and k_f is the original function to be broadened as defined in (4.33). One interesting finding from (4.35) is that there are two r_0 satisfy the requirement. They are conjugated to each other in the complex angle sense [133]. For beamforming implementation purpose, the $r_0 < 1$ will be taken.

4.3.5 Algorithms for the Synthesis of Flat Top Beam Pattern

With the preparation of the previous sub-section, the algorithm for the synthesis of flat-top beam pattern could then be described as a 3 steps process. Firstly, based on the input requirement of number of antenna elements N and SLL value or Beamwidth, the $N - 3$ zeros of the $N - 2$ elements Chebyshev array are calculated. Secondly, based on the requirement of the allowed variation, the last two zeros location are calculated. In the end, the complete N weights are derived from the whole $N - 1$ zeros. The details of the algorithm are described below.

Algorithm 1 Synthesis of Zero Placement Controlled Flat Top Beam Pattern

Require: Input($N, sll, bw, d, \lambda, \delta$) N : Number of Antenna Elements sll : Sidelobe Level bw : Null to Null Mainlobe Beamwidth d : Antenna Element Space λ : Wave Length of Incident Signal δ : Allowed Variation in the mainlobe beam

```
1: //Derive  $R_0$  for  $(N - 2)$  elements based on  $sll$  or  $bw$ 
2: if  $sll = null$  then
3:    $L = 10^{sll/20}$ 
4:    $R_0 = \cosh(\frac{\text{acosh}(L)}{(N-3)});$ 
5: else
6:    $R_0 = \cos(\frac{\pi}{2(N-3)}) \cdot 1/\cos(\pi \frac{d}{\lambda} \cdot \sin(\frac{bw}{2}))$ 
7: end if
8: //Find all zeros for Chebyshev sub-polynomial
9: for  $i$  in 1 to  $(N - 3)$  do
10:   $z_{i+2} \leftarrow e^{j \cdot 2 \cdot \text{acos}(\frac{1}{R_0} \cos(\frac{(2i-1)\pi}{2(N-3)})}$ 
11: end for
12: //Find a proper controlling factor  $k$  based on allowed variation  $\delta$ 
13:  $k = 2(\delta - \sqrt{\delta^2 - \delta}) - 1$ 
14: //Derive shape parameter  $k_f$  for the second order Taylor expansion of Chebyshev
    Response
15:  $k_f = \frac{2\sqrt{R_0^2 - 1}}{R_0(N-3)}$ 
16: //Derive  $r_0$  for the broadening zero location
17:  $r_0 = (1 + \frac{1}{4}(kk_f \pm \sqrt{(kk_f)^2 + 8kk_f})) \cdot \alpha$ 
18:  $z_1 \leftarrow r_0$ 
19:  $z_2 \leftarrow -1$ 
20:  $C(z) \leftarrow \prod_{i=1}^{N-1} (1 - z_i z^{-1})$ 
21: for  $i$  in 0 to  $N-1$  do
22:   $w(i + 1) \leftarrow$  coefficient of  $z^{-i}$ 
23: end for
```

For a N element Uniform Linear Array (ULA), there are total $N - 1$ zeros for distribution. In steps 1 to 11, $N - 3$ zero are used to build the Chebyshev array using

the SLL or Beamwidth constraints. The left two zeros are used for the broadening effect. In steps 12-13, the controlling factor is decided, there is some flexibility for the value of k and it depends on how much variation is allowed inside the main beam. In steps 14-15, the second order Taylor expansion is used to approximate the Chebyshev response, so that the broadening theory developed using the second order polynomial could be used to calculate the shape parameter k_f . Then in steps 17-18, the location of the broadening zero r_0 is derived. During implementation, an optional adjustable factor α could be applied to r_0 to compensate for the approximation error. In practice, $\alpha = 0.9$ gives a good matching result. In step 19, an extra zero is placed at $(-1,0)$ to balance the effect of r_0 for remaining low SLL.

4.4 Numerical Simulation and Analysis

To verify the performance of the proposed ZPFT algorithm, two simulations are set up for the comparison with two types of popular algorithms, window method and numerical optimization method. The third simulation is to show the ripple effect of the k factor and the easy steering of the flat-top main beam. The window method based on FIR algorithm is popular due to its simplicity although not optimum[52] as it just applies a window function to an ideal filter response to smooth out the transition band. Recently, the convex optimization for beam pattern synthesis becomes more and more popular with the readily available optimization packages like CVX [134]. When shaped beam pattern synthesis is formulated as an optimization problem, the constraints on the amplitude in the pass band is often non-convex. One of the most promising way to apply convex optimization is to use the Semi-definite Relaxation (SDR) algorithm which drops the rank one requirement of the correlation matrix to make it a convex optimization program [135, 136, 137].

4.4.1 Lower SLL or Narrower Null to Null Beamwidth Compared with Window Method

In the first simulation, ZPFT is compared with window method based on FIR and Dolph-Chebyshev to demonstrate that ZPFT is able to deliver the same main beam as the window methods but with much lower SLL or narrower null to null beamwidth. A 7 elements ULA with flat-top beam pattern with -52dB SLL as designed in [112] is used for comparison for FIR based algorithm. The design parameter is listed below in

Table (4.1).

Table 4.1: Design Parameter for Simulation of Comparison with Window Method Based on FIR

Parameter	Name	Value
N	Number of Elements	7
bw	Null to Null Beamwidth	$\leq 120^\circ$
sll	Sidelobe Level	$\leq -52dB$
d	Space between Element	half wavelength
ξ	Steering Direction	0

Fig. 4.4 shows the performance of the synthesized beam pattern following the requirements in Table (4.1). ZPFT algorithm can be controlled by beamwidth or SLL. Both methods are used in this simulation for comparison. It shows clearly that while FIR algorithm used in [112] does make a flat-top beam pattern, the synthesized SLL is around -52.7dB. In contrast, the proposed ZPFT algorithm by beamwidth gives a much lower SLL of around -75dB with the same broadened flat-top main beam width of 25° , the same null to null beamwidth of 60° and a negligible ripple of 0.25dB as shown from the zoomed view of the flat top pattern in Fig. 4.4. When SLL is a design parameter, the proposed ZPFT algorithm by SLL gives the much narrower null to null beamwidth of 102° with the same SLL level of around -52dB and the same flat-top main beamwidth of 25° . As for the Dolph-Chebyshev algorithm, although it achieves the lowest SLL of around -110dB, it has no control of the beam pattern of the main beam.

Table (4.2) shows the synthesized array using the 3 algorithms where ZPFT is simulated twice with two different controlling parameter. The null to null beamwidth controlled ZPFT is labeled as ZPFT-bw while SLL controlled ZPFT is labeled as ZPFT-sll.

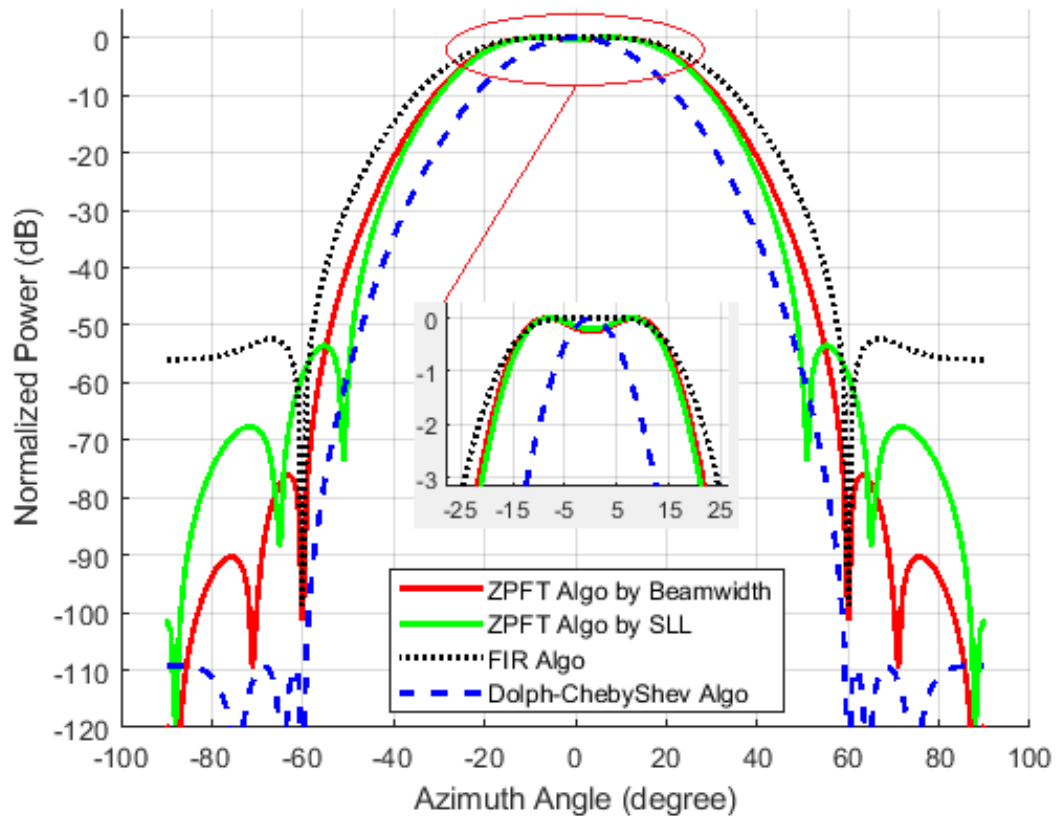


Figure 4.4: Synthesized Beam Pattern Comparison between FIR, ZPFT and Dolph-Chebyshev

Table 4.2: Synthesized ULA for Dolph-Chebyshev, FIR and ZPFT

Weight	Dolph-Chebyshev	FIR	ZPFT-bw	ZPFT-sll
1	1	-0.0345	1	1
2	5.7194	0	4.1955	3.9514
3	13.8972	0.2849	6.5144	6.1855
4	18.3554	0.4992	3.7567	4.2607
5	13.8972	0.2849	-0.8395	0.3377
6	5.7194	0	-1.8773	-1.1795
7	1	-0.0345	-0.6000	-0.4907

For the listed three algorithms, the parameter of the beam width and SLL are interlinked and can't be controlled independently. In the above simulation, the same width of the flat main beam pattern is achieved for both FIR and ZPFT. But as demonstrated, when null to null beamwidth is specified, ZPFT-bw gives much better attenuation in the sidelobe which is around 22dB lower than the FIR algorithm. When

the SLL is specified, ZPFT gives a much narrower null to null beamwidth which is around 18° narrower. Although the Dolph-Chebyshev synthesized pattern has the lowest SLL, it is not suitable for the intended usage where flat top beam pattern is needed for robust beamforming to cater for DOA mismatch.

4.4.2 Faster Calculation Speed Compared with Numerical Optimization Method

The second simulation is set up to demonstrate that compared with the iteration based global optimisation methods like SDR, the proposed ZPFT can deliver the same optimal beam performance but with much lower computation complexity. The design parameter is listed in Table (4.3).

Table 4.3: Design Parameter for Simulation of Comparison with SDR

Parameter	Name	Value
N	Number of Elements	8
bw	Null to Null Beamwidth	106°
d	Space between Element	half wavelength
ξ	Steering Direction	0
pr	Passband Ripple	$\leq 2\text{dB}$

Fig. 4.5 shows the synthesized beam. The optimization objective is set to minimize the stop band response and the pass band ripple is set to less than 2dB. ZPFT achieves the same pass band performance. Only at the first sidelobe as shown in the zoomed view in Fig. 4.5, ZPFT shows around 2dB lesser attenuation. But at the far end, it achieves much better attenuation.

Table (4.4) shows the synthesized array with the two algorithm SDR and ZPFT.

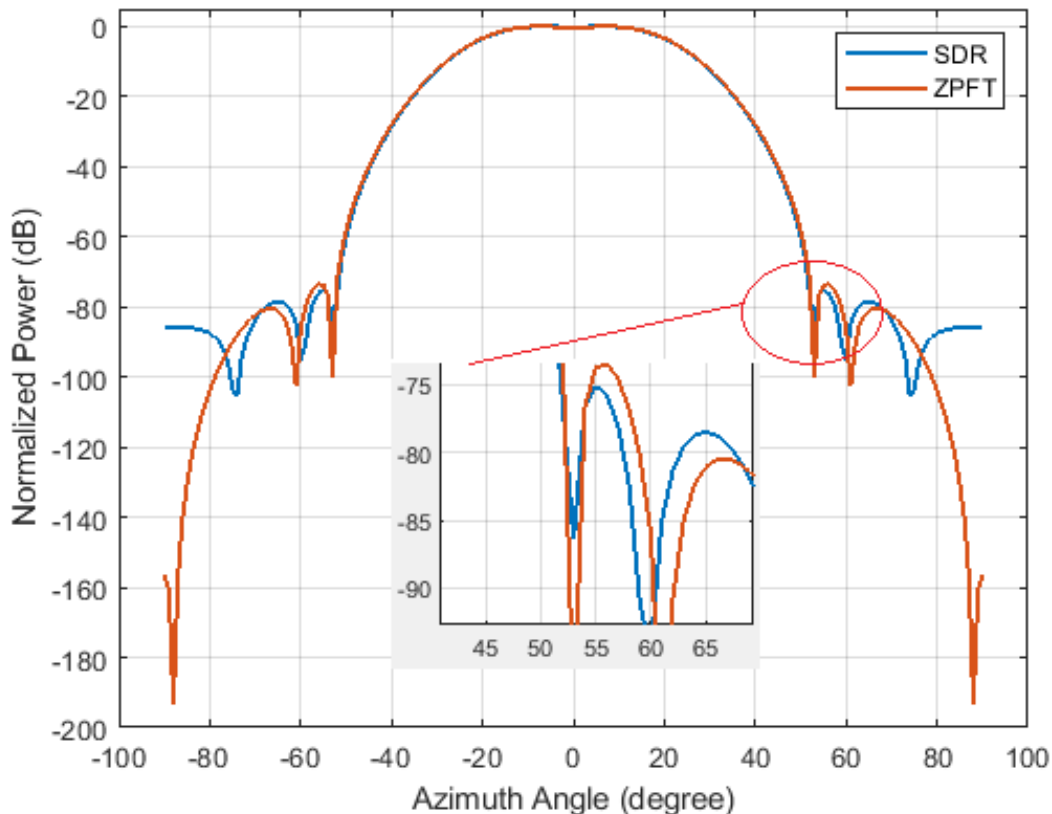


Figure 4.5: Synthesized Beam Pattern Comparison between SDR and ZPFT

Table 4.4: Synthesized ULA for SDR and ZPFT

Weight	Semi-definite Relaxation	ZPFT
1	-0.0321730	1
2	-0.1107191	4.94610614
3	-0.0667814	10.0811574
4	0.27006853	10.2004021
5	0.64181062	4.14318630
6	0.63031549	-1.2397797
7	0.30998210	-1.8366604
8	0.06326148	-0.5190451

With this comparable performance, ZPFT takes only 0.003 seconds. Compared with 1.15 seconds of the SDR method, ZPFT runs 383 times faster than SDR in an Intel Core i7 Windows laptop where CVX [134] 2.2 software is used for the SDR implementation. This makes it suitable for real time applications as required in high

speed rail scenario.

4.4.3 Impact of k Factor and Steering of Main Beam by Angle Shift

The third simulation is set up to illustrate the effects of shape factor k on the flattened pattern. To verify the impact of the controlling factor, a simulation for 8 elements antenna with different controlling factor k is conducted. The design parameter is listed below in Table (4.5)

Table 4.5: Design Parameter for Impact of Shape Factor k Simulation

Parameter	Name	Value
N	Number of Elements	8
bw	Null to Null Beamwidth	100°
d	Space between Element	half wavelength
ξ	Steering Direction	0
pr	Passband Ripple	$\leq 3\text{dB}$

Fig. 4.6 shows the effect of k on the beam shape. It is clear that the higher the value of k , the narrower the beam width. The broadening of the beam width comes with a price of increased SLL. When k decrease from 10 to 0.5, the SLL increased from -58dB to -50dB. From the zoomed view of the main beam in Fig. 4.6, it is clear that when k is decreasing from 10 to 0.5, the ripple in the main beam increases from 0 to 3dB.

Since the ZPFT algorithm is directly working in the spatial angular domain, the steering of the main beam becomes straight forward. It could be implemented by just shifting the angle of the derived zeros. To illustrate the shifting capability, the design parameter is listed below in Table (4.6)

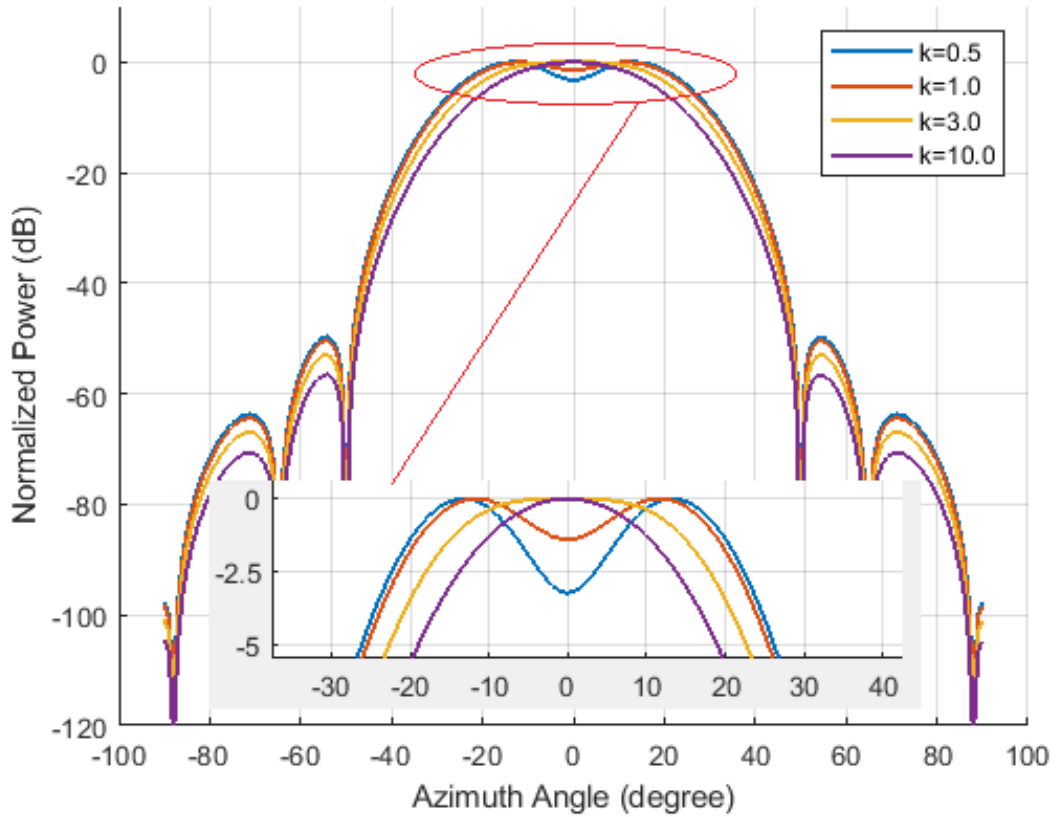
Figure 4.6: Beam Pattern Effect of Controlling Factor k

Table 4.6: Design Parameter for Main Beam Shifting Simulation

Parameter	Name	Value
N	Number of Elements	20
bw	Null to Null Beamwidth	50°
d	Space between Element	half wavelength
ξ	Steering Direction	$-15^\circ, 0^\circ, 15^\circ, 20^\circ$
pr	Passband Ripple	$\leq 1\text{dB}$

Fig. 4.7 shows the steering of the DOA of the synthesized 20 elements ULA with the above parameter.

In practical scenario, a value of 1-3 would be recommended for k to get a flat top beam pattern with pass band ripple less than 1dB. In this chapter, $k = 1$ is set for the first simulation, while $k = 2$ is set for the rest of simulations.

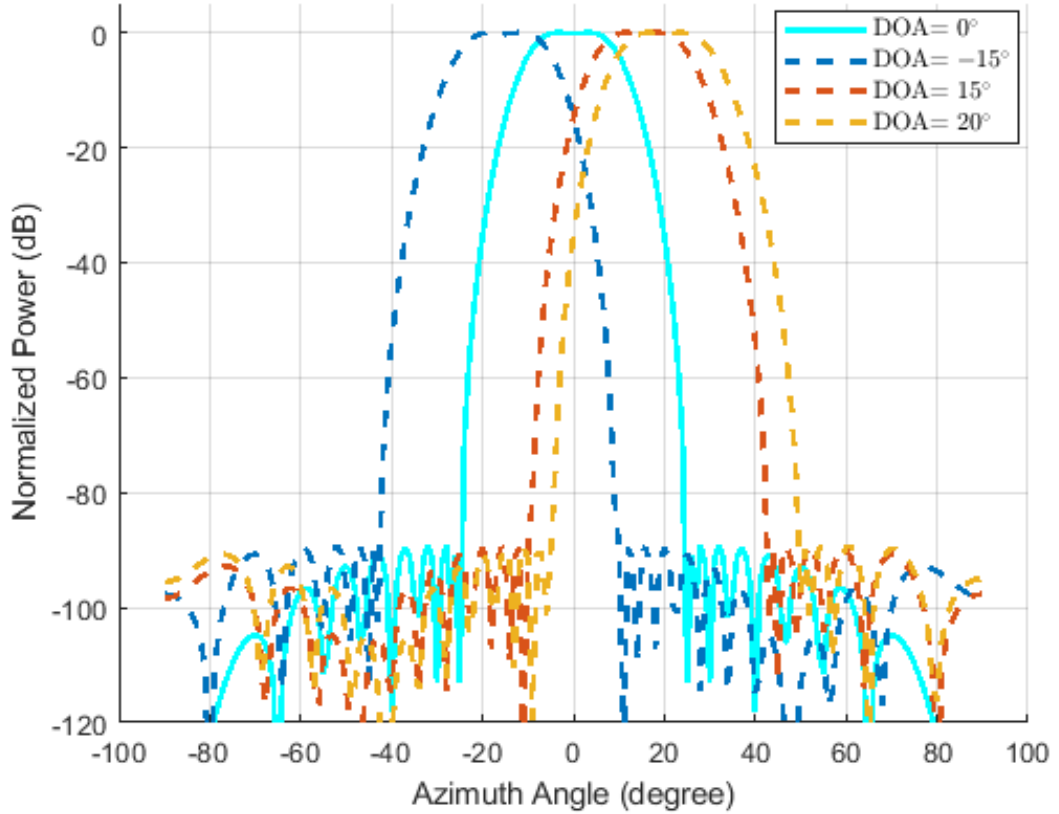


Figure 4.7: Main Beam Steering Control for ZPFT Algorithm

4.5 Summary

By breaking the array factor into two separate parts, a flat-top and narrow main beam with low SLL could be synthesized directly in the Z domain. The beam width requirement with low SLL is realized through the use of Dolph-Chebyshev array or other suitable window methods. The flat-top constraints is realized through two reserved zeros in the real axis where one of the zero is derived from the analysis of the broadening effect of two quadratic functions and the other zero is placed for keeping the SLL low. The simulation results confirm that ZPFT can achieve 22dB lower SLL while maintaining the same main beam performance as compared with FIR method for a 7 elements ULA. It can achieve the same optimal performance as demonstrated by the iteration based global optimisation techniques, with about 380 times less computing time in an Intel Core i7 platform. ZPFT can steer the main beam easily in real time by just doing an angle shift in the unit circle which makes it suitable for high mobility application where the DOA is changing fast.

Chapter 5

Adaptive Beamformer Design and Implementation in Transportation Market

5.1 Introduction

Adaptive Beamforming is a widely used technique in wireless communication [15], acoustic sensors array [138], medical imaging [18] and other fields to improve signal quality. The fundamental task of adaptive beamforming is to combine the output from an array of spatially separated sensors in a way to minimize a predefined cost function adaptively so that a particular performance criteria could be satisfied. Working as a spatial filter, it can enhance signal from an interested look direction and reject noise or interference from other directions. In intelligent transportation systems like HSR, the high mobility creates unique challenges for the wireless communication [32]. The time varying DOA [139] is a known issue that adaptive beamformer needs to tackle. The rapid change of DOA in these kinds of scenarios put even higher demand on the calculation speed for the adaptive beamformer. This chapter introduces a fast Blocking Matrix generating algorithm named SZPA for GSC [140] adaptive beamformer to improve the calculation speed. As a general Blocking Matrix generating algorithm, the SZPA can be used for any GSC application.

As a widely used beamforming architecture, GSC has the benefit of converting a constrained optimization problem to an unconstrained problem [5] while maintaining the same performance as LCMV as proved in [141]. Thus many adaptive algorithm like LMS, NLMS, RLS etc. could be directly applied in the noise cancellation path.

The major components of a GSC beamformer include fixed beamformer, blocking matrix, and adaptive controller. The fixed beamformer in GSC controls the quiescent response. It could be implemented by many radiation pattern synthesis techniques like Sample Matrix Inversion (SMI) and various iterative methods that are based on adaptive beamformer principle which includes Iterative Fourier Transform method [142, 16] and the latest virtual jammer based methods [143]. The adjustable step size has been investigated in [3] and the included references.

Blocking matrix is a critical component [140] for GSC beamformer which blocks out the desired signals from being leaked to the cancellation path and thus being canceled as interference. A systematic approach for deriving the blocking matrix has been documented in [144]. As summarized in [39, p. 40], there are two major methods to derive the blocking matrix. When the SOI is from the broadside or the received signal from each sensor has been aligned to be synchronized towards the SOI, the blocking matrix could be implemented as a simple Cascaded Differential Column (CCD) as in the original GSC proposal by Griffiths [140]. But its usage is limited to broadside beamformer or systems that have delay adjustment for each sensor element. To support beamforming towards arbitrary directions without pre-processing, SVD [145] based method is normally used to get the null basis of the constraint matrix. But SVD method is known to be computation intensive.

In scenarios like vehicle to roadside sensor communication where the DOA changes rapidly, the signal cancellation caused by the DOA mismatch [146] becomes more severe. Various Robust Beamforming Algorithms (RBF) has been investigated in the past decades to address this issue. The RBF based on Diagonal Loading [147] reduces the sensitivity to the SOI mismatch by adding a diagonal matrix to the covariance matrix, which is equivalent to putting a quadratic inequality constraint on the weight vector [45, p. 506]. But there is no systematic way for deriving the loading factor. The more recent RBF based on Interference plus Noise Covariance (IPNC) Matrix Reconstruction algorithm address this issue by removing the SOI component from IPNC matrix and make a better estimation of SOI based on Capon spatial spectrum weighted reconstruction [148] or Maximum Entropy Power Spectrum (MEPS) weighted reconstruction [92]. But it requires expensive matrix inversion and integration operation and might not be suitable for the DOA rapid changing scenarios. The RBF based on Derivative Constraint for the weight vector in the direction of SOI is first proposed in [65] and proves to be effective. Later the derivative constraint concept is extended

to GSC architecture by [149] which controls the flatness of the null in the blocking matrix. Both methods require additional degree of freedom in the blocking matrix for each derivative constraint put in. The other promising way is to increase the speed of DOA estimation or tracking, and at the same time improve the calculation speed of the weight vector. It would require the blocking matrix to be recalculated more frequently to reduce the SOI mismatch.

So clearly there is a need to improve the blocking matrix generation speed in a rapidly changing signal environment since every constraint angle change will trigger a recalculation of the blocking matrix. As predicted in [149], the only requirement for the blocking matrix is that the basis vectors need to be independent. Orthogonality is not really necessary for the blocking matrix. So by relaxing on the orthogonality requirement, the basis vectors for the blocking matrix could be found by methods other than SVD.

In this chapter, a fast algorithm working in the \mathbf{Z} domain that combines zero placement generated polynomial and a simple linear independent sub-polynomials to derive a set of null space vectors is proposed and simulated. The novelty of this new algorithm is that it finds the null space basis vector directly in the \mathbf{Z} domain with polynomial methods. This eliminates the needs for null basis finding methods like SVD which is known to be computation demanding. It achieves more than 9 times faster speed with the same performance as SVD based methods. One additional advantage for this new method is that it makes adding the derivative constraints at the DOA straightforward, although it still requires extra degree of freedom as in [149].

The rest of the chapter is organized in 4 sections. After the problem and its context are defined in section 5.2, the proposed solution is explained in section 5.3. Then numerical simulation and analysis are presented in section 5.4. Finally, the section 5.5 summarize the proposed solution.

5.2 Problem Formulation

5.2.1 Vehicle to Roadside Challenge

A major challenge for making beamforming working properly in rapid changing scenarios like railway communication is its reduced coherence time as reported in various channel modeling and experiments. In [150] coherence time of around 5-8 millisecond is reported with a speed of around 60km/h. For explicit beamforming which requires

more frequent channel sounding, various methods have been proposed in reducing the overhead for transmitting the CSI. In [151], an analog channel estimator is proposed to improve the channel sounding speed. But all these will increase the overhead and reduce the bandwidth efficiency.

A typical scenario where a wireless base station deployed along the track side is illustrated in Fig. 5.1. For situations like in HSR, where the train travels at speed



Figure 5.1: Base Station Installed along Track Side

as high as more than 320km/h [152] and the base station is just 5 meters away as listed in [153], the peak angle change speed could be around 16° per millisecond. So in less than one milli-second, although it is still within the coherence time around 1.4 milli-seconds according to the experiment and investigation in [153], the DOA change could make beamforming degrade very significantly due to the angle mismatch. In this scenario, the explicit channel sounding process becomes too slow and the outdated channel information actually makes the beamforming performance worse. So every time when the train passing by the base station the abrupt increase in DOA changing speed will make the beamforming algorithm break if not handled properly. The smaller cell size adopted in 5G and WiFi deployment makes the situation worse. In the cases where cell size is around 150 meter or less, the performance drop might occur in a frequency of every several milli-seconds.

To apply adaptive beamforming in this kind of scenario, the beamformer needs to adjust its weight fast enough after getting an updated DOA. With deep learning technology applied to DOA estimation [154], the speed and accuracy could be improved

significantly. As for the beamformer weight update speed, although GSC is able to automatically adapt to received data and form a null dynamically in the direction of interference which is not specified inside the constraint, it takes many steps to converge. But in many scenarios, especially high speed cases, it has limited time window to converge to forming the null in the interference direction. As indicated in [155], when the interference could be detected early, it is often better to put it inside the constraint matrix so that the required attenuation is achieved without an adaptation process. HSR scenario is a very good example of that.

A simplified system model illustrated in Fig. 5.2 shows the unique problem that requires the beamformer to derive the weight vector fast and frequent when train moving along the track and communicating with the base station.

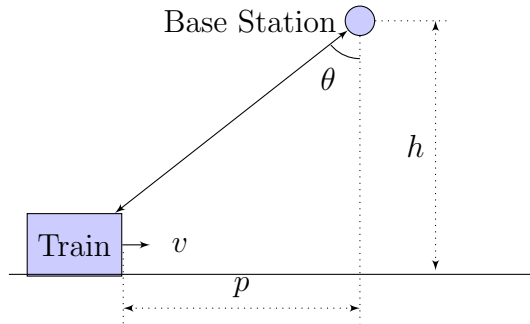


Figure 5.2: DOA Change Effect for Vehicle to Infrastructure

In Fig. 5.2, the train moving along the rail with velocity v . The base station is deployed along the road with a distance of h to rail. In actual case, there are multiple base stations deployed along the road every several hundred meters as indicated in Fig. 5.1. Here only one is illustrated for clarity. The instantaneous DOA $\theta(t)$ at time t is related to the v and the relative position in the road $p(t)$ by the following equation:

$$p(t) = h \tan(\theta(t)) \quad (5.1)$$

Taking derivative of (5.1), we can derive the instantaneous $\theta(t)$ changing speed in (5.2).

$$\dot{\theta}(t) = \frac{v}{h} \cos^2(\theta(t)) \quad (5.2)$$

It is clear from (5.2) that when train is near base station, $\theta(t)$ is small and the DOA changes fast as illustrated Fig. 5.3. And the changing speed is inversely proportional to the distance h as illustrated in Fig. 5.4

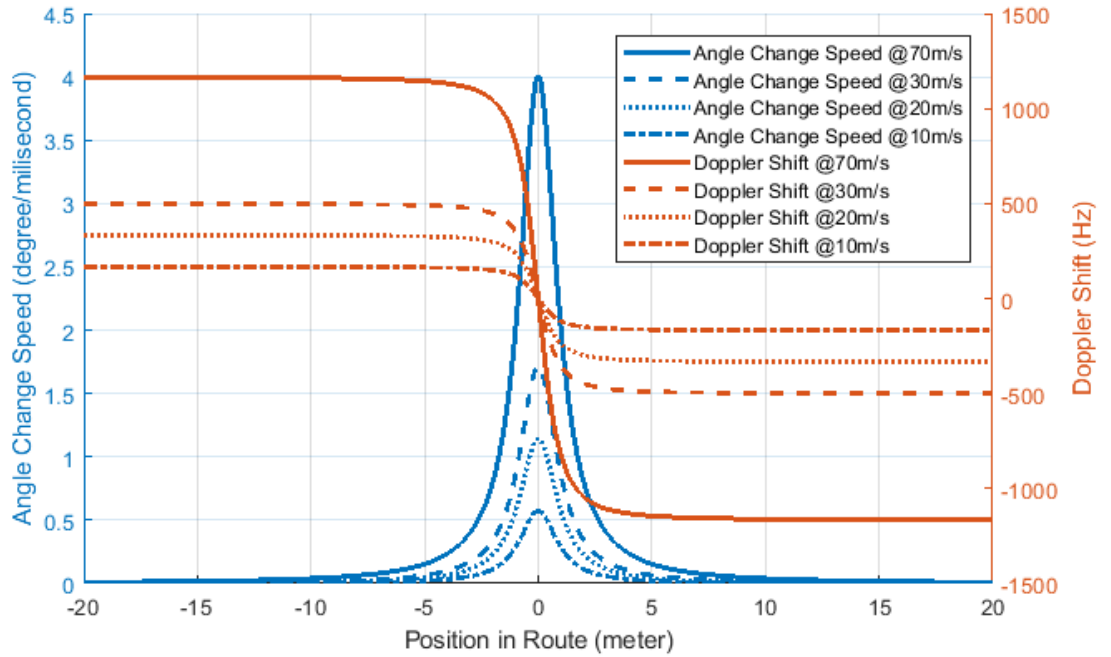


Figure 5.3: Angle Change Speed Spike when Passing By Base Station

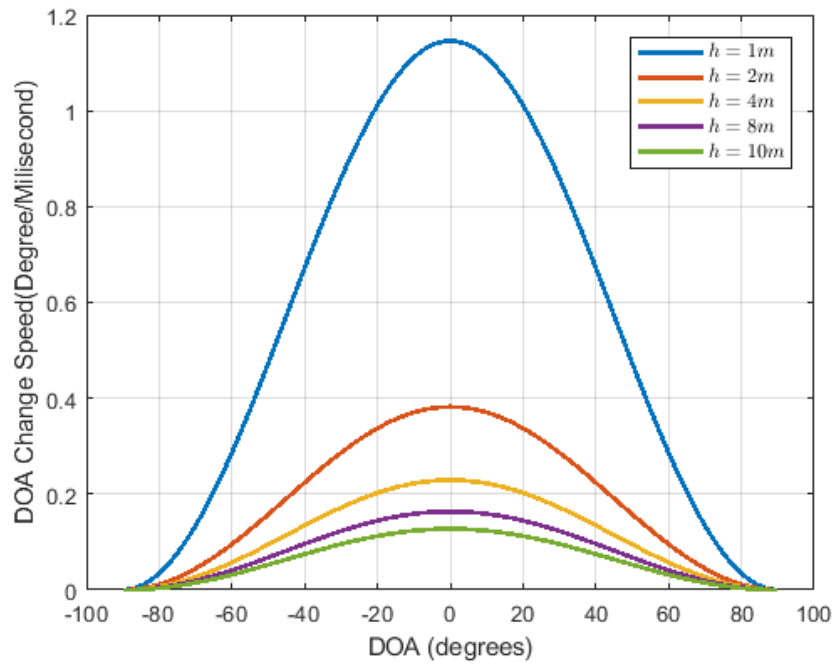


Figure 5.4: Angle Change Speed Increases when Distance h Decreases

The Doppler shift induced by the high travelling speed could be mitigated by the transmit beamforming as reported in [30] where multiple beams are formed and each angle is compensated separately before transmitting out. But it doesn't solve the rapid DOA change problem. So the DOA change speed is a unique problem for vehicle to road side scenarios when the distance h between the base station and the route is small.

It could be around 1-10 meters which is much shorter than usual 5G base station to vehicle.

5.2.2 GSC Architecture

A typical GSC beamformer is illustrated in Fig. 2.10. Here we highlight the blocking matrix component \mathbf{B} that our proposed algorithm aims to improve in green color in Fig. 5.5. It consists of a fixed beamformer \mathbf{w}_f which controls the quiescent response for input vector \mathbf{x} from M receivers, a blocking matrix \mathbf{B} which projects the input vector \mathbf{x} to the null space of the constraint matrix as vector \mathbf{u} that is further adaptively combined to produce the estimated interference \hat{y} for cancellation and an unconstrained beamformer \mathbf{w}_a which is adaptively controlled through an adaptive algorithm block.

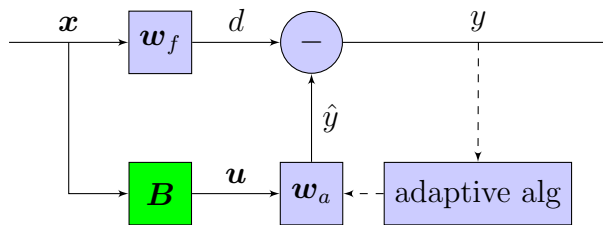


Figure 5.5: Beamformer Implementation with GSC Structure

The blocking matrix \mathbf{B} plays a critical role in mitigation of the signal cancellation problem where any signal leaked through the lower path of the GSC will be treated as noise and get cancelled through the adaptive algorithm. So when the DOA of incoming input \mathbf{x} changes rapidly, \mathbf{B} also needs to be updated accordingly.

5.3 Proposed Solution

5.3.1 Simplified Zero Placement Algorithm

Since any $M - N$ independent vectors in the null space of C^H span the whole null space, it might be simpler to just find $M - N$ vectors that satisfy equation (2.56). It turns out to be straightforward when looking from this perspective. For weight vectors \mathbf{b}_i that satisfies (2.56), their \mathbf{Z} transform $\mathbf{H}_B(z)$ could be separated into two parts. The first one contains the zeros for all the constraints.

$$C(z) = \prod_{i=1}^N (1 - z_i z^{-1}) \quad (5.3)$$

where N is the total number of constraints, z_i represents the zero location of the spatial frequency corresponding to the directions of interference and signals in the constraint matrix. The full $\mathbf{H}_B(z)$ then could be represented as

$$\mathbf{H}_B(z) = G(z)C(z) \quad (5.4)$$

where $G(z)$ represents the leftover $M - N - 1$ degree of polynomial. Since the signals from the N constrained direction correspond to the N embedded z_i in (5.4), any signal from those directions will result in 0 output. So any valid $G(z)$ would make $\mathbf{H}_B(z)$ a valid transform for vectors in null space of constraint matrix. So the task is simplified to just choose $M - N$ linearly independent polynomials to make up the null basis vectors. And we can choose the simplest ones which is easy for hardware implementation and guaranteed to be independent.

$$G(z) = \{1, z^{-1}, z^{-2}, \dots, z^{-(M-N-1)}\} \quad (5.5)$$

Since the z^{-1} is just a delay operator, the $M - N$ vectors that form the null basis is just the $M - N$ shifted version of the core vector that produces the zero response for all the constraints. The algorithm is described as follows.

Algorithm 2 SZPA: Calculate zero location for \mathbf{B} based on constraint matrix \mathbf{C}_{MN}

Require: $M \geq N$

- 1: **for** i in 1 to N **do**
 - 2: $\xi_i \leftarrow \frac{d \sin(\theta_i)}{\lambda_i}$ //Convert to spatial frequency
 - 3: $z_i \leftarrow e^{j2\pi\xi_i}$
 - 4: **end for**
 - 5: $C(z) \leftarrow \prod_{i=1}^N (1 - z_i z^{-1})$
 - 6: **for** i in 1 to N **do**
 - 7: $\mathbf{h}(i) \leftarrow$ coefficient of z^{-i}
 - 8: **end for**
 - 9: **for** i in 1 to $M-N$ **do**
 - 10: $\mathbf{B}(:, i) = [\text{zeros}(i - 1, 1); \mathbf{h}; \text{zeros}(M - 1 - N - i, 1)]$
 - 11: **end for**
-

The shifting operation is equivalent to add additional zeros in the origin for the \mathbf{Z} transform. So effectively in step 10 we are getting all the required independent vectors

in null space by a simple shifting operation. It is a very efficient and light operation. To our best knowledge, it has not been reported in the literature before.

5.3.2 Derivative Constraint based Robust Beamforming

By constraints with the first, second or even higher derivative of the beam pattern with respect to the DOA to zero, the beamformer can cater for larger signal DOA mismatch [65, 138]. In the framework of GSC, the derivative constraint is enforced in the noise cancellation path. By controlling the flatness of the null direction in the blocking matrix, the signal cancellation could be made less sensitive to the angle change in the vicinity of the SOI. This section looks the problem of derivative constraint in the Z domain and gives the way to implement the derivative constraint in the proposed SZPA algorithm.

The norm of $G(z)$ is constant by choosing (5.5) as the left over polynomial. This gives an additional advantage when investigating the beampattern of blocking matrix. Combine (5.4) and (5.5), it is apparent that the beam pattern is totally controlled by $C(z)$ which in turn is determined by the zero placement location.

$$P_B(z) = C(z)C^*(z) \quad (5.6)$$

To find the beam pattern over the DOA, (5.6) can be evaluated over the unit circle:

$$\begin{aligned} P_B(z)|_{z=e^{j\xi}} &= \prod_{i=1}^N (z - z_i)(z - z_i)^* \\ &= 2^N \prod_{i=1}^N (1 - \cos(\xi - \xi_i)) \end{aligned} \quad (5.7)$$

By taking the derivative with respect to ξ , we have:

$$\frac{dP_B}{d\xi} = 2^N \sum_{i=1}^N (\sin(\xi - \xi_i) \prod_{j \neq i} (1 - \cos(\xi - \xi_j))) \quad (5.8)$$

It is clear from (5.8) that for the first order derivative at ξ_i to be 0, at least one of ξ_j needs to equal to ξ_i . This means that by putting two zeros at the specified location, we can enforce their first derivative to be 0. And this will consume one more degree of freedom as expected. Keep taking derivative over (5.8), it can be found that for higher order of derivatives, we can just put more zeros to the specified location.

A simple simulation could illustrate the idea better. Different number of zeros are placed at a specific incoming angle 30° for a half wavelength spaced array, the power transfer function is then calculated and illustrated in Fig.5.6.

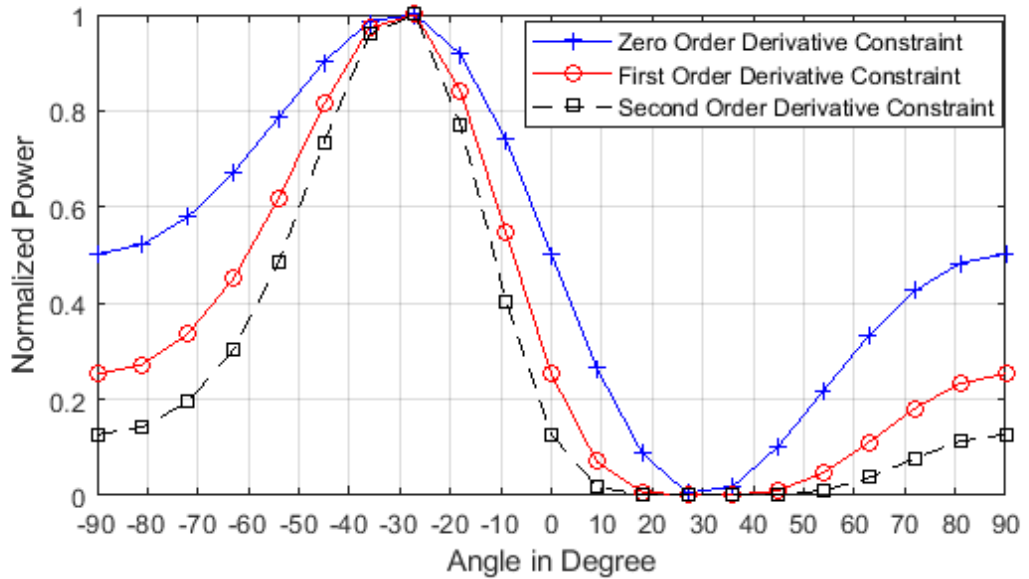


Figure 5.6: Derivative Constraint and Number of Zeros Effect

In Fig. 5.6, it is clear that the pattern curve is flattened in the vicinity of degree 30° when derivative constraint is put on 30° . The higher the derivative order, the flatter the curve at the constrained angle. A side effect can be noticed in Fig. 5.6 is that the derivative constraint put on angle 30° would create a steeper peak at angle -30° . This is an expected behavior according to (5.7). It becomes more obvious when viewed from the Z plane as in Fig. 5.7 where the $\Re(\cdot)$ and $\Im(\cdot)$ indicates the real and imaginary part of z respectively. When z moves around the unit circle, the norm $|z - \xi_i|$ experience the minimum of 0 at the zero location $z_i = e^{j\xi_i}$ and maximum at $e^{j(\xi_i+\pi)}$. For each

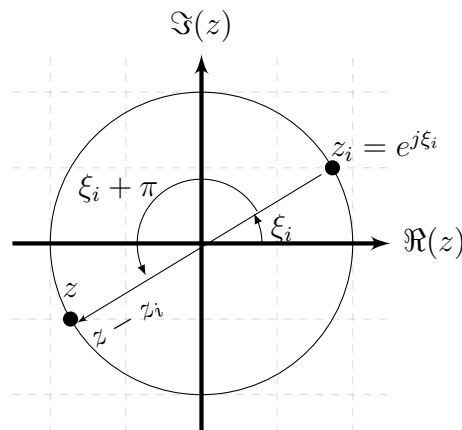


Figure 5.7: Each Zero Located at ξ_i Has a Corresponding Peak at $\xi_i + \pi$ for the Norm $|z - \xi_i|$

zero placement of ξ_i , there is a corresponding peak at $\xi_i + \pi$. So for DOA of 30° , the corresponding ξ_i is $\frac{\pi}{2}$. The peak would appear at $\arcsin(-\frac{1}{2})$ which corresponds to -30° .

The side effect of peak doesn't affect blocking capability since only the zero location has the blocking capability. This makes adding the derivative constraint in SZPA a straightforward step. The flatness of the nulls in the blocking matrix is controlled by the duplication number of zeros. For making the beamformer robust against SOI mismatch, we can just duplicate the required number of zeros when calculating the blocking matrix in step 5 of SZPA.

5.4 Numerical Simulation and Analysis

The main advantage of this new blocking matrix calculation algorithm SZPA is its fast computational speed for multiple constraints with no requirement on the pre-steering of sensors. Simpler blocking matrix that acts as a high pass filter like CCD and its variant [156, 139] requires pre-steering delay thus limited its usage. For scenarios that require multiple constraint angles like in HSR scenario, no pre-steering GSC [157] should be used where the Blocking Matrix is in the left null space of constraint matrix. So the comparison is conducted with the SVD method denoted as normal GSC [39, p. 60]. Since the simulation is designed to show performance of Blocking Matrix generation, any GSC algorithm like LMS GSC, NLMS GSC, Conjugate Gradient GSC [158] can serve the purpose and the angles used in constraints matrix are assumed to be derived by tracking or estimation through location aided scheme [159, 160] or other fast schemes like deep learning algorithm [154] etc. In this simulation we choose NLMS as it makes the selection of step size normalized and easy for comparison. With NLMS GSC chosen, the performance comparison can be done just by swapping the generated Blocking Matrix. Several simulations have been setup to demonstrate its effectiveness. The results are obtained from three simulations. The first simulation is to show that the calculation speed is substantially faster and insensitive to the number of constraints. The second simulation is to show that the optimum state performance is unaffected by using the SZPA generated blocking matrix. The third simulation is to show that the learning speed is also not affected by using the SZPA generated blocking matrix.

5.4.1 Calculation Performance Simulation

The blocking matrix \mathbf{B} calculation time comparison is shown in Fig. 5.8. An ULA with 20 antenna elements spaced at half carrier wavelength is simulated in a MATLAB running on a Dell laptop with Intel i7 CPU. The angle of constraints increased from 1 to 15 for this antenna array which could happen in multiple user scenarios. The calculation time is averaged over 20 times of running.

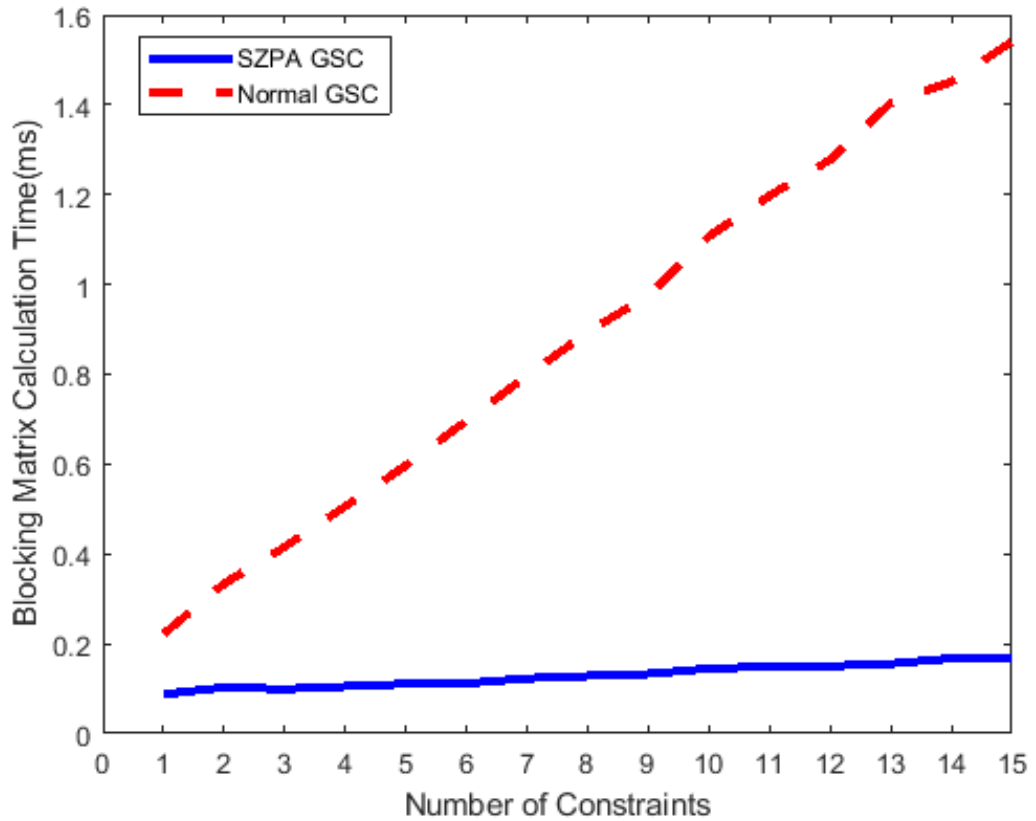


Figure 5.8: Blocking Matrix Calculation Time Comparison with Respect to Number of Constraints

It clearly shows that the proposed algorithm has very stable performance over the different number of constraints. In comparison, the calculation time for the SVD in normal GSC increases linearly with the increased number of constraints. There are two factors that limit the calculation speed for the normal GSC and give the SZPA the calculation advantage. Firstly, the normal GSC requires to build the constraint matrix from each of the specified angle and SZPA just needs to convert each specified angles to spatial frequency. Secondly, the matrix inversion and SVD operation used to find the null space basis are known to be expensive and SZPA replaces those expensive operation with simple polynomial operation. While required time for SZPA increase from 0.087ms to 0.168ms when constraints increased from 1 to 15, the SVD method

used in normal GSC increase from 0.22ms to 1.541ms. So it is obvious that SZPA calculation time is faster and insensitive to number of constraints. For 15 constraints, the speed to calculate the blocking matrix using SZPA is more than 9 times faster than Normal GSC. The required calculation time incremental for each additional constraint with SZPA is only around $\frac{1}{16}$ of SVD method.

5.4.2 Optimum Beam Pattern Performance Simulation

The beam pattern performance comparison is illustrated in Fig. 5.9. For clarity, the scenario with two angles constraints is depicted for an 8 element ULA where the desired signal is from 20° , a constrained interference is from 40° and an unconstrained interference is from 50° .

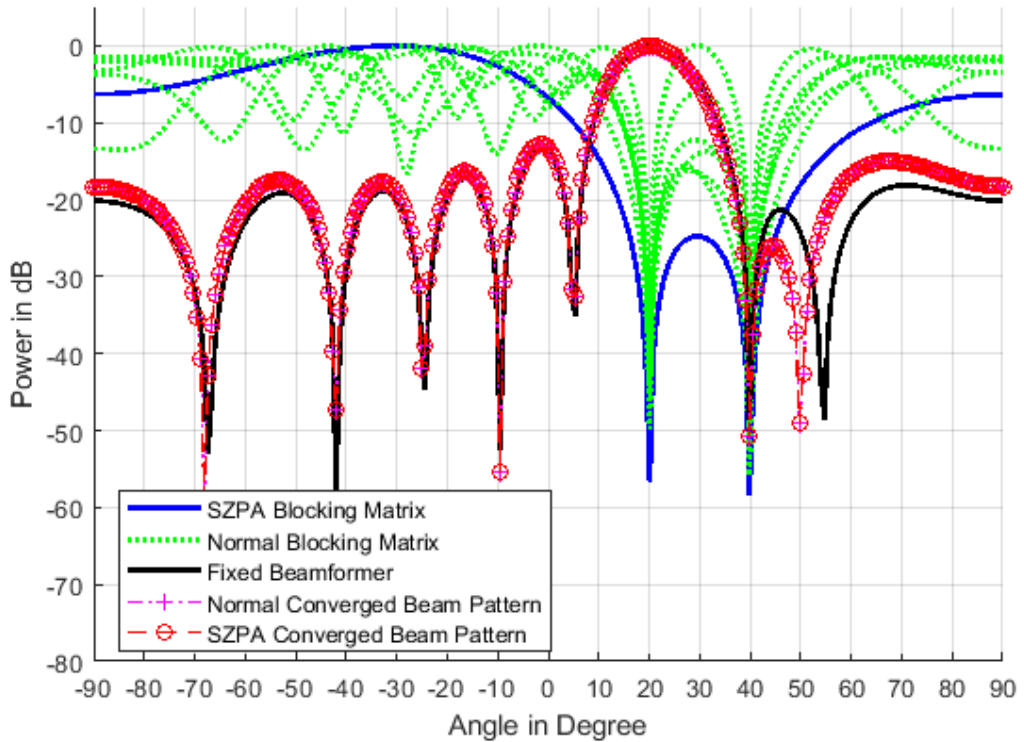


Figure 5.9: Converged Beam Pattern Performance Comparison

The blocking matrix prevents the constrained signal from being leaked to the cancellation path thus there are nulls formed at 20° and 40° . The overall converged beam patterns confirm that the main beam is untouched and nulls are formed at the constrained interference direction 40° and unconstrained direction 50° . The green dotted lines show patterns for each vector of the normal blocking matrix. But vectors of the SZPA blocking matrix are just shifted versions of each other, their amplitude response is the same thus the blue pattern appears as only one track. The overall converged

state beam pattern shows that both algorithms achieve exactly the same optimum performance. This behavior is expected from (2.55). The difference in \mathbf{B} will result in different input for the unconstrained adaptive filter in the cancellation path. But the adaptive process will reach different optimum value for the \mathbf{w}_a and finally the combined effect for the cancellation path $\mathbf{B}\mathbf{w}_a$ will be the same.

5.4.3 Learning Curve and SNR Performance Comparison

The Blocking Matrix generated by SZPA is not guaranteed to be orthogonal as compared to SVD based normal GSC Blocking Matrix generation algorithm. To evaluate the impact of the orthogonality in the adaptive speed of the noise cancellation path, different step size for the NLMS with 0.001, 0.01, 0.1 is used for the simulation. QPSK is used for the modulation scheme since it is the most basic QAM scheme which is widely used in many wireless standards. The results are average of 20 times of run. The simulation setup parameter is detailed in Table 5.1.

Table 5.1: Adaptive Speed Impact Simulation Setup

Parameters	Value
Modulation Scheme	QPSK
Number of Sensors	8
Desired Signal Angle of Arrival	30°
Interference Angle of Arrival	60°
Interference to Signal Ratio	35dB
Signal to Noise Ratio	20dB
Monte Carlo Simulation Runs	20
Adaptive Algorithm Used in GSC	NLMS
Number of Samples Simulated	10000
Step Size used	0.001, 0.01, 0.1

The learning curve and Signal to Noise Ratio (SNR) for the same GSC beamformer with Normal Blocking Matrix and SZPA Blocking Matrix is illustrated in Fig. 5.10 and Fig. 5.11.

It shows clearly in Fig. 5.10 that the learning curve is a typical NLMS algorithm based learning curve. For different step size, the learning speed is the same for both

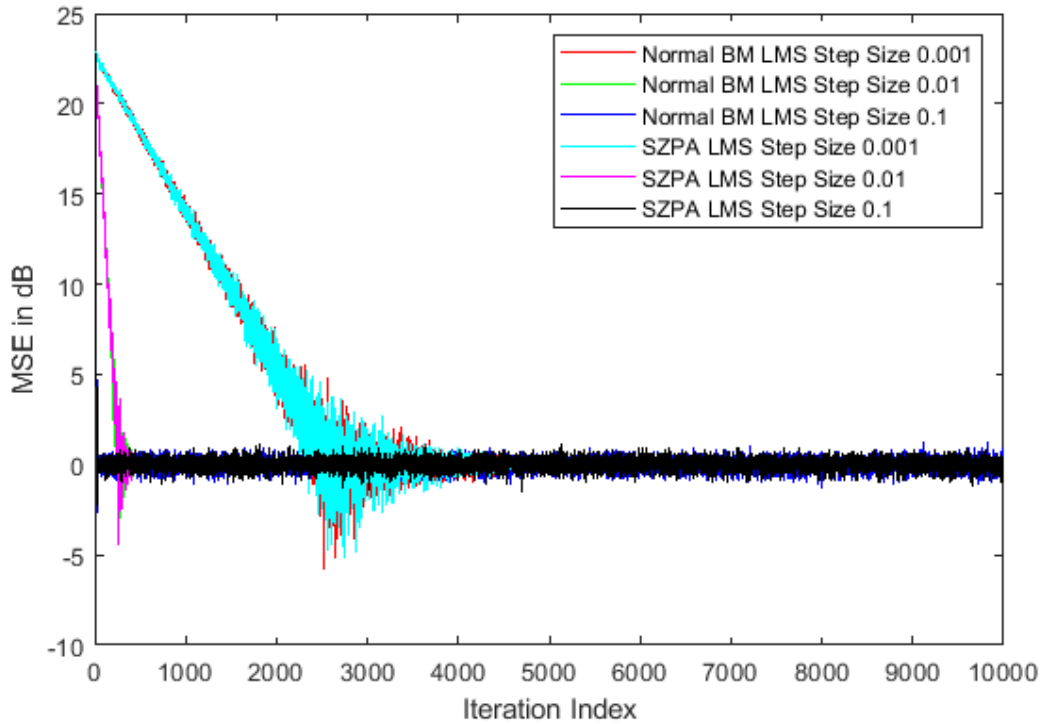


Figure 5.10: Learning Curve Performance Comparison with Different Step Size

algorithm generated Blocking Matrix.

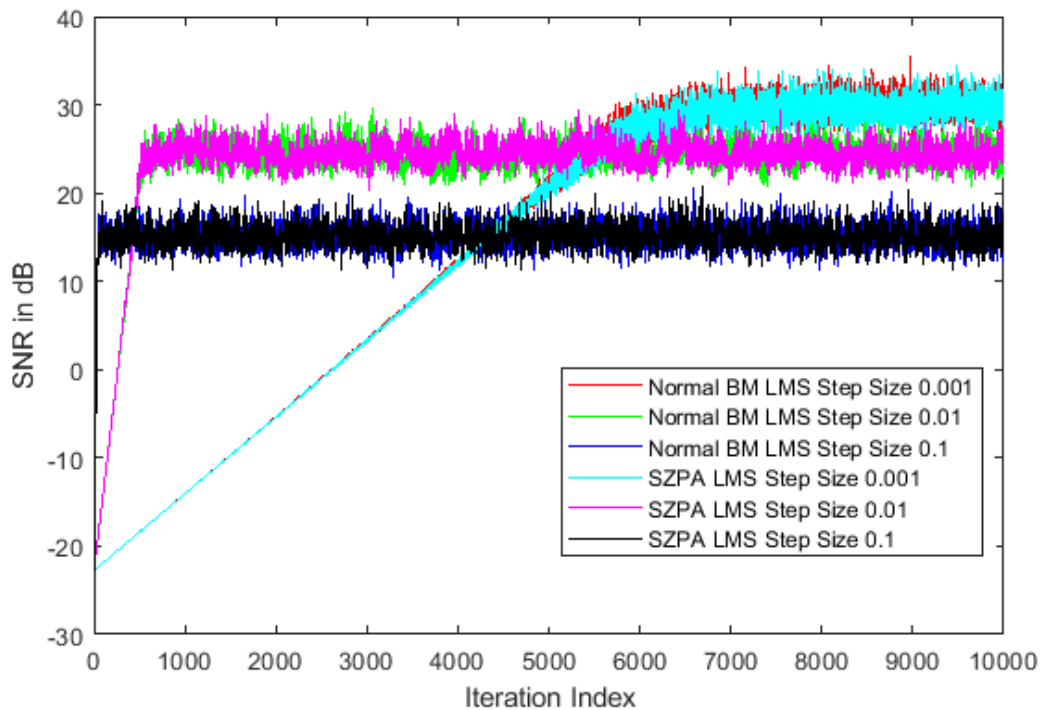


Figure 5.11: SNR Performance Comparison

From Fig. 5.11, it is clear that the SNR performance is also the same for both algorithms under different step sizes. The step size is well known to have great impact

on the adaptive speed and steady state SNR performance. As investigated in [161], variable step size could achieve both fast speed and low steady state MSE. A variety of Variable Step Size algorithm [3] could be employed to improve both performance. Since the main objective for this chapter is on the blocking matrix generation algorithm, the investigation on variable step size to achieve high learning speed and good performance will not be in the scope of this chapter.

5.5 Summary

A simplified zero placement algorithm (SZPA) to generate the blocking matrix is proposed and simulated. Working in the Z domain, the proposed SZPA is fast and also straightforward to support derivative based robust beamformer algorithms. The novelty of this new algorithm is that it finds the null space basis vector directly in the Z domain with polynomial methods and simple shift operations. The simulation results confirm the effectiveness of the proposed method. It could be more than 9 times faster than the conventional SVD based Normal GSC method for scenarios with 15 constraints and even more advantageous for more constraints. The optimum beam pattern performance of the whole GSC using the Blocking Matrix generated by the SZPA and SVD methods are the same. And from the simulation, the learning speed characteristics is also not compromised. In conclusion, this fast blocking matrix generation algorithm is suitable for any scenario that requires multiple constraints and frequent update like HSR train to infrastructure communication. It makes the real time update for Blocking Matrix possible for HSR scenario so that the signal loss due to DOA mismatch could be reduced.

Chapter 6

Conclusion and Future Work

6.1 Conclusion

Adaptive beamforming and switching in smart antenna system is investigated in this dissertation with the focus in adaptive beamforming. GSC architecture is selected to implement the adaptive beamforming algorithms due to its advantage of using unconstrained optimization algorithm in place of constrained optimization algorithm. The three main component of GSC is then individually investigated to address unique challenge in high speed transportation market which has rapid DOA change and dynamic channel characteristics.

A PSO based algorithm to generate colored Non-Gaussian noise that meets both the requirements of PSD and PDF is proposed in chapter 3. The numerical simulation result confirms its effectiveness. The benefit of this new method is that the complexity of deriving the required pre-distortion for the filter is replaced with a simple PSO search method. And once the required filter coefficients are found, the generation of non-Gaussian noise could be done in real time by filtering and ITS. Compared to block based methods or other analytical methods, it is more suitable for real time wireless channel simulation. The limitation for the proposed method is that the inverse of the required PDF needs to be available. Future investigation would be suggested on the verification of the validity for various PDFs and PSDs that might be useful for wireless channel gain simulation. The colored Non-Gaussian noise generation algorithm proposed in chapter 3 provides a way to evaluate the performance of various adaptive beamforming algorithms under different profiles of angle spread, delay spread and Doppler spread which is still an active measurement, modeling and research area for V2X scenarios.

A fast algorithm to synthesize a data independent flat top beam pattern named ZPFT that makes use of Chebyshev window and Schelkunoff algorithm is proposed in Chapter 4 which can achieve the same optimal performance as iteration based global optimization method with much less computing time in the designed simulation. The majority of the content is published in [2]. By breaking the array factor into two separate parts, a flat-top and narrow main beam with low SLL could be synthesized directly in the Z domain. The beam width requirement with low SLL is realized through the use of Dolph-Chebyshev array or other suitable window methods. The flat-top constraints are realized through two reserved zeros in the real axis where one of the zero is derived from the analysis of the broadening effect of two quadratic functions and the other zero is placed for keeping the SLL low. The simulation results confirm that ZPFT can achieve 22dB lower SLL while maintaining the same main beam performance as compared with FIR method for a 7 elements ULA. It can achieve the same optimal performance as demonstrated by the iteration based global optimisation techniques, with about 380 times less computing time in an Intel Core i7 platform. In the controlled simulation, ZPFT synthesizes the required beam pattern in 3 milliseconds. Compared with 1.15 seconds using the Semi-Definite Relax (SDR) method, it is clear that ZPFT can steer the main beam easily in real time while the overall optimum state performance remains the same by just doing an angle shift in the unit circle which makes it suitable for high mobility application where the DOA is changing fast.

A fast algorithm named SZPA to generate the Blocking Matrix of GSC is detailed in Chapter 5. The majority of the content is published in [1]. The proposed new algorithm finds the null space basis vector directly in the Z domain with polynomial methods and simple shift operations. The simulation results confirm the effectiveness of the proposed method. It could be more than 9 times faster than the conventional SVD based Normal GSC method for scenarios with 15 constraints and even more advantageous for more constraints. The optimum beam pattern performance of the whole GSC using the Blocking Matrix generated by the SZPA and SVD methods are the same. And from the simulation, the learning speed characteristics is also not compromised. In conclusion, this fast blocking matrix generation algorithm is suitable for any scenario that requires multiple constraints and frequent update like HSR train to infrastructure communication. It makes the real time update for Blocking Matrix possible for HSR scenario so that the signal loss due to DOA mismatch could be reduced.

In summary, this thesis proposes a GSC structure of adaptive beamformer which is suitable for high speed transportation market after incorporating two designed algorithms: ZPFT and SZPA. To facilitate the simulation of adaptive beamforming performance, an algorithm to generate colored non-Gaussian noise is also proposed.

6.2 Future Work

The work and algorithms derived from this thesis could be further enhanced in the following aspects:

1. To explore the knowledge of constrained route in transportation market to improve the speed and accuracy of DOA estimation,
2. To extend the SZPA and ZPFT to non-uniform distributed array,
3. To extract random variable characteristics from field wireless sounding measurement result to simulate various scenarios in railway wireless communication.

6.2.1 Further Explore the Knowledge of Constrained Route

As the estimated DOA is still needed for steering the main beam in the proposed GSC structure, a faster and more accurate DOA estimation would be helpful. The algorithm proposed in 2.5.2 using Kalman algorithm to fuse multiple sensors is simplified for illustration of concept only. It could be further explored with the help of the pre-defined constrained route. It can be further improved with more state variables like accelerator, Global Positioning System (GPS) sensor etc. which are also available in modern train or car.

One of the challenges for the Kalman filter assisted algorithm is the parameter setting for the measurement noise and process noise. In many implementation, the measurement noise is set arbitrarily [162]. In the rail way context, there is no proven algorithm to set them in an optimum way. Yet they have a big impact on how Kalman filter performs. More work needs to be done to improve the Kalman filter model.

6.2.2 Extend the SZPA and ZPFT Algorithm to Non-Uniform Distributed Scenario

The Zero Placement based algorithms SZPA and ZPFT could be further extended to non-uniform distributed AE scenario where each AE could have an correction factor to match to the uniform distributed case as discussed in this dissertation.

Even in ULA, the calibration error and component variance will cause some level of perturbation on the actual AE location. This non-uniformity will cause DOA mismatch if not being taken into consideration. The impact is analyzed in [45, p 1091].

6.2.3 Use the Right Random Variable Profile for Fast Railway Wireless Communication Simulation

The Non-Gaussian Colored noise generation algorithm proposed in chapter 3 could be used for wireless communication simulation with various adaptive beamforming algorithms. In stochastic modeling, the wireless channel gain random variable carries information about the profile of delay spread, angle spread and Doppler spread. With different measurement conducted by various projects [163, 164, 165], the random variable model could be established and the proposed algorithm could be used for fast wireless channel simulation so that different adaptive beamforming algorithm could be verified in different scanerio.

Abbreviations

AD/DA Analog/Digital and Digital/Analog Converter.

AE Antenna Element.

AP Access Point.

APA Affine Projection Algorithm.

AWGN Additive White Gaussian Noise.

BER Bit Error Rate.

BLUE Best Linear Unbiased Estimator.

BPSK Binary Phase Shift Keying.

BSS Blind Source Separation.

C-V2X Cellular Vehicle to Everything.

CCD Cascaded Differential Column.

CDF Cumulative Distribution Function.

CLT Central Limit Theorem.

CMA Constant Modulus Algorithm.

CPFSK Continuous Phase Frequency Shift Keying.

CSI Channel State Information.

CSIT Channel State Information at the Transmitter.

CSMA/CA Carrier Sense Multiple Access/Collision Avoidance.

CVSS Cyclic Variable Step Size.

DBF Digital Beamforming.

DCF Distributed Coordination Function.

DIFS Distributed Coordination Function (DCF) Interframe Space.

DMI Direct Matrix Inversion.

DOA Direction of Arrival.

ESPRIT Estimation of Signal Parameters by Rotational Invariance Techniques.

EVM Error Vector Magnitude.

FIR Finite Impulse Response.

FPGA Field Programmable Gate Array.

FSK Frequency Shift Keying.

GPS Global Positioning System.

GSC Generalized Sidelobe Cancellation.

HSR High Speed Rail.

ICA Independent Component Analysis.

IOT Internet of Things.

IPP Industrial Post-graduate Program.

IQ In-phase and Quadrature component.

ITS Inverse Transform Sampling.

LCMV Linear Constraint Minimum Variance.

LMS Least Mean Square.

LP Linear Programming.

LS Least Square.

MEPS Maximum Entropy Power Spectrum.

MIMO Multiple In Multiple Out.

MinMax Minimum Maximum.

MMSE Minimum Mean Square Error.

MPDR Minimum Power Distortionless Response.

MRC Maximum Ratio Combining.

MSE Mean Square Error.

MU-MIMO Multiple User Multiple Input Multiple Output.

MUSIC Multiple Signal Characterization.

MVDR Minimum Variance Distortionless Response.

NDP Null Data Packet.

NLMS Normalized LMS.

NR-V2X New Radio Vehicle to Everything.

OFDM Orthogonal Frequency Division Multiplexing.

PA Power Amplifier.

PCA Principle Component Analysis.

PDE Partial Derivative Equation.

PDF Probability Density Function.

PSD Power Spectral Density.

PSK Phase Shift Keying.

PSO Particle Swarm Optimization.

QAM Quadrature Amplitude Modulation.

QPSK Quadrature Phase Shift Keying.

RAB Robust Adaptive Beamformer.

RF Radio Frequency.

RLS Recursive Least Square.

RV Random Variable.

SD Steepest Descent.

SDA Signed Data Algorithm.

SDMA Space Division Multiple Access.

SDR Semi-Definite Relax.

SEA Signed Error Algorithm.

SINR Signal to Interference and Noise Ratio.

SISO Single Input Single Output.

SLL Sidelobe Level.

SMI Sample Matrix Inversion.

SNR Signal to Noise Ratio.

SOI Signal of Interest.

SVD Singular Value Decomposition.

SZPA Simplified Zero Placement Algorithm.

TTD True Time Delay.

UCA Uniform Circular Array.

ULA Uniform Linear Array.

V2I Vehicle to Infrastructure.

V2X Vehicle to Everything.

VGA Variable Gain Amplifier.

WRM Weighted Residual Method.

ZPFT Zero Placement Flat Top.

Bibliography

- [1] S. Dai, M. Li, Q. H. Abbasi, and M. A. Imran, “A fast blocking matrix generating algorithm for generalized sidelobe canceller beamformer in high speed rail like scenario,” *IEEE Sensors Journal*, 2020.
- [2] S. Dai, M. Li, Q. H. Abbasi, and M. A. Imran, “A zero placement algorithm for synthesis of flat top beam pattern with low sidelobe level,” *IEEE Access*, vol. 8, pp. 225935–225944, 2020.
- [3] S. Dai, M. Li, Q. H. Abbasi, and M. Imran, “Hardware efficient adaptive beamformer based on cyclic variable step size,” in *2018 IEEE International Symposium on Antennas and Propagation & USNC/URSI National Radio Science Meeting*, pp. 191–192, IEEE, 2018.
- [4] S. Dai, Q. H. Abbasi, M. Li, and M. Imran, “Beamforming optimization based on kalman filter for vehicle in constrained route,” in *2019 IEEE International Symposium on Antennas and Propagation and USNC-URSI Radio Science Meeting*, pp. 1365–1366, IEEE, 2019.
- [5] S. Dai, M. Li, Q. H. Abbasi, and M. Imran, “Improve tracking speed of beamformer with simplified zero placement algorithm,” in *2019 IEEE MTT-S International Wireless Symposium (IWS)*, pp. 1–3, IEEE, 2019.
- [6] S. Dai, M. Li, Q. H. Abbasi, and M. Imran, “Non-gaussian colored noise generation for wireless channel simulation with particle swarm optimizer,” in *2020 14th European Conference on Antennas and Propagation (EuCAP)*, pp. 1–4, IEEE, 2020.
- [7] S. Dai, M. Li, Q. H. Abbasi, and M. Imran, “A fast blocking matrix generating algorithm for generalized sidelobe canceller beamforming,” in *2020 IEEE International Symposium on Antennas and Propagation and North American Radio Science Meeting*, pp. 291–292, IEEE, 2020.

- [8] P. Ioannides and C. A. Balanis, "Uniform circular arrays for smart antennas," *IEEE Antennas and Propagation Magazine*, vol. 47, no. 4, pp. 192–206, 2005.
- [9] R. Mudumbai, G. Barriac, and U. Madhow, "On the feasibility of distributed beamforming in wireless networks," *IEEE Transactions on Wireless communications*, vol. 6, no. 5, pp. 1754–1763, 2007.
- [10] H. Ochiai, P. Mitran, H. V. Poor, and V. Tarokh, "Collaborative beamforming for distributed wireless ad hoc sensor networks," *IEEE Transactions on Signal Processing*, vol. 53, no. 11, pp. 4110–4124, 2005.
- [11] T.-D. Chiueh, P.-Y. Tsai, L. I-Wei, and T.-D. Chiueh, *Baseband receiver design for wireless MIMO-OFDM communications*. Wiley Online Library, 2012.
- [12] H. T. Hui, "The performance of the maximum ratio combining method in correlated rician-fading channels for antenna-diversity signal combining," *IEEE Transactions on Antennas and Propagation*, vol. 53, no. 3, pp. 958–964, 2005.
- [13] S. M. Alamouti, "A simple transmit diversity technique for wireless communications," *IEEE Journal on Selected Areas in Communications*, vol. 16, no. 8, pp. 1451–1458, 1998.
- [14] L. Zheng and D. N. C. Tse, "Diversity and multiplexing: A fundamental trade-off in multiple-antenna channels," *IEEE Transactions on Information Theory*, vol. 49, no. 5, pp. 1073–1096, 2003.
- [15] L. C. Godara, "Application of antenna arrays to mobile communications. ii. beam-forming and direction-of-arrival considerations," *Proceedings of the IEEE*, vol. 85, no. 8, pp. 1195–1245, 1997.
- [16] C. Carroll and B. V. Kumar, "Iterative fourier transform phased array radar pattern synthesis," in *Real-Time Signal Processing X*, vol. 827, pp. 73–85, International Society for Optics and Photonics, 1987.
- [17] H. Cox, "Resolving power and sensitivity to mismatch of optimum array processors," *The Journal of the Acoustical Society of America*, vol. 54, no. 3, pp. 771–785, 1973.

- [18] J. F. Synnevag, A. Austeng, and S. Holm, “Adaptive beamforming applied to medical ultrasound imaging,” *IEEE transactions on ultrasonics, ferroelectrics, and frequency control*, vol. 54, no. 8, pp. 1606–1613, 2007.
- [19] P. Stoica, R. L. Moses, *et al.*, “Spectral analysis of signals,” 2005.
- [20] L. R. Vega and H. Rey, *A rapid introduction to adaptive filtering*. Springer Science & Business Media, 2012.
- [21] S.-Y. Lien, D.-J. Deng, C.-C. Lin, H.-L. Tsai, T. Chen, C. Guo, and S.-M. Cheng, “3gpp nr sidelink transmissions toward 5g v2x,” *IEEE Access*, vol. 8, pp. 35368–35382, 2020.
- [22] M. H. C. Garcia, A. Molina-Galan, M. Boban, J. Gozalvez, B. Coll-Perales, T. ahin, and A. Kousaridas, “A tutorial on 5g nr v2x communications,” *IEEE Communications Surveys Tutorials*, vol. 23, no. 3, pp. 1972–2026, 2021.
- [23] G. Naik, B. Choudhury, and J.-M. Park, “Ieee 802.11 bd & 5g nr v2x: Evolution of radio access technologies for v2x communications,” *IEEE Access*, vol. 7, pp. 70169–70184, 2019.
- [24] M. Di Renzo, H. Haas, A. Ghayeb, S. Sugiura, and L. Hanzo, “Spatial modulation for generalized mimo: Challenges, opportunities, and implementation,” *Proceedings of the IEEE*, vol. 102, no. 1, pp. 56–103, 2013.
- [25] O. El Ayach, S. Rajagopal, S. Abu-Surra, Z. Pi, and R. W. Heath, “Spatially sparse precoding in millimeter wave mimo systems,” *IEEE Transactions on Wireless Communications*, vol. 13, no. 3, pp. 1499–1513, 2014.
- [26] S. Han, I. Chih-Lin, Z. Xu, and C. Rowell, “Large-scale antenna systems with hybrid analog and digital beamforming for millimeter wave 5g,” *IEEE Communications Magazine*, vol. 53, no. 1, pp. 186–194, 2015.
- [27] X. Yu, J. Zhang, and K. B. Letaief, “Doubling phase shifters for efficient hybrid precoder design in millimeter-wave communication systems,” *Journal of Communications and Information Networks*, vol. 4, no. 2, pp. 51–67, 2019.
- [28] T. Lin, J. Cong, Y. Zhu, J. Zhang, and K. B. Letaief, “Hybrid beamforming for millimeter wave systems using the mmse criterion,” *IEEE Transactions on Communications*, vol. 67, no. 5, pp. 3693–3708, 2019.

- [29] F. Sofrabi and W. Yu, “Hybrid digital and analog beamforming design for large-scale antenna arrays,” *IEEE Journal of Selected Topics in Signal Processing*, vol. 10, no. 3, pp. 501–513, 2016.
- [30] W. Guo, W. Zhang, P. Mu, F. Gao, and H. Lin, “High-mobility wideband massive mimo communications: Doppler compensation, analysis and scaling laws,” *IEEE Transactions on Wireless Communications*, vol. 18, no. 6, pp. 3177–3191, 2019.
- [31] L. Zexian and H. Do, “Final 5g v2x radio design,” *5G-PPP 5GCAR Deliverable D3.3*, Nov,2019.
- [32] J. Wu and P. Fan, “A survey on high mobility wireless communications: Challenges, opportunities and solutions,” *IEEE Access*, vol. 4, pp. 450–476, 2016.
- [33] T. Zugno, M. Drago, M. Giordani, M. Polese, and M. Zorzi, “Toward standardization of millimeter-wave vehicle-to-vehicle networks: Open challenges and performance evaluation,” *IEEE Communications Magazine*, vol. 58, no. 9, pp. 79–85, 2020.
- [34] S. Zeadally, M. A. Javed, and E. B. Hamida, “Vehicular communications for its: standardization and challenges,” *IEEE Communications Standards Magazine*, vol. 4, no. 1, pp. 11–17, 2020.
- [35] H. Guo, B. Makki, D.-T. Phan-Huy, E. Dahlman, M.-S. Alouini, and T. Svensson, “Predictor antenna: A technique to boost the performance of moving relays,” *IEEE Communications Magazine*, vol. 59, no. 7, pp. 80–86, 2021.
- [36] S. D. Stearns, “Adaptive signal processing,” 1985.
- [37] S. Dai, M. Li, Q. H. Abbasi, and M. Imran, “Hardware efficient adaptive beamformer based on cyclic variable step size,” in *2018 IEEE International Symposium on Antennas and Propagation USNC/URSI National Radio Science Meeting*, pp. 191–192, July 2018.
- [38] J. Li and P. Stoica, *Robust adaptive beamforming*, vol. 88. John Wiley & Sons, 2005.
- [39] W. Liu and S. Weiss, *Wideband beamforming: concepts and techniques*, vol. 17. John Wiley & Sons, 2010.

- [40] D. Zhu, B. Li, and P. Liang, “A novel hybrid beamforming algorithm with unified analog beamforming by subspace construction based on partial csi for massive mimo-ofdm systems,” *IEEE Transactions on Communications*, vol. 65, no. 2, pp. 594–607, 2016.
- [41] R. Compton, “The power-inversion adaptive array: concept and performance,” *IEEE Transactions on Aerospace and Electronic Systems*, no. 6, pp. 803–814, 1979.
- [42] H. Nyquist, “Certain topics in telegraph transmission theory,” *Transactions of the American Institute of Electrical Engineers*, vol. 47, no. 2, pp. 617–644, 1928.
- [43] A. Alkhateeb, S. Alex, P. Varkey, Y. Li, Q. Qu, and D. Tujkovic, “Deep learning coordinated beamforming for highly-mobile millimeter wave systems,” *IEEE Access*, vol. 6, pp. 37328–37348, 2018.
- [44] A. Pezeshki, B. D. Van Veen, L. L. Scharf, H. Cox, and M. L. Nordenvaad, “Eigenvalue beamforming using a multirank mvdr beamformer and subspace selection,” *IEEE Transactions on Signal Processing*, vol. 56, no. 5, pp. 1954–1967, 2008.
- [45] H. L. Van Trees, *Optimum array processing: Part IV of detection, estimation, and modulation theory*. John Wiley & Sons, 2004.
- [46] D. Schlichtharle, *Digital filters*. Springer, 2014.
- [47] F. J. Harris, “On the use of windows for harmonic analysis with the discrete fourier transform,” *Proceedings of the IEEE*, vol. 66, no. 1, pp. 51–83, 1978.
- [48] S. J. Orfanidis, “Electromagnetic waves and antennas,” 2002.
- [49] D. Schlichthärle, *Digital filters: basics and design*. Springer, 2010.
- [50] W. Fraser, “A survey of methods of computing minimax and near-minimax polynomial approximations for functions of a single independent variable,” *Journal of the ACM (JACM)*, vol. 12, no. 3, pp. 295–314, 1965.
- [51] H. Xu, W. Zeng, X. Zeng, and G. G. Yen, “An evolutionary algorithm based on minkowski distance for many-objective optimization,” *IEEE Transactions on Cybernetics*, vol. 49, no. 11, pp. 3968–3979, 2018.

- [52] M. Okuda, M. Ikehara, and S. Takahashi, “Fast and stable least-squares approach for the design of linear phase fir filters,” *IEEE Transactions on Signal Processing*, vol. 46, no. 6, pp. 1485–1493, 1998.
- [53] H. Schjær-Jacobsen and K. Madsen, “Synthesis of nonuniformly spaced arrays using a general nonlinear minimax optimisation method,” *IEEE Transactions on Antennas and Propagation*, vol. 24, no. 4, pp. 501–506, 1976.
- [54] M. Qian, J. Jen, Z. Aliyazicioglu, and H. Hwang, “Phase array antenna pattern design using the minimax algorithm,” in *Proceedings of 2011 IEEE CIE International Conference on Radar*, vol. 1, pp. 342–346, IEEE, 2011.
- [55] J. C. Mason and D. C. Handscomb, *Chebyshev polynomials*. CRC press, 2002.
- [56] R. Buck, “Alternation theorems for functions of several variables,” *Journal of Approximation Theory*, vol. 1, no. 3, pp. 325–334, 1968.
- [57] T. Parks and J. McClellan, “Chebyshev approximation for nonrecursive digital filters with linear phase,” *IEEE Transactions on Circuit Theory*, vol. 19, no. 2, pp. 189–194, 1972.
- [58] F. Taylor, *Digital filters: principles and applications with MATLAB*, vol. 30. John Wiley & Sons, 2011.
- [59] M. Z. Komodromos, S. F. Russell, and P. T. P. Tang, “Design of fir hilbert transformers and differentiators in the complex domain,” *IEEE Transactions on Circuits and Systems I: Fundamental Theory and Applications*, vol. 45, no. 1, pp. 64–67, 1998.
- [60] P. Woodward and J. Lawson, “The theoretical precision with which an arbitrary radiation-pattern may be obtained from a source of finite size,” *Journal of the Institution of Electrical Engineers-Part III: Radio and Communication Engineering*, vol. 95, no. 37, pp. 363–370, 1948.
- [61] J. Capon, “High-resolution frequency-wavenumber spectrum analysis,” *Proceedings of the IEEE*, vol. 57, no. 8, pp. 1408–1418, 1969.
- [62] J. R. Schott, *Matrix analysis for statistics*. John Wiley & Sons, 2016.
- [63] T. K. Moon and W. C. Stirling, *Mathematical methods and algorithms for signal processing*. No. 621.39: 51 MON, 2000.

- [64] Z. Zheng, Y. Zheng, W.-Q. Wang, and H. Zhang, "Covariance matrix reconstruction with interference steering vector and power estimation for robust adaptive beamforming," *IEEE Transactions on Vehicular Technology*, vol. 67, no. 9, pp. 8495–8503, 2018.
- [65] M. Er and A. Cantoni, "Derivative constraints for broad-band element space antenna array processors," *IEEE Transactions on Acoustics, Speech, and Signal Processing*, vol. 31, no. 6, pp. 1378–1393, 1983.
- [66] J. Li, P. Stoica, and Z. Wang, "On robust capon beamforming and diagonal loading," *IEEE Transactions on Signal Processing*, vol. 51, no. 7, pp. 1702–1715, 2003.
- [67] O. Forst, "An algorithm for linearly constrained adaptive processing," *Proc. IEEE*, vol. 60, no. 8, pp. 926–935, 1972.
- [68] J. Xu, G. Liao, S. Zhu, and L. Huang, "Response vector constrained robust lcmv beamforming based on semidefinite programming," *IEEE Transactions on Signal Processing*, vol. 63, no. 21, pp. 5720–5732, 2015.
- [69] B. D. Van Veen and K. M. Buckley, "Beamforming: A versatile approach to spatial filtering," *IEEE ASSP magazine*, vol. 5, no. 2, pp. 4–24, 1988.
- [70] J. Treichler and B. Agee, "A new approach to multipath correction of constant modulus signals," *IEEE Transactions on Acoustics, Speech, and Signal Processing*, vol. 31, no. 2, pp. 459–472, 1983.
- [71] J.-F. Cardoso, "Blind signal separation: statistical principles," *Proceedings of the IEEE*, vol. 86, no. 10, pp. 2009–2025, 1998.
- [72] A. Hyvärinen and E. Oja, "Independent component analysis: algorithms and applications," *Neural networks*, vol. 13, no. 4-5, pp. 411–430, 2000.
- [73] E. Oja, A. Hyvarinen, and J. Karhunen, *Independent Component Analysis*. Nashville, TN: John Wiley & Sons, 2001.
- [74] B. Widrow, J. McCool, and M. Ball, "The complex lms algorithm," *Proceedings of the IEEE*, vol. 63, no. 4, pp. 719–720, 1975.
- [75] B. Farhang-Boroujeny, *Adaptive filters: theory and applications*. John Wiley & Sons, 2013.

- [76] J. W. Brown and R. V. Churchill, *Complex variables and applications eighth edition*. McGraw-Hill Book Company, 2009.
- [77] R. Hunger, “An introduction to complex differentials and complex differentiability,” 2007.
- [78] A. H. Sayed, *Adaptive filters*. John Wiley & Sons, 2011.
- [79] R. A. Monzingo and T. W. Miller, *Introduction to adaptive arrays*. Scitech publishing, 2004.
- [80] B. Widrow, “Thinking about thinking: the discovery of the lms algorithm,” *IEEE Signal Processing Magazine*, vol. 22, no. 1, pp. 100–106, 2005.
- [81] B. Widrow and M. E. Hoff, “Adaptive switching circuits,” tech. rep., Stanford Univ Ca Stanford Electronics Labs, 1960.
- [82] S. S. Haykin, B. Widrow, and B. Widrow, *Least-mean-square adaptive filters*, vol. 31. Wiley Online Library, 2003.
- [83] L. Griffiths, “A simple adaptive algorithm for real-time processing in antenna arrays,” *Proceedings of the IEEE*, vol. 57, no. 10, pp. 1696–1704, 1969.
- [84] K. Ozeki and T. Umeda, “An adaptive filtering algorithm using an orthogonal projection to an affine subspace and its properties,” *Electronics and Communications in Japan (Part I: Communications)*, vol. 67, no. 5, pp. 19–27, 1984.
- [85] A. Gersho, “Adaptive filtering with binary reinforcement,” *IEEE Transactions on Information Theory*, vol. 30, no. 2, pp. 191–199, 1984.
- [86] K. Ozeki, *Theory of affine projection algorithms for adaptive filtering*. Springer, 2016.
- [87] S. Banerjee and A. Roy, *Linear algebra and matrix analysis for statistics*. Crc Press, 2014.
- [88] R. E. Kalman, “A new approach to linear filtering and prediction problems,” 1960.
- [89] R. G. Brown, *Introduction to random signals and Kalman filtering*. John Wiley, 1992.

- [90] R. Schmidt, "Multiple emitter location and signal parameter estimation," *IEEE Transactions on Antennas and Propagation*, vol. 34, no. 3, pp. 276–280, 1986.
- [91] F. Shen, F. Chen, and J. Song, "Robust adaptive beamforming based on steering vector estimation and covariance matrix reconstruction," *IEEE Communications Letters*, vol. 19, no. 9, pp. 1636–1639, 2015.
- [92] S. Mohammadzadeh, V. H. Nascimento, R. C. de Lamare, and O. Kukrer, "Maximum entropy-based interference-plus-noise covariance matrix reconstruction for robust adaptive beamforming," *IEEE Signal Processing Letters*, vol. 27, pp. 845–849, 2020.
- [93] S. Arikawa and Y. Karasawa, "A simplified mimo channel characteristics evaluation scheme based on ray tracing and its application to indoor radio systems," *IEEE Antennas and Wireless Propagation Letters*, vol. 13, pp. 1737–1740, 2014.
- [94] X. Mao, J. Jin, and J. Yang, "Wireless channel modeling methods: Classification, comparison and application," in *2010 5th International Conference on Computer Science & Education*, pp. 1669–1673, IEEE, 2010.
- [95] E. Biglieri, J. Proakis, and S. Shamai, "Fading channels: Information-theoretic and communications aspects," *IEEE Transactions on Information Theory*, vol. 44, no. 6, pp. 2619–2692, 1998.
- [96] F. P. Font en and P. M. Espi eira, *Modelling the wireless propagation channel: a simulation approach with Matlab*, vol. 5. John Wiley & Sons, 2008.
- [97] E. Perahia and R. Stacey, *Next generation wireless LANs: 802.11 n and 802.11 ac*. Cambridge university press, 2013.
- [98] H. Jiang, Y. Lu, and S. Yao, "Random matrix based method for joint dtd and doa estimation for large scale mimo radar in non-gaussian noise," in *2016 IEEE International Conference on Acoustics, Speech and Signal Processing (ICASSP)*, pp. 3031–3035, IEEE, 2016.
- [99] V. G. Chavali and C. R. da Silva, "Classification of digital amplitude-phase modulated signals in time-correlated non-gaussian channels," *IEEE Transactions on Communications*, vol. 61, no. 6, pp. 2408–2419, 2013.

- [100] E. Eweda, N. J. Bershad, and J. C. M. Bermudez, “Stochastic analysis of the lms and nlms algorithms for cyclostationary white gaussian and non-gaussian inputs,” *IEEE Transactions on Signal Processing*, vol. 66, no. 18, pp. 4753–4765, 2018.
- [101] J. E. Gentle, *Random number generation and Monte Carlo methods*. Springer Science & Business Media, 2006.
- [102] J. C. S. Santos Filho and M. D. Yacoub, “Coloring non-gaussian sequences,” *IEEE Transactions on Signal Processing*, vol. 56, no. 12, pp. 5817–5822, 2008.
- [103] S. Kay, “Representation and generation of non-gaussian wide-sense stationary random processes with arbitrary psds and a class of pdfs,” *IEEE Transactions on Signal Processing*, vol. 58, no. 7, pp. 3448–3458, 2010.
- [104] J. Kennedy and R. Eberhart, “Particle swarm optimization,” in *Proceedings of ICNN’95-international conference on neural networks*, vol. 4, pp. 1942–1948, IEEE, 1995.
- [105] D. Tse and P. Viswanath, *Fundamentals of wireless communication*. Cambridge university press, 2005.
- [106] A. M. Jaradat, J. M. Hamamreh, and H. Arslan, “Modulation options for ofdm-based waveforms: classification, comparison, and future directions,” *IEEE Access*, vol. 7, pp. 17263–17278, 2019.
- [107] W. Kibble, “An extension of a theorem of mehlér’s on hermite polynomials,” in *Mathematical Proceedings of the Cambridge Philosophical Society*, vol. 41, pp. 12–15, Cambridge University Press, 1945.
- [108] D. W. Boeringer and D. H. Werner, “Particle swarm optimization versus genetic algorithms for phased array synthesis,” *IEEE Transactions on Antennas and Propagation*, vol. 52, no. 3, pp. 771–779, 2004.
- [109] K. I. Pedersen, J. B. Andersen, J. P. Kermoal, and P. Mogensen, “A stochastic multiple-input-multiple-output radio channel model for evaluation of space-time coding algorithms,” in *Vehicular Technology Conference Fall 2000. IEEE VTS Fall VTC2000. 52nd Vehicular Technology Conference (Cat. No. 00CH37152)*, vol. 2, pp. 893–897, IEEE, 2000.

- [110] C.-Y. Chen and P. P. Vaidyanathan, “Quadratically constrained beamforming robust against direction-of-arrival mismatch,” *IEEE Transactions on Signal Processing*, vol. 55, no. 8, pp. 4139–4150, 2007.
- [111] B. Liao, C. Guo, L. Huang, Q. Li, and H. C. So, “Robust adaptive beamforming with precise main beam control,” *IEEE Transactions on Aerospace and Electronic Systems*, vol. 53, no. 1, pp. 345–356, 2017.
- [112] Y. Zhang, W. He, W. Hong, and Z. Song, “Flat topped radiation pattern synthesis based on fir filter concept,” in *2017 IEEE Asia Pacific Microwave Conference (APMC)*, pp. 751–754, IEEE, 2017.
- [113] A. Reyna, L. I. Balderas, and M. A. Panduro, “Time-modulated antenna arrays for circularly polarized shaped beam patterns,” *IEEE Antennas and Wireless Propagation Letters*, vol. 16, pp. 1537–1540, 2017.
- [114] Y. Xu, X. Shi, W. Li, and J. Xu, “Flat-top beampattern synthesis in range and angle domains for frequency diverse array via second-order cone programming,” *IEEE Antennas and Wireless Propagation Letters*, vol. 15, pp. 1479–1482, 2015.
- [115] A. K. Singh, M. P. Abegaonkar, and S. K. Koul, “Wide angle beam steerable high gain flat top beam antenna using graded index metasurface lens,” *IEEE Transactions on Antennas and Propagation*, vol. 67, no. 10, pp. 6334–6343, 2019.
- [116] J. Wang, Y. Yao, J. Yu, and X. Chen, “Broadband compact smooth horn with flat-top radiation pattern,” *Electronics Letters*, vol. 55, no. 3, pp. 119–120, 2018.
- [117] J. Khalilpour, J. Ranjbar, and P. Karami, “A novel algorithm in a linear phased array system for side lobe and grating lobe level reduction with large element spacing,” *Analog Integrated Circuits and Signal Processing*, pp. 1–11, 2020.
- [118] S. Das, G. R. Hardel, P. Chakravorty, D. Mandal, R. Kar, and S. P. Ghoshal, “Optimization of antenna arrays for sll reduction towards pareto objectivity using ga variants,” in *2015 IEEE Symposium Series on Computational Intelligence*, pp. 1164–1169, IEEE, 2015.
- [119] S. A. Schelkunoff, “A mathematical theory of linear arrays,” *The Bell System Technical Journal*, vol. 22, no. 1, pp. 80–107, 1943.

- [120] C. L. Dolph, "A current distribution for broadside arrays which optimizes the relationship between beam width and side-lobe level," *Proceedings of the IRE*, vol. 34, no. 6, pp. 335–348, 1946.
- [121] G. B. Arfken, *Mathematical Methods for Physicists, 6th Edition*. Academic Press, jul 2005.
- [122] H. Riblet, "Discussion on a current distribution for broadside arrays which optimizes the relationship between beamwidth and side-lobe level," *Proc. Ire*, vol. 35, pp. 489–492, 1947.
- [123] T. T. Taylor, "Design of line-source antennas for narrow beamwidth and low side lobes," *Transactions of the IRE Professional Group on Antennas and Propagation*, vol. 3, no. 1, pp. 16–28, 1955.
- [124] A. T. Villeneuve, "Taylor patterns for discrete arrays," *IEEE Transactions on Antennas and Propagation*, vol. 32, no. 10, pp. 1089–1093, 1984.
- [125] G. Buttazzoni and R. Vescovo, "Gaussian approach versus dolph-chebyshev synthesis of pencil beams for linear antenna arrays," *Electronics Letters*, vol. 54, no. 1, pp. 8–10, 2017.
- [126] M. Matijašćić and G. Molnar, "Design of linear arrays forming pencil beams based on derivatives of chebyshev polynomials," in *2019 42nd International Convention on Information and Communication Technology, Electronics and Microelectronics (MIPRO)*, pp. 117–121, IEEE, 2019.
- [127] G. T. F. de Abreu and R. Kohno, "A modified dolph-chebyshev approach for the synthesis of low sidelobe beampatterns with adjustable beamwidth," *IEEE Transactions on Antennas and Propagation*, vol. 51, no. 10, pp. 3014–3017, 2003.
- [128] W. Fan, C. Zhang, and Y. Huang, "Flat beam design for massive mimo systems via riemannian optimization," *IEEE Wireless Communications Letters*, vol. 8, no. 1, pp. 301–304, 2018.
- [129] D. Mandal, K. S. Kola, J. Tewary, V. P. Roy, and A. K. Bhattacharjee, "Synthesis of steered flat-top beam pattern using evolutionary algorithm," *Advanced Electromagnetics*, vol. 5, no. 3, pp. 86–90, 2016.

- [130] B. Misra and A. Deb, “Synthesis of antenna arrays with flat-top pattern using conventional and random drift particle swarm optimization algorithms,” in *2018 Emerging Trends in Electronic Devices and Computational Techniques (EDCT)*, pp. 1–5, IEEE, 2018.
- [131] A. B. Gershman, N. D. Sidiropoulos, S. Shahbazpanahi, M. Bengtsson, and B. Ottersten, “Convex optimization-based beamforming,” *IEEE Signal Processing Magazine*, vol. 27, no. 3, pp. 62–75, 2010.
- [132] R. C. Hansen, “Array pattern control and synthesis,” *Proceedings of the IEEE*, vol. 80, no. 1, pp. 141–151, 1992.
- [133] A. Boyajian, “Physical interpretation of complex angles and their functions,” *Journal of the American Institute of Electrical Engineers*, vol. 42, no. 2, pp. 155–164, 1923.
- [134] M. Grant and S. Boyd, “CVX: Matlab software for disciplined convex programming, version 2.1.” <http://cvxr.com/cvx>, Mar. 2014.
- [135] Z.-Q. Luo, W.-K. Ma, A. M.-C. So, Y. Ye, and S. Zhang, “Semidefinite relaxation of quadratic optimization problems,” *IEEE Signal Processing Magazine*, vol. 27, no. 3, pp. 20–34, 2010.
- [136] X. Zhang, Z. He, X. Zhang, and W. Peng, “High-performance beampattern synthesis via linear fractional semidefinite relaxation and quasi-convex optimization,” *IEEE Transactions on Antennas and Propagation*, vol. 66, no. 7, pp. 3421–3431, 2018.
- [137] B. Fuchs, “Application of convex relaxation to array synthesis problems,” *IEEE Transactions on Antennas and Propagation*, vol. 62, no. 2, pp. 634–640, 2013.
- [138] O. Hoshuyama, A. Sugiyama, and A. Hirano, “A robust adaptive beamformer for microphone arrays with a blocking matrix using constrained adaptive filters,” *IEEE Transactions on Signal Processing*, vol. 47, no. 10, pp. 2677–2684, 1999.
- [139] D.-C. Chang and B.-W. Zheng, “Adaptive generalized sidelobe canceler beamforming with time-varying direction-of-arrival estimation for arrayed sensors,” *IEEE Sensors Journal*, 2019.

- [140] L. Griffiths and C. Jim, “An alternative approach to linearly constrained adaptive beamforming,” *IEEE Transactions on Antennas and Propagation*, vol. 30, no. 1, pp. 27–34, 1982.
- [141] B. R. Breed and J. Strauss, “A short proof of the equivalence of lcmv and gsc beamforming,” *IEEE Signal Processing Letters*, vol. 9, no. 6, pp. 168–169, 2002.
- [142] W. P. Keizer, “Low-sidelobe pattern synthesis using iterative fourier techniques coded in matlab [em programmer’s notebook],” *IEEE Antennas and Propagation Magazine*, vol. 51, no. 2, pp. 137–150, 2009.
- [143] X. Zhang, Z. He, B. Liao, X. Zhang, and Y. Yang, “Pattern synthesis via oblique projection based multi-point array response control,” *IEEE Transactions on Antennas and Propagation*, 2019.
- [144] C.-Y. Tseng and L. J. Griffiths, “A systematic procedure for implementing the blocking matrix in decomposed form,” in *Twenty-Second Asilomar Conference on Signals, Systems and Computers*, vol. 2, pp. 808–812, IEEE, 1988.
- [145] G. A. Seber, *A matrix handbook for statisticians*, vol. 15. John Wiley & Sons, 2008.
- [146] Y. Zhao, W. Liu, and R. J. Langley, “Adaptive wideband beamforming with frequency invariance constraints,” *IEEE Transactions on Antennas and Propagation*, vol. 59, no. 4, pp. 1175–1184, 2011.
- [147] B. D. Carlson, “Covariance matrix estimation errors and diagonal loading in adaptive arrays,” *IEEE Transactions on Aerospace and Electronic systems*, vol. 24, no. 4, pp. 397–401, 1988.
- [148] Y. Gu and A. Leshem, “Robust adaptive beamforming based on interference covariance matrix reconstruction and steering vector estimation,” *IEEE Transactions on Signal Processing*, vol. 60, no. 7, pp. 3881–3885, 2012.
- [149] K. Buckley and L. Griffiths, “An adaptive generalized sidelobe canceller with derivative constraints,” *IEEE Transactions on Antennas and Propagation*, vol. 34, no. 3, pp. 311–319, 1986.

- [150] L. Wang, B. Ai, D. He, K. Guan, J. Zhang, J. Kim, and Z. Zhong, "Vehicle-to-infrastructure channel characterization in urban environment at 28 ghz," *China Communications*, vol. 16, no. 2, pp. 36–48, 2019.
- [151] V. V. Ratnam and A. F. Molisch, "Periodic analog channel estimation aided beamforming for massive mimo systems," *IEEE Transactions on Wireless Communications*, vol. 18, no. 3, pp. 1581–1594, 2019.
- [152] J. Guzinski, M. Diguët, Z. Krzeminski, A. Lewicki, and H. Abu-Rub, "Application of speed and load torque observers in high-speed train drive for diagnostic purposes," *IEEE Transactions on Industrial Electronics*, vol. 56, no. 1, pp. 248–256, 2008.
- [153] D. He, B. Ai, K. Guan, Z. Zhong, B. Hui, J. Kim, H. Chung, and I. Kim, "Channel measurement, simulation, and analysis for high-speed railway communications in 5g millimeter-wave band," *IEEE Transactions on Intelligent Transportation Systems*, vol. 19, no. 10, pp. 3144–3158, 2017.
- [154] H. Huang, J. Yang, H. Huang, Y. Song, and G. Gui, "Deep learning for super-resolution channel estimation and doa estimation based massive mimo system," *IEEE Transactions on Vehicular Technology*, vol. 67, no. 9, pp. 8549–8560, 2018.
- [155] L. Griffiths and K. Buckley, "Quiescent pattern control in linearly constrained adaptive arrays," *IEEE Transactions on Acoustics, Speech, and Signal Processing*, vol. 35, no. 7, pp. 917–926, 1987.
- [156] S. Gannot, D. Burshtein, and E. Weinstein, "Signal enhancement using beamforming and nonstationarity with applications to speech," *IEEE Transactions on Signal Processing*, vol. 49, no. 8, pp. 1614–1626, 2001.
- [157] K. Wu and T. Su, "Design of generalised sidelobe canceller-based adaptive wide-band beamformer without pre-steering delays," *Electronics Letters*, vol. 52, no. 3, pp. 177–179, 2015.
- [158] L. Wang and R. C. de Lamare, "Constrained adaptive filtering algorithms based on conjugate gradient techniques for beamforming," *IET Signal Processing*, vol. 4, no. 6, pp. 686–697, 2010.

- [159] K. Xu, Z. Shen, Y. Wang, and X. Xia, "Location-aided mmimo channel tracking and hybrid beamforming for high-speed railway communications: An angle-domain approach," *IEEE Systems Journal*, 2019.
- [160] C. Zhang, J. Zhang, Y. Huang, and L. Yang, "Location-aided channel tracking and downlink transmission for hst massive mimo systems," *IET Communications*, vol. 11, no. 13, pp. 2082–2088, 2017.
- [161] L. Shi, H. Zhao, and Y. Zakharov, "Performance analysis of shrinkage linear complex-valued lms algorithm," *IEEE Signal Processing Letters*, vol. 26, no. 8, pp. 1202–1206, 2019.
- [162] S. Park, M.-S. Gil, H. Im, and Y.-S. Moon, "Measurement noise recommendation for efficient kalman filtering over a large amount of sensor data," *Sensors*, vol. 19, no. 5, p. 1168, 2019.
- [163] R. He, Z. Zhong, B. Ai, G. Wang, J. Ding, and A. F. Molisch, "Measurements and analysis of propagation channels in high-speed railway viaducts," *IEEE Transactions on Wireless Communications*, vol. 12, no. 2, pp. 794–805, 2012.
- [164] R. He, B. Ai, Z. Zhong, A. F. Molisch, R. Chen, and Y. Yang, "A measurement-based stochastic model for high-speed railway channels," *IEEE Transactions on Intelligent Transportation Systems*, vol. 16, no. 3, pp. 1120–1135, 2014.
- [165] R. Zhang, X. Lu, J. Zhao, L. Cai, and J. Wang, "Measurement and modeling of angular spreads of three-dimensional urban street radio channels," *IEEE Transactions on Vehicular Technology*, vol. 66, no. 5, pp. 3555–3570, 2016.